New nanocomposite materials based on nanochitin and essential oils

eman ta zabal zazu

Universidad
del País Vasco

Euskal Herriko
Unibertsitatea

Rut Fernández Marín

2021

New nanocomposite materials based on nanochitin and essential oils

A dissertation presented by

Rut Fernández Marín

In Fulfilment of the Requirements for the Degree

Doctor of Philosophy by the University of the Basque Country

In the program Renewable Materials Engineering

Under the supervision of

Dr. Susana C M Fernandes and Dr. María Ángeles Andrés Sánchez

Tutor: Dr. Jalel Labidi

Chemical and Environmental Engineering Department

DONOSTIA - SAN SEBASTIÁN 2021

"*I am one of those who think that science has a great beauty. A scientist in his laboratory is not only a technician: he is also a child placed in front of natural phenomena that impress him like a fairy tale.*"

Marie Curie

Summary

In recent years, the isolation of chitin, which is the second most abundant natural polymer after cellulose, from crustacean shell waste has generated great interest for its application in different fields. This is due to its interesting properties such as biocompatibility and biodegradability. Chitin is a support material in nature, and presents a highly organised micro and nanofibrillated structure, which makes it possible to obtain nanochitin (nanocrystals and nanofibres). These have excellent properties such as low density, low toxicity, and high biodegradability. Additionally, they improve the mechanical properties by acting as reinforcement of films. On the other hand, essential oils are a complex mixture of volatile compounds extracted from different parts of plants that are a good source of bioactive metabolites with antioxidant and antimicrobial properties. Therefore, the aim of this thesis was to develop nanocomposite films based on nanochitin and (bio)polymers (in particular chitosan as matrix) and including essential oils as bioactive compounds, in order to promote the revalorisation of marine waste.

The thesis is divided into 5 parts: Context, Introduction, General methodology, Results and discussion and Conclusions and future works. Part 4, Results and discussion, is divided into 2 subsections, with a total of 5 chapters. The first subsection includes two chapters (Chapter 1 and 2) dedicated to the extraction and characterisation of nanochitin from yellow lobster, shrimp and squid pen and essential oil from *Curcuma longa* L. using the microwave-assisted extraction technique. The second Sub-section focuses on materials development and is divided in 3 chapters (Chapter 3, 4 and 5). Chapter 3, assess the effects that the deterpenation of essential oil fractions from *Origanum majorana* L. has on the final properties of chitosan/β-chitin nanofibre nanocomposites

films. In the Chapter 4, chitosan/α-chitin nanocrystal films were developed to change colour by the effect of ammonium gas and different pH by the incorporation of curcuma oil and anthocyanin extracts. In the last chapter (Chapter 5), poly(vinyl alcohol) films were investigated by the effect of different concentrations of *Origanum vulgare* oil and the reinforcement of α-chitin nanocrystals to improve the final properties.

The results showed that the addition of nanochitin reinforced the films and, moreover, the essential oils improved their functional properties, including their biological activity (antioxidant and antifungal). They could therefore be applied as smart food packaging.

ABBREVIATIONS

CH	Chitin
CS	Chitosan
EOs	Essential oils
CHNC	Chitin nanocrystals
CHNF	Chitin nanofibres
α-NCH$_S$/ α-NCH$_L$	α-nanochitin from shrimp/ α-nanochitin from lobster
β-NCH$_{Sp}$	β-nanochitin from squid pen
RSM	Response surface methodology
BBD	Box-Behnken design
ATR-FTIR	Attenuated Total Reflection-Fourier Transform Infrared Radiation
^{13}C-NMR	^{13}C nuclear magnetic resonance
XRD	X-ray diffraction
SEM	Scanning electron microscopy
AFM	Atomic force microscopy
MAE	Microwave-assisted technique
TGA	Thermogravimetric analysis
GC/MS	Gas chromatography and mass spectrometry
UV/Vis	Ultraviolet/visible
DA	Degree of N-acetylation
CI	Crystallinity Index
MC	Moisture content

WS	Water solubility
WCA	Water contact angle
YM	Young´s modulus
E	Elongation
TS	Tensile strength
TPC	Total phenolic content
DPPH assay	(2,2-diphenyl-1-picrylhydrazyl) free radical scavenging assay
FRAP assay	ferric reducing ability of plasma assay
ABTS assay	2,2'-Azino-bis(3-ethylbenzothiazoline-6-sulfonic acid) assay
FGI	Fungal growth inhibition
PVA	Poly(vinyl alcohol)
OEO	*Origanum vulgare* essential oil
OM	*Origanum majorana* L.

AGRADECIMIENTOS

Agradecimientos formales

Quisiera dar las gracias al grupo BioRP del departamento de Ingeniería química y Medio Ambiente de la Universidad del País Vasco/Euskal Herriko Unibertsitatea (UPV/EHU) por acogerme estos 4 años de tesis.

En especial quiero agradecer a mi tutor el Dr. Jalel Labidi y a mis directoras la Dra. María Ángeles Andrés Sánchez y la Dra. Susana Cristina de Matos Fernandes por darme la oportunidad de crecer tanto personal como científicamente dejándome probar todas mis locuras en esta tesis. Sobretodo agradecer al Dr. Jalel Labidi por depositar su confianza ciega en mi para desarrollar la tesis y a la Dr. Susana C. M. Fernandes por su ayuda sobre todo durante estos últimos meses.

Además, querría agradecer a la Dra. Corinne Nardin y al grupo Manta dirigido por la Dra. Susana C. M. Fernandes por acogerme durante 3 meses pudiendo desarrollar mi estancia en el IPREM, Université de Pau et des Pays de L'Adour (Pau, Francia).

También quiero dar las gracias a SGIker (UPV/EHU) por el apoyo técnico y humano ofrecido sin el cual no hubiera podido realizar esta tesis. Sobretodo destacar a Loli por su inestimable ayuda y por su amabilidad.

Por último, me gustaría agradecer al Departamento de Desarrollo Económico y Competitividad del Gobierno Vasco por concederme esta oportunidad de formarme mediante la beca de jóvenes investigadores.

AGRADECIMIENTOS

4 años desde que comenzó este largo camino en el que he pasado momentos intensos, a veces muy duros, y otros muy divertidos, en los que he llorado y he reído. En estos años he aprendido mucho tanto en la parte profesional como en la personal. A lo largo de estos años me he caído muchísimas veces, pero a pesar de ello he tenido la suerte de tener siempre a alguien para tenderme su mano para ayudar a levantarme. Esta tesis es el resultado de la pasión, dedicación y del trabajo duro. Es por ello que se la quiero agradecer a:

A Rebujitos

Gracias de corazón a Amaia, Leyre, Fabio, Xabi, Jonatan, Izas y Patri por convertiros en mi familia durante estos años. Por esos viajes locos, *Skypotes*, celebraciones de cumpleaños y de cualquier otra cosa…¡Siempre es buen momento para juntarnos! Pero sobre todo por aguantarme, apoyarme y consolarme cuando las cosas no salían bien y celebrarlo conmigo cuando ocurría algún milagroso éxito, aplaudiendo estas victorias como si fueran vuestras. Sin vosotros no habría logrado acabar este largo camino.

Thank you !!

Eskerrik asko!!
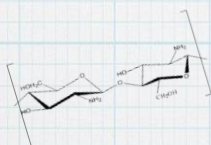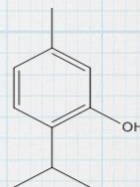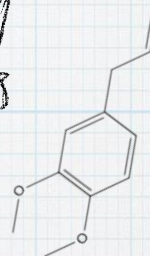
manta

Gracias a todos los miembros de MANTA por acogerme en estos momentos tan difíciles de *pandemia mundial* que estamos viviendo. Espero conoceros más en mejores condiciones y qué podamos colaborar en el futuro.

Sobretodo tengo que agradecer a Nelly que me incluyera en los planes y tareas del grupo desde el primer momento y hacerme sentir como una más. Sigue con esa alegría que tienes y con todas tus buenas ideas para mantener al grupo unido.
Además, quiero dar las gracias a Sheila por ser tan alegre y cercana conmigo y conseguir que me sintiera como en casa.

A los "de arriba"

Gracias a Iratxe, Julen, Joseba y Mireia por esas comidas de desconexión y esos largos cafés donde arreglábamos el mundo.
Sobre todo, quiero agradecer a Iratxe por aguantarme tantos años y por esas sesiones de psicólogo que me has ahorrado jajaja. Gracias por esas charlas en las que nunca nos da tiempo a contarnos todo y tenemos que ir corriendo a por el último bus. Por supuesto gracias a esos equipos de investigación en el "Alemán" junto a Ander.

Oregano

Th (90) 232.0381	N (7) 14.00674	K (19) 39.0983	Y (39) 88.90585	O (8) 15.9994	U (92) 238.0289
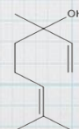
BioRP

Gracias a los compañeros del grupo **BioRP** *con los que he trabajado mano a mano durante este largo y duro proceso.*

En especial quiero dar las gracias a **Leyre, Amaia, Fabio, Xabi, Izas y Jonatan** por enseñarme a que el trabajo en equipo siempre es mejor que poner la zancadilla. También a **Belén** tengo que agradecer su amistad durante tantos años en todas las universidades de la UPV/EHU.

Sobre todo, quiero dar las gracias a los que han tenido que partir:

A **Patricia**, gracias por enseñarnos tanto, por hacernos espabilar y darnos un chute de energía y alegría siempre.

A **Asier** gracias por todo. Tanto dentro como fuera del laboratorio. Por enseñarme Donosti sobre ruedas y estar dispuesto a prestarme tu ayuda siempre que la he necesitado dando igual el momento del día.
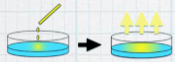
sgiker

Quiero darle las gracias a **Loli**. Por ayudarnos tanto y acudir en nuestra ayuda cuando lo hemos necesitado.

*Gracias **Alvar** por estar ahí siempre y hacerme grande cuando me hacía pequeña. Por escuchar con paciencia mis días malos (¡qué han sido muchos!). Y sacarme siempre una sonrisa con cualquier tontería.*

Gracias por cumplir conmigo la teoría de la aceituna y aparecer en mi vida en el momento adecuado. AMZ

Mis amigos

¡Qué deciros que no sepáis ya! Tantas batallas vividas y las que aún nos quedan por vivir. Tengo que agradeceros vuestra alegría que me da chute de energía y por aguantarme en lo bueno y en lo malo. Gracias por ser mi media pera.

A mi familia

A **mis padres**, ¡¡tengo tantísimo qué agradeceros!!

Gracias por enseñarme todo lo que sé en la vida, aunque no siempre lo aplique...

Por apoyarme incondicionalmente decida lo que decida.

A ti **Beatriz**, por motivarme siempre en cualquier ámbito de la vida y sobre todo cuando pensaba que no podía continuar con este largo viaje. ¡mi gran científica!

De mayor quiero ser como tú (aunque alcance la mitad).

Gracias **Nacho** por llevarnos de excursión a conocer nuevos mundos y esas tardes de invierno comiendo gominolas disfrutando de los Alpes.

A **mis primos y tíos**, gracias por sacarme siempre una sonrisa y estar siempre ahí.

¡¡¡No sé qué haría sin vosotros!!!

Gracias a todos por guiarme en la vida sin desdibujar mi propio camino.

Table of contents

Chapter 1

Optimization of microwave irradiation for the isolation of nanochitin from different origins by response surface methodology: an eco-friendly alternative

Chapter 2

Microwave-assisted extraction of Curcuma longa L. oil: Optimization, chemical structure and composition, antioxidant activity and comparison with conventional Soxhlet extraction

Chapter 3

Effect of deterpenated Origanum majorana L. essential oil on the physicochemical and biological properties of chitosan/ β-chitin nanofibres nanocomposite films

Chapter 4

Halocromic and antioxidant capacity of smart pH- and volatile ammonia-sensitive chitosan/chitin nanocrystals nanocomposite films prepared with curcuma oil and anthocyanins

Chapter 5

Using α-chitin nanocrystals to improve the final properties of poly (vinyl alcohol) films with Origanum vulgare essential oil

PART I: CONTEXT

PART I: CONTEXT

1. Outline of the Thesis

In our society, we are increasingly dependent on fossil resources such as coal, natural gas and oil. These resources have become indispensable to our lives because they are a source of energy, chemicals and materials. It is estimated that in 10 years the demand for fossil resources will rise by around 50 to 60 % [1]. Therefore, as a consequence of this ever-increasing use, they will be totally depleted in approximately 100-200 years [2]. Moreover, the production of these fossil resources generates environmental pollution and contributes to climate change; and, the materials produced, such as plastics, take long periods of time to degrade, around 1000 years [3,4]. Furthermore, in recent years there have been major problems with the nano-plastics that are generated, as around 150 million tonnes per year can reach the oceans, polluting them and killing marine life [5,6]. All of these factors have contributed to the search for renewable sources of biomass for some time now. These include those obtained from marine bioresources that are mainly composed of proteins, glycosaminoglycans and polysaccharides (alginates, chitin and chitosan) [7,8].

Seafood in particular generates the largest amount of waste and is estimated to be in the region of 6-8 million tonnes per year worldwide. Most of this waste is disposed of in landfills, used as animal feed meal or dumped into the sea [9]. The most important polysaccharide obtained from this waste is chitin, a poly (β-(1-4)-N-acetyl-D-glucosamine), which is considered and of the most abundant biopolymer on the planet. Two main compounds can be obtained from this biopolymer: 1) Nanochitin; and 2) Chitosan. Nanochitin, in the form of nanofiber or nanocrystals, can be

isolated from chitin because in nature it is a support material and presents a structure with highly organised micro- and nanofibrils. In addition, it has unique properties such as biocompatibility, small size, non-toxicity, biodegradability that make it highly valuable in numerous applications in the industrial sector. As for chitosan, which is a cationic biopolymer, it is obtained by deacetylation of chitin and its properties include antimicrobial, biocompatibility, biodegradability, low toxicity and a great ability to generate film [10]. Because of these unique intrinsic properties, these two raw materials had shown to be great candidates for the design and development of new (nano)composites for several applications [11–13].

On the other hand, throughout the history of humanity, knowledge of bioactive compounds, in particular essential oils (EOs), from the plant world has generated a great deal of interest, especially for their use in food and for health [14]. Essential oils are a mixture of low molecular weight molecules found in flowers, bark, leaves and seeds. Thanks to their antimicrobial and antioxidant properties, they can be used as bioactive agents in matrix materials such as chitosan, poly(vinyl alcohol) (PVA), starch and others to improve their functional properties [15,16]. Recently, chitosan in the form of coatings, capsules, emulsions or films have been used as matrix for EOs.

In this context, the work of this thesis report the development of nanocomposite materials based nanochitin and other (bio)polymers, in particular chitosan, as matrix and EOs as bioactive compound in order to promote the valuation of marine waste and reduce pollution.

2. Main and specific objectives

The general objective of the thesis was to design and develop nanocomposite films based on nanochitin and chitosan and analyse the effect of the incorporation of essential oils as bioactive compound on the final properties of the materials. To do so, the valorisation of marine wastes was investigated, by the extraction of nanochitin (nanocrystals and nanofibres) using a new green approach. The optimization of the extraction of *Curcuma longa* L. oil was also assessed.

2.1. Specific objectives

- **Objective 1** (Chapter 1)

To optimise the isolation of α-chitin nanocrystals from shrimp and yellow lobster and β-chitin nanofibres from squid pen by using a green approach - the microwave-assisted extraction technique - employing a Box-Behnken experimental design by surface response methodology.

- **Objective 2** (Chapter 2)

To optimise the extraction yield of *Curcuma longa* L. oil by using a green approach - microwave-assisted extraction technique - using Box-Behnken experimental design with response surface methodology.

- **Objective 3** (Chapter 3)

To investigate the effect of different fractions of *Origanum majorana* L. oil on the final properties of nanocomposite films based on chitosan and beta-chitin nanofibres from squid pen.

- **Objective 4** (Chapter 4)

To develop ammonia gas and pH-color change biocomposite films by incorporating *Curcuma longa* L. oil and anthocyanin extract into chitosan matrix and alpha-nanocrystals chitin from lobster.

- **Objective 5** (Chapter 5)

To study the effect of different concentrations of *Origanum vulgare* essential oil on the final properties of PVA/α-chitin nanocrystals from shrimp and lobster nanocomposite films.

PART II: INTRODUCTION

Part II: INTRODUCTION

1. Chitin and its derivates

In 1823, A. Odier, isolated, from beetles in alkaline solutions, an insoluble compound, which it called chitin (CH), a word that comes from the Greek << χιτών >> and means tunic or covering [17]. Chitin, poli (β-(1-4)-N-acetyl-D-glucosamine), is after cellulose the second most abundant natural polysaccharide on earth. This natural polymer is found in the exoskeleton of crustaceans, cell walls of fungi and yeast and in insect cuticles [18], [19].The Figure II- 1 shows the CH structure.
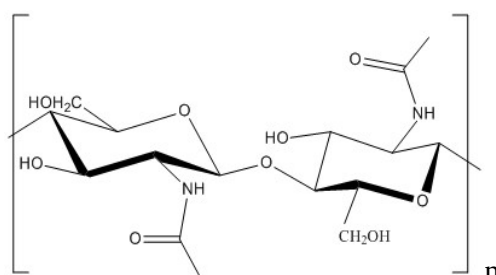
Figure II- 1. Chitin chemical structure.

CH presents three polymorphic crystalline structures: α, β and γ. The structures differ in the arrangement of the chains. The α-CH contains antiparallel chains alternatively, in the β structure all the chains are stacked parallel while the γ structure is formed by two parallel chains alternated with an antiparallel (Figure II-2) [20], [18].
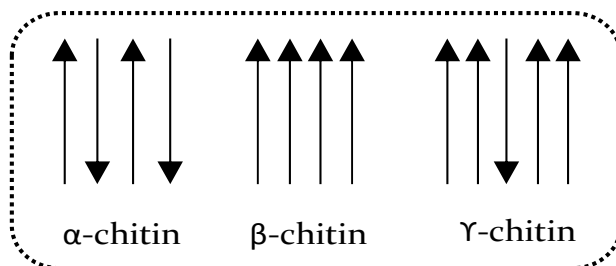
Figure II- 2. Scheme of the three polymorphic crystalline structures of chitin.

Chitin occurs in a complex matrix in conjunction with other substances such as proteins, pigments and other polysaccharides. Therefore, it is isolated (normally by the shellfish waste) by a three-step treatment such as shows the Figure III-3. The first step is deproteinization in which proteins are solubilized by a basic treatment (NaOH, KOH) or by enzymatic hydrolysis. The second step consists in an acid treatment (HCl, H_2SO_4) to eliminate the calcium carbonate. Finally, lipids and pigments are eliminated by bleached treatment (with acetone and reflux with ethanol). Depending on the raw material, when they are rich in minerals, the step of demineralization precedes that of deproteinization [18,21].
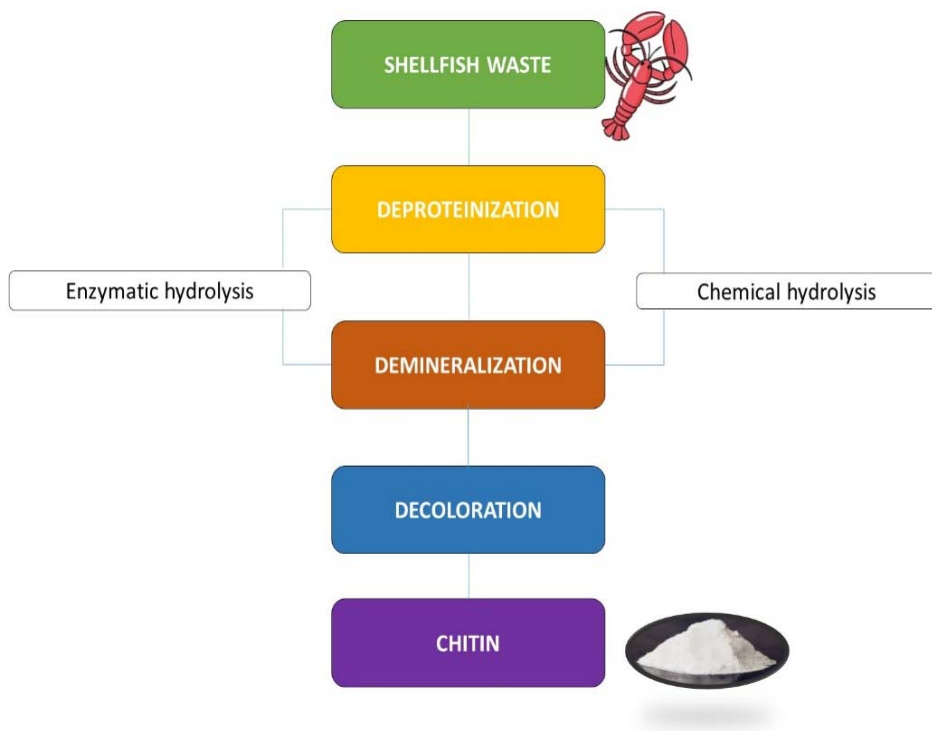
Figure II-3. Chitin extraction procedure.

CH has several advantages such as biocompatibility, biodegradability and is no toxic. However, it is insoluble in common solvents like water, organic solvents and diluted acids and bases, which makes its applications limited. This stability is owing to the stable equatorial disposition of the substituents and to the link $\beta(1\text{-}4)$ of the pyranose rings. The configuration β of the glycosidic bonds allows straight chains structures with strong interchain hydrogen bonds [18].

In recent years, chitin has been used in the form of nanocrystals/nanohiskers and nanofibers. Chitin presents a highly organized structure of microfibrils and nanofibrils, because is a structural material in nature and therefore contains crystalline and amorphous

domains [19], [22]. Depending on the biological material or isolation conditions, it can be isolated in the form of nanofibers (10-100 nm in width and many micrometres in length) and nanocrystals (6-60 nm in width and 100-800 nm in length) [10], [23]. The traditionals methods to isolated chitin nanofibers are ultrasonic techniques, mechanical approaches and electrospinning method [10], [24], [25]. On the other hand, to obtained chitin nanocrystals methods are acid hydrolysis, ionic liquids, partial deacetylations and TEMPO-mediated oxidation [26], [10].

Several studies have been reported its unique properties such as low density, large surface, small size, high cytocompatibility, low toxicity and also antimicrobial and antioxidant properties [27], [28], [29], [30]. Their main application is as reinforcing agent in nanocomposites materials and in numerous studies it has been demonstrated that they improve the mechanical, thermal properties and antifungal activity [31], [32]. According to its excellent properties, chitin nanoforms have generate a high interest in food, medical, textile and cosmetics industrial sectors.

However, the most commonly used derivative of CH is Chitosan (CS), which is a cationic polymer obtained from the deacetylation of chitin by a basic strong hydrolysis. The Figure II-4 shows the CS structure. Several studies have demonstrated that CS presents diverse biological activities, namely antioxidant, antimicrobial or anti-inflammatory, among others [33],[28], [34]. Moreover, chitosan presents excellent properties such as biocompatibility, biodegradability, low toxicity, solubility in weak acids and the ability of forming active edible films [35], [36], [37], coatings [38], [39], [40], emulsions [41], [42] and encapsulations [43], [44]. This makes CS a versatile material for different applications in the fields of medicine, food, agriculture and cosmetics.
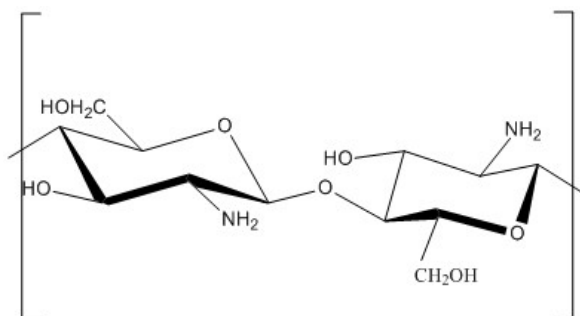
Figure II-4. Chitosan chemical structure.

2. Chitosan-based materials as templates for essential oils

2.1. Why use Chitosan as a carrier of Essential oils (EOs)?

Currently, there is increased demand for antioxidant and antimicrobial materials from naturally occurring agents and with a low negative impact on human health and the environment. An alternative to synthetic bioactive substances is the use of chitosan-based materials. CS, (Figure II-4) is a cationic natural polymer obtained from the deacetylation of CH by alkaline hydrolysis. CS shows bioactive properties namely antimicrobial, antioxidant or anti-inflammatory effects, [28,45,46]. Moreover, it also presents other excellent properties such as biocompatibility, biodegradability, low toxicity, solubility in weak acids and great film-forming ability [47].

Furthermore, the antioxidant and antimicrobial properties of CS can be improved with the association of supplemental bioactive substances. As such, essential oils (EOs) are good candidates for the design of this type of material due to their intrinsic properties. Indeed, these compounds have

PART II: INTRODUCTION

shown their therapeutic potential as antioxidants [48,49], antifungal [15], insecticidal [50] or antimicrobials [51–53].

EOs are highly complex mixtures of low molecular weight compounds obtained from different parts of plants such as flowers, barks, roots, leaves, seeds and fruit peels [54,55]. They are secondary metabolites constituted of two main groups: (i) terpenes (also called isoprenes); and (ii) terpenoids (also called isoprenoids). The terpenes group is made up of monoterpenes, which contain 10 carbon atoms, and by sesquiterpenes that contain 15 carbon atoms and have mono-, bi- or tricycles structures (Figure II-5). The terpenoids group is composed of oxygenated dreivatives of isoprenes (Figure II-5) [54,56]. Most of them fall into the Generally Recognized as Safe (GRAS) category, as defined by the US Food and Drug Administration (USFDA) [57].
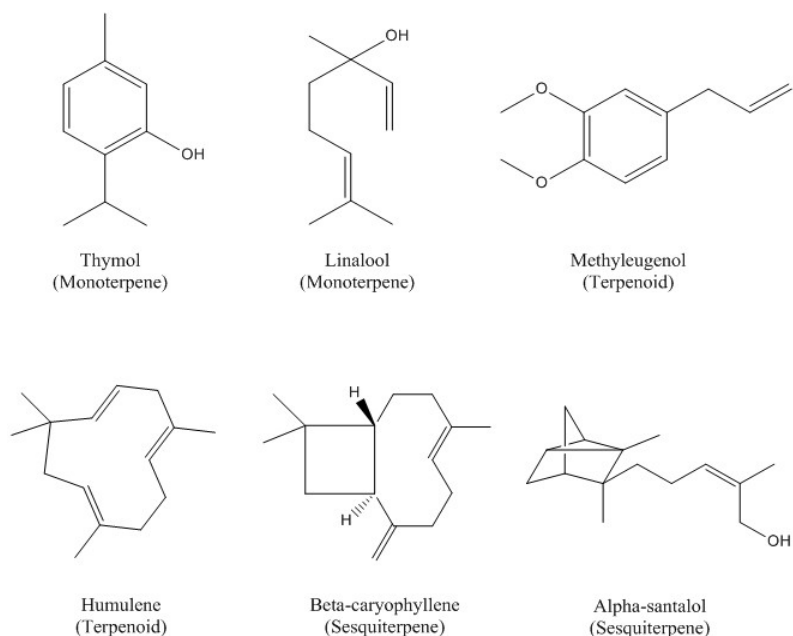
Figure II-5. Chemical structure of some typical essential oils.

EOs are extracted using different techniques, which can be divided two groups: (i) conventional methods and, the generally more eco-friendly, (ii) new methods as summarized in Figure II-6. Among the conventional methods are hydrodistillation, organic-solvent based extraction, steam-distillation and clevenger distillation [58]. In recent years, innovation in EO extraction has grown, with the use of methods such as microwave assisted extraction, microwave hydrodiffusion, microwave steam distillation, solvent free microwave extraction, supercritical fluid extraction and subcritical liquid extraction [54,58].
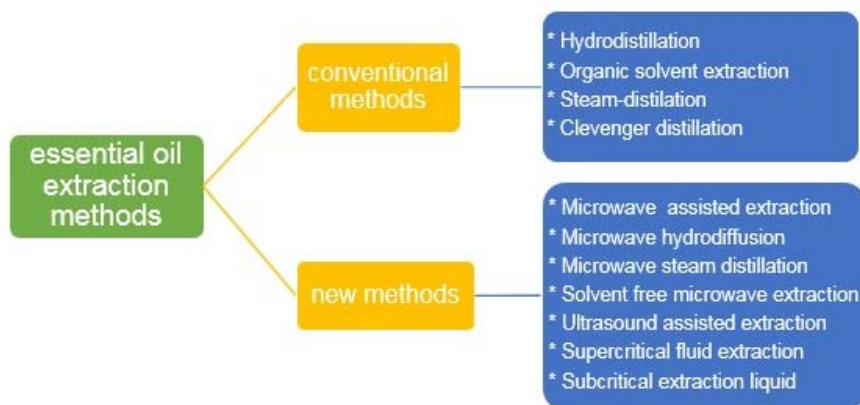
Figure II-6. Essential oils extraction methods.

EOs are very volatile compounds, and can easily be degraded during handling or on exposure to oxygen, heat or ultraviolet light [59]. For this reason, they are protected through incorporation in emulsions [41,42], particles [44,60], films [37,61] or coatings [38,60] using different biopolymers such as lignocellulosic materials, soy protein, alginate, gelatine and, the focus of this chapiter CS [62–66].

The aim of this chapter is to report the most recent and relevant advances concerning the use of CS as templates, in the form of films,

coating, capsules, gels and emulsions of EOs. For instance, CS active (i) films have been made with *Cinnamon verum, Zingiber officinale, Thymus moroderi and Thymus piperella* [35–37], (ii) coatings with *Zataria multiflora, Corum copticum* and *Camelia sinensis* [38–40], (iii) emulsions with *Zea mays* [41,42] and (iv) encapsulations with *Coriandrum sativum L.* and *Summer savory* [43,44]. These show the potential of CS as a versatile material for different applications in particular in food industry as well as fields as diverse as medicine, agriculture and cosmetics.

2.2. CS-based EOs coatings and films

Coatings and films are generally applied in liquid form before solidifying [67]. In this way, the first step of their preparation is solubilizing CS in an acidic aqueous solution (e.g. acetic acid) [38,68,69]. Then, in order to improve flexibility a plasticizer and/or surfactants are added, such as glycerol or Tween 80 and Tween 20 respectively [61,70,71]. In the final step, several methods are used to apply the coating on foodstuffs, for example solvent-casting, spray-coating, dipping and extrusion (Figure II-7), [72].
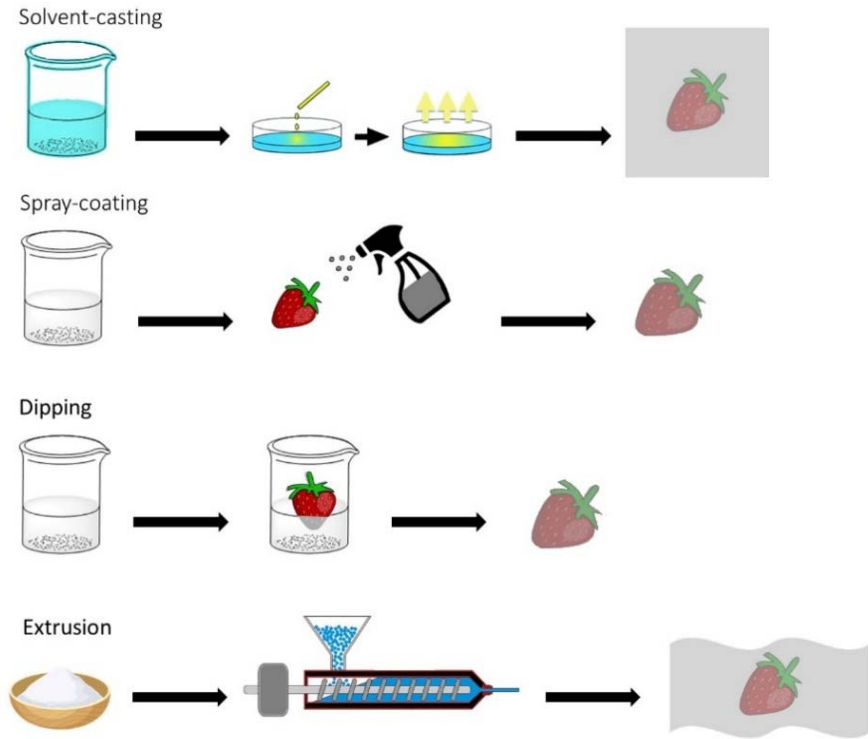
Figure II-7. Different methods to prepare CS-based films or coatings.

In the last few years, CS-based films and coatings combined with natural bioactive agents such as essential oils have increasingly gained the interest of researchers due to their useful properties. They are used to (i) protect food against gases, water vapour, UV-vis radiation and proliferation of microbial organisms; (ii) improve the mechanical properties of the material; (iii) and to release bioactive agents in order to maintain the quality and the organoleptic properties of food [72,73]. CS provides antimicrobial and antioxidant properties, which are further improved by incorporating essential oils into solution (Table II-1). Adding EOs may improve other properties like water vapour permeation and elongation at break [28,51].

Table II-1. Summary of CS-based EOs coatings and films materials and their properties.

Essential oil	Matrix	Coating or films method	Final bioactive properties	References
Zataria multiflora Boiss and Sumac extract	CS coating	Dip-coating	Antioxidant and antimicrobial	[38]
Prunus armeniaca	CS-N-methyl-2-pyrrolidone nanoparticles films	Solvent-casting	Antioxidant and antimicrobial	[28]
Carum copticum	CS film reinforced with cellulose nanofibers or lignocellulose nanofibers	Solvent-casting	Antioxidant and antimicrobial	[51]
Cinnamon verum, Cumbopogon citrates and *Origanum vulgare*	CS film	Solvent-casting	Antifungal	[74]
Myrcia ovata Cambessedes	CS coatings	Dip-coating	Antimicrobial	[75]

Citrus reticulata	N-palmitoyl CS based-coating containing nanoemulsion	Spray-coating	Antimicrobial	[76]
Citrus reticulata	N-palmitoyl CS based-coating nanoemulsion	Spray-coating	Antimicrobial	[77]
Origanum vulgare	Cassava starch-CS film	Extrusion	Antimicrobial	[16]

2.3. CS emulsions and (nano) gels of EOs

In the food industry, nanogels and emulsions are increasingly studied as carriers of EOs to control their release and their stability in order to extend the shelf life of food [76,78].

Emulsions are a mixture of at least two immiscible liquids, usually oil and water. One of the liquids is dispersed (dispersed phase) in the form of small spherical droplets in the other (continuous phase or dispersing phase). There are two types of emulsions: (i) hydrophilic emulsions, in which the oil droplets are dispersed in water (oil-in-water emulsion, O / W) and (ii) hydrophobic emulsions, in which there are water droplets dispersed in oil (water-in-oil emulsion, W / O).

Emulsions are thermodynamically unfavourable systems, which tend to break down over time [76,79]. For this reason, stabilizing the drops of the emulsion can be performed by reducing the interfacial tension using surfactants or hydrocolloids and water-soluble proteins [80]. One of the

most common ways to stabilize emulsions is the use of particles, known as Pickering emulsions. In this type of emulsion, an accumulation of dispersed particles occurs at the water-oil interface which forms a mechanical barrier to protect the drops against coalescence [81]. As shown in Figure II-8, these particles can take a number of different morphologies, shapes and appearances, such as platelets, globules, surfactants and fibrils.
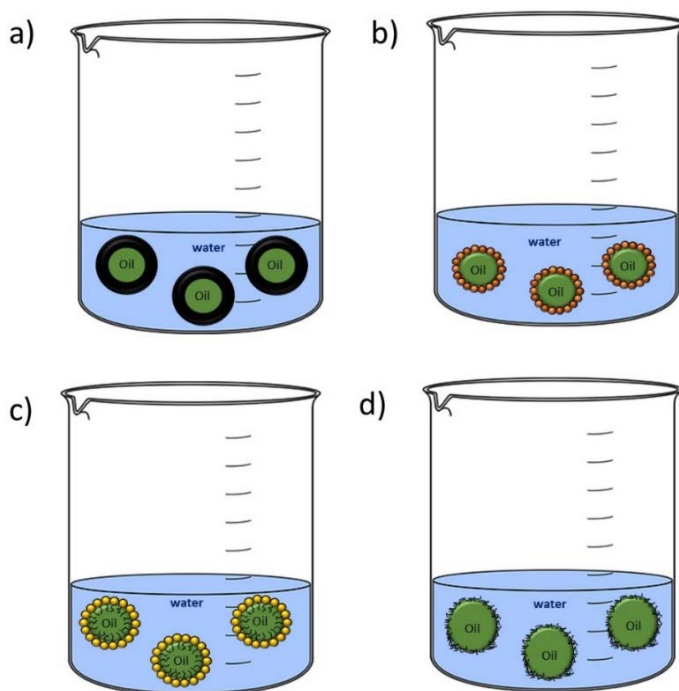
Figure II-8. Nanoparticle stabilized and surfactant stabilized emulsions.

In factories producing foodstuffs proteins, starch, flavonoids and nanocrystals of chitin or cellulose are used as stabilizing particles to make Pickering emulsions [41,82,83]. The use Chitin and CS nanoparticles in Pickering emulsions has been the subject of numerous recent studies because of their biocompatiblity and absence of toxicity. However, because these polysaccharides are poorly water-soluble, the addition of surfactants and other components is required for their use in emulsions such as: Tween

20 or Tween 80, gelatin, benzoic acid, cinnamic acid, caffeic acid or glycerol among others [42,84,85].

Nanogels are colloidal systems with a semi-solid appearance that flow when subjected to relatively weak forces. Normally, they are divided into two broad groups: (i) hydrogels, which absorb water, and (ii) organogels (micelles) which are hydrophobic and have a tendency oleo substances substances [78]. Structurally, nanogels are by self-assembled three-dimensional networks connected by covalent bonds [34,84]. They can be made using proteins, organic or inorganic compounds, and polymers such as CS.

In brief, adding emulsions of EOs into CS films can decrease solubility, increase elongation at break values and increase antimicrobial performance [86,87]. When nanogels are encapsulated, release of EOs is sustained over an extended time period, improving antioxidant and antimicrobial activity [78,85]. Some of the oils incorporated as emulsions or nanongels are sunflower oil [80], garlic oil [86], corn oil [41] or rosemary oil [34].

2.4. CS (nano) capsules for EOs encapsulation

Encapsulation is a technique widely used in food and medicine to release bioactive substances such as terpenes, terpenoids, and phenolic compounds mainly for their antioxidant and antimicrobial properties [88]. Encapsulations are individual particles of an active agent in a core that is surrounded by a membrane called shell (Figure II-9.) The size of (nano)capsulates is usually from 1 to 1000 μm [89].

The core can be liquid (the case of EOs), solid or a dispersion. The shell can be made up of polysaccharides and simple sugars (gum, cellulose, starch), lipids (oils, waxes, parafilms), proteins (soy, gelatin, casein) or biodegradable polymers (poly(vinyl-alcohol), poly(D,L-lactide), CS) [21,90].
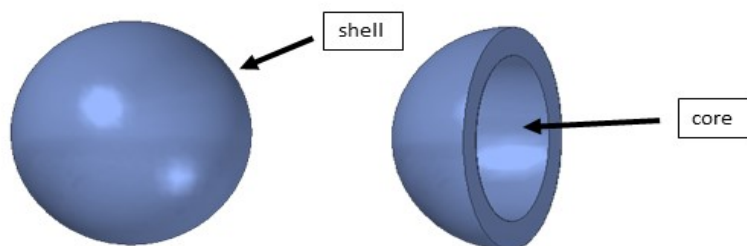
Figure II-9. A simple structure of capsule.

The stability of the (nano)capsulate depends on factors like pressure, temperature or pH and the method of encapsulation.

The encapsulation methods most effective for EOs (nano)capsulates appear to be ionic gelation, spray drying and coacervation [58,91]. Ionic gelation encapsulation makes use of the electrostatic interactions between the negative groups of the polyanion (for example: tripolyphosphate) and the positive charges of the primary amines of CS [59]. Spray drying is a method in which a solution is atomized in small droplets, followed a drying step in a heated gas. Coacervation is the separation of two liquid phases in a colloidal solution. These two phases are called coacervates, one polymer-rich, and another in which there is no polymer - an equilibrium solution. There are two main types of coacervation: simple – involving a single polymer, and complex – involving two or more polymer [54].

In the last decade, many studies have used encapsulated EOs for diverse applications, as compiled in Table II-2.

Table II-2. Summary of CS-based EOs nanocapsules and their properties.

EOs	Template	Encapsulation method	Size	Final bioactive properties	References
Syzygium aromaticum	CS–TPP nanoparticles	Ionic gelation	129 – 1288 nm	Antifungal	[91]
Mentha spicata and green *Camellia sinensis*	CS	Emulsification- ionic gelation	20-256 nm	Antioxidant and antibacterial activities for food and medical	[88]
Coriandrum sativum	CS	Spray-drying	400 nm- 7μm	Antimicrobial and antioxidant	[21]
Mentha piperita	CS–cinnamic acid nanogel	Ionic gelation	< 100 nm	Antimicrobial	[84]
Pimenta dioica (L.) Merrill	CS/k-carrageenan	Complex coacervation	1172 -1224 μm	Antimicrobial and antioxidant	[58]
Origanum vulgare	CS–TPP nanoparticles	Ionic gelation	40- 80 nm	bioactive food components delivery systems	[59]
Curcuma longa	CS	Spray-drying	80-120 nm	Antiinflamatory agent	[92]
Eugenol	CS-TPP nanoparticles	Ionic gelation	80-100 nm	Antioxidant for the thermal processing in food packaging	[93]
Lippia sidoides	CS/ cashew gum nanogel	Complex coacervation	335-558 nm	Larvicide	[94]

TPP: tripolyphosphate

2.5. Antioxidants activity in CS as templates for EOS

One of the biggest problems for food preservation is the oxidation of lipids that occurs during handling, thermal treatments and storage of finished foods products. This affects nutritional and sensory properties (changes in taste, smell, texture and loss of vitamins) ultimately shortening shelf life and potentially causing consumer health problems [33].

CS has the potential to prevent or slow some of the oxidation. Indeed, several studies have shown CS may scavenge free radicals through interaction with residual free amino groups, leading to stable macromolecular radicals and ammonium groups [36,95]. This scavenging activity can be increased with the addition of EOs and plant extracts containing monoterpenes, terpenes and polyphenols or other molecules with antioxidant activity [36,96].

The most commonly used assays to measure antioxidant activity are the Folin-Ciocalteau method, DPPH assay (radical 2,2-diphenyl-1-picrylhydrazyl), ABTS assay (2,2′-azino-bis(3-ethylbenzothiazoline-6-sulfonic acid) diammonium salt and FRAP assay (Ferric Ion Reducing Antioxidant Power Assay):

2.5.1. Antioxidant activity assays

Folin-Ciocalteau assay

The Folin-Ciocalteu assay is a simultaneous reaction of HAT (Hydrogen Atoms Transfer reactions) and SET (single electron transfer reactions) and is used to determine and quantify total polyphenol content.

The Folin-Ciocalteu reagent contains a mixture of sodium molybdate and sodium tungstate, which react with the phenolic compounds present in the sample under alkaline conditions. Molybdenum (VI) during the reaction is reduced by the electrons of the phenolic compounds to an oxidation state of 5. This change in the oxidation state produces a change in the colour of the solution, from yellow to blue. The intensity of the blue colour increases with the content of phenolic compounds. The Follin-Ciocalteau assay is measured by spectroscopy at 765 nm and the results are represented by a calibration curve of gallic acid and expressed in gallic acid equivalents [70,97].

$$Na_2WO_4/Na_2MO_4 \rightarrow (phenol - MoW_{11}O_{40})^{4-}$$

$$Mo\ (VI) + e^- \rightarrow Mo\ (V)$$
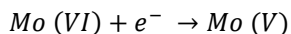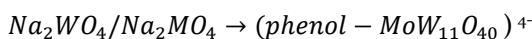
DPPH assay (radical 2,2-diphenyl-1-picrylhydrazyl)

Among antioxidant assays, the most widely used is the DPPH assay (radical 2,2-diphenyl-1-picrylhydrazyl), because of its simplicity, speed and low cost.

The method measures the capacity of a substance to give a hydrogen to the DPPH radical. When the antioxidant substance is exposed to the DPPH in a violet methanol solution, DPPH is reduced resulting in a loss of color (Figure II-10). Absorbance is measured at 517 nm, greater loss of intensity indicates greater antioxidant activity of the substance analysed [51,96,98].
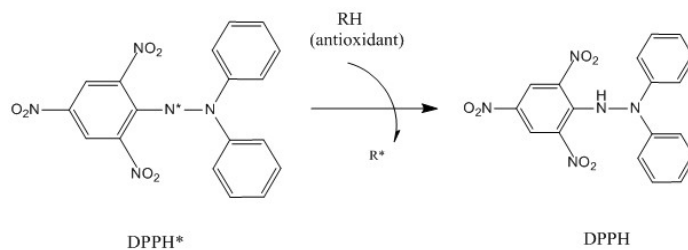
Figure II- 10. The mechanism between the DPPH radical and an antioxidant to generate DPPH.

TEAC (Trolox Equivalent Antioxidant Capacity) or ABTS (2,2′-azino-bis(3-ethylbenzothiazoline-6-sulfonic acid) diammonium salt

The TEAC (Trolox equivalent antioxidant capacity) or ABTS (2,2'-azino-bis(3-ethylbenzothiazoline-6-sulfonic acid) diammonium salt) assays belong to SET reaction and was developed by Miller in 1993 [99] to easily determine the antioxidant capacity. In this method, the Trolox (6-hydroxy-2, 5, 7, 8-tetramethylchroman-2-carboxylic acid) reagent is used as the standard to measure the antioxidant capacity. The assay is based on the reaction of an aqueous solution of ABTS with potassium persulfate solution in the dark for 12-16 h. During that time, the radical ABTS•+ is generated (blue / green chromophore), which has three absorption maxima at the wavelengths of 645, 734 and 815 nm. At this stage, the antioxidant compounds to be tested, are placed in contact with the radical and reduce it to ABTS (Figure II-11), producing a decolouration in the solution and consequently, a decrease in the absorbance measured at a wavelength of 734 nm [37,97].
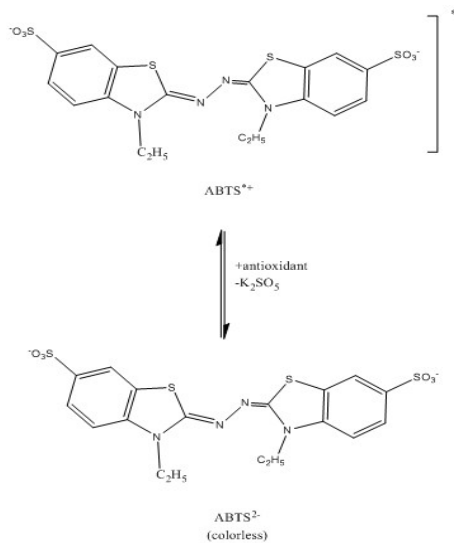
Figure II-11. Structure of radical ABTS•+ before and after the reaction with an antioxidant.

FRAP assay (Ferric Ion Reducing Antioxidant Power Assay)

The FRAP assay belongs to the SET reactions and was developed by Benzi & Strain in 1996 in order to measure the reducing power in plasma samples. This method consists in measuring the reduction of the 2,4,6-tripyridyls-triazine complex (TPTZ) to the ferrous complex by the action of an antioxidant compound in an acidic environment (Figure II-12). This reaction produces a variation in color which is measured at a wavelength of 593-595 nm. The results are represented by a calibration curve using Trolox reagent as standard and are expressed in Trolox equivalents (μmol Trolox / g or μmol Trolox / L) [86,97].
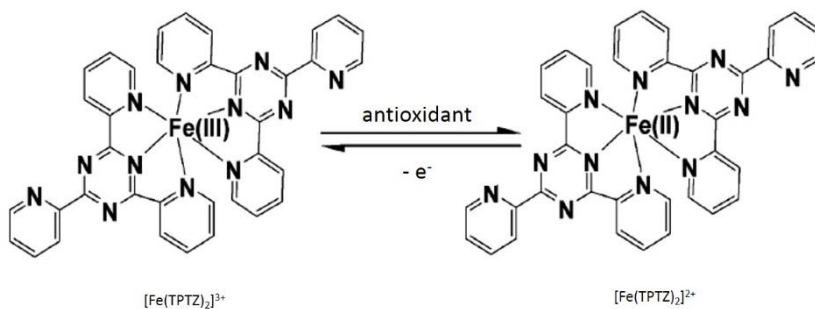
Figure II-12. Reaction mechanism of FRAP assay.

The Table II-3 summarises the antioxidant assays involving CS as templates of essential oil and their applications.

Table II-3. Antioxidant assay and CS as templates of essential oils and their applications.

Essential oil or extract	Template	Antioxidant assay	Application	Reference
Helianthus annuus	Pickering emulsion CS-stearic acid nanogel	TBARS	Food manufacturers	[80]
Mentha piperita and *Camellia sinensis*	CS nanoparticles: encapsulation	DPPH	Nutraceuticals, cosmetic and pharmaceutica	[88]
Zingiber officinale	Gelatin/CS films	ABTS	Food packaging	[100]
Lippia origanoide	Nanogel emulsion CS-p-coumaric acid: encapsulation	DPPH ABTS	Antioxidant	[101]
Lepidium sativum	CS film	DPPH FRAP	Food active-packaging	[102]

		Folin-Ciocalteu		
Zataria multiflora	CS coating	TBARS	Food packaging (Beef steaks)	[38]
Brassica napus oil *α-tocopherol/cinnamaldehyde* *α-tocopherol/Allium sativum* *α-tocopherol/cinnamaldehyde* *Allium sativum oil*	Gelatin-CS based films that incorporate nanoemulsions	DPPH ABTS FRAP	Food packaging	[86]
Prunus armeniaca	CS-N-methyl-2-pyrrolidone nanoparticles films	DPPH	Bread	[28]
Apple peel polyphenols	CS film	DPPH ABTS	Food packaging	[103]
Rosmarinus officinalis	CS-benzoic acid nanogel encpaulation	DPPH	Beef cutlets during storage	[34]
Carum copticum	CS film reinforced with cellulose nanofibers or lignocellulose nanofibers	DPPH	Active packaging	[51]
Coriandrum sativum L.	Microencapsulated CS	DPPH	Packaging technology in the food industry	[43]
Satureja hortensis L.	CS nanoparticles	DPPH	Packaging	[44]

		DPPH		
Eucalyptus globulus	CS film	Folin-Ciocalteu NO H$_2$O$_2$	Packaging	[70]
Carum carvi	CS film	DPPH	Active packaging	[104]
Green Camellia sinensis	CS coating	Folin-Ciocalteu	Fresh walnut kernel	[40]
Cinnamomum verum	CS-oleic acid film	ABTS	Strawberry	[37]
Thymus serpyllum L.	CS microbeads	Folin-Ciocalteu	Food applications	[105]
Pimenta dioica	Microencapsulated CS/k-carrageenan	DPPH	Meat	[21]
Zataria multiflora Boiss and *grape seed extract*	CS film	DPPH Folin-Ciocalteu	Food packaging	[106]
Green Camellia sinensis	CS film	DPPH Folin-Ciocalteu	Active packaging	[95]

DPPH assay: radical 2,2-diphenyl-1-picrylhydrazyl; ABTS assay: 2,2'-azino-bis(3-ethylbenzothiazoline-6-sulfonic acid) diammonium salt; FRAP assay: Ferric Ion Reducing Antioxidant Power Assay; NO: nitric oxide radical scavenging activity; H$_2$O$_2$: Hydrogen peroxide radical scavenging.

2.5.2. *Antioxidant properties of CS-EOs coating and films*

Many researchers have studied how different essential oils in films or coating influences antioxidant activity, and how this relates to the quality of the food and its preservation.

Hromiš et al. [104] used caraway seed oil and beeswax with CS as packaging films. Using the DPPH assay, they measured the antioxidant activity of the films after 2.5, 4 and 24 h. The results showed that the antioxidant activity of the CS (around 29% after 24 h) significantly increased when the oil was added (80% after 24 h). Jahed et al. [107] also used as *Carum copticum* seed essential oil and CS to make bionanocomposites for food preservation. To elaborate the bionanocomposite CS films, they reinforced *Carum copticum* oil (CCO) with lignocellulosenanofibers (LCNF) or cellulose nanofibers (CNF). The highest value of antioxidant activity was observed in the CS films with 5% (w / w) of CCO with a value around 37% using the DPPH assay. This is due to the high content of carvacrol and ϒ-terpinene in the oil. The polymers used to reinforce the bionanocomposites also had an effect, those with LCNF showing greater antioxidant activity than those with CNF, reducing DPPH intensity 27% and 23%, respectively. Priyadarshi et al. [28] developed CS films with apricot kernel oil at different concentrations for active food packaging. Apricot kernels contain high percentages of oleic acid and in N-methyl-2-pyrrolidone with antioxidant activities. Increasing the concentration of apricot kernel oil in the film increased antioxidant activity as evaluated by DPPH. Pure CS films showed 21.8% DPPH scavenging activity and with the AKEO ratios of 0.125:1 (with respect to CS), increased DPPH from 25.9% to 35.3%.

Similar results were obtained by Moradi et al. [38] when adding *Zataria multiflora Boiss* oil in CS films, reaching around 38 % DPPH scavenging activity with a ratio of 1:0.5 (CS:oil). *Zataria multiflora* oil (ZEO) was also used together with hydroalcoholic extract of sumac (SE) in edible CS coating in modified-atmosphere packaged of beef

meat during 20 days of storage. This kind of substrate contains a high protein and lipid contents, for this reason, oxidation was measured using thiobarbituric acid reactive substances (TBARS) at 532 nm. The TBARS assay measures the concentration of the compounds that give off an unpleasant odour or taste resulting from lipid oxidation. Films with CS-SE showed a value of TBARS of 1.77 mg malonaldehyde / kg meat after 20 days of storage and it was observed that when adding the ZEO oil this value was decreased to 1.56 mg malonaldehyde / kg meat. The addition of the EO increases antioxidant activity of the film and aides in the preservation of bovine meat [38].

Perdones et al. [37] used the ABTS (TEAC) assay to evaluate the antioxidant activity of CS films with cinnamon leaf essential oil and oleic acid. Their conclusions mirrored that of other studies, showing that the adding the essential oil decreases the TEAC values, indicating high antioxidant activity.

DPPH, Folin-Ciocalteu and FRAP assays were used by Kadam & Lele et al. [102] to study antioxidant activity in CS films with *Lepidium sativum* seedcake phenolic extract, intended for use as active-packaging. Extracts were extracted in water and in 50% and 95% ethanol. In both DPPH and FRAP assays, antioxidant activity was higher with water extracts. Furthermore, increasing the concentration of the oil also increased the antioxidant activity. These results followed polyphenol content as determined by the Folin-Ciocalteu method, with the most found in the water extract, followed by the 50% ethanol and 95% ethanol extracts.

Despite using different EOs in the films and coatings, and the use of variety methods to evaluate antioxidant activity, the studies

unanimously showed that EOs provide supplemental antioxidant properties and that increasing their concentration results in higher antioxidant activity.

2.5.3. *Antioxidant properties of CS-EOs emulsions and (nano)gels*

Antioxidant and antimicrobial activity of *Rosmarinus officinalis (RO)* essential oil encapsulated in CS-benzoic acid (CS-BA) nanogels on beef cutlets were studied by Hadian et al. [46]. DPPH radical scavenging activity assay was used to dermine the antioxidant activity of free RO essential oil, CS-BA nanogel and CS-BA nanogel-encapsulated essential oils. Results showed that at the beginning of the experiment, free RO had higher radical-scavenging activity, but over time, its effect stabilized. On the other hand, CS-BA nanogel demonstrated an increase in the radical-scavenging activity until 100 h, and CS-BA nanogel-encapsulated essential oil showed the best DPPH radical scavenging ability, with an 85% decrease in intensity.

Similar results were reported by Damasceno et al. [101], who studied the antioxidant activity of *Lippia origanoides* oil encapsulated in a nanogel made with p-coumaric acid and CS using DPPH and ABTS assays. In both assays the CS modified with p-coumaric acid had increased antioxidant activity as compared to pure CS. However, the addition of EOs further increased antioxidant activity, possibly due to compounds such as thymol and carvacrol that are H+ donors.

Pérez-Córdoba et al. [86] developed gelatin-CS films loaded with oil/water emulsions, employing canola oil, α-tocopherol/cinnamaldehyde; α-tocopherol/garlic oil; or α-

tocopherol/cinnamaldehyde and garlic oil. The film loaded with nanoemulsion encapsulatin α-tocopherol/ cinnamaldehyde showed the highest antioxidant acitivity, as measured by DPPH and ABTS assays. Using the FRAP assay, however the material with α - tocopherol/garlic oil obtained greatest antioxidant activity with an increase from 51% to 91% when compared with control. This increase was probably due to the fact that during the reaction the FRAP reagent is in direct contact with the film samples.

2.5.4. Antioxidant properties of chitin or CS-EOs encapsulations

CS can be used, to directly encapsulate EOs and several studies have looked into resulting antioxidant activity. The most commonly used method to study antioxidant capacity for CS-encapsulated EOs is the DPPH assay.

Shetta et al. [88] researched the encapsulation of peppermint (PO) and green tea oil (GTO) in CS-TPP (tripolyphosphate nanoparticles) with the emulsification-ionic gelation technique for food and pharmaceutical applications. DPPH assay was used to analyse the antioxidant capacity of the encapsulation. The results of the antioxidant activity were assessed using the IC_{50} (concentration required to scavenge DPPH radicals by 50%) of each composite. CS-TPP showed relatively high values (116.07 mg $\cdot$ mL^{-1}) perhaps due TPP masking CS amino groups, which are the groups that react with DPPH. The highest values of antioxidant activity were observed in the encapsulations containing GTO and PO with with IC_{50} values attained at 0.34 mg $\cdot$ mL^{-1} and 1.61 mg $\cdot$ mL^{-1}, respectively. Of the two oils, the one with the highest antioxidant activity was GTO, possibly

due to the greater amount of phenolic compounds it contains. These results agree with those obtained by Dima et al. [56]. These authors, showed how the encapsulation of pimento (*Pimenta dioica L. Merr*) oil with CS / k-carrageen, using the complex coacervation method, shows greater antioxidant activity than pure CS and K-carrageen. This is because this EO contains a high percentage of eugenol and methyl eugenol. In addition, they observed that the CS-EO encapsulation had greater antioxidant activity than k-carrageen-EO, most probably from the synergy of CS and the EO [56]. Moreover, Duman et al. [21], observed that coriander oil (*Coriandrum sativum L.*) encapsulated by spray drying method CS showed high DPPH antioxidant activity value of 60%. They also observed that the antioxidant activity of CS was dependant on factors such as molecular weight and degree of acetylation.

Despite the method of encapsulation used, all results show that by adding essential oil, antioxidant activity increases. On the one hand, it is due to their capacity to donate hydrogen atoms and to capture the free radicals that increase the antioxidant activity. On the other hand, the encapsulation shell helps to protect the bioactive compounds from factors such as humidity, pH, temperature and pressure among others, making them be slowly released and thus prolonging effects.

2.6. Antibacterial activity in CS as templates for EOS

One of the most important causes of food spoilage is the growth of microorganisms and pathogens [108]. These can accelerate the lipid

oxidation, resulting in changes in the organoleptic properties, creating toxicity or and potential pathogenicity in humans [109]. To combat these problems and extend food shelf life, several studies have shown the high potential of natural compounds such as CS and EOs [80,103,110].

CS is usually used as food preservative due to its antimicrobial activity against a wide range of yeast, bacteria and fungi, its biocompatibility and low toxicity [21,78,111]. The mechanism of CS antimicrobial activity of CS is not yet known, however there are several different hypotheses. One of these hypotheses is that cell permeability changes due to the interaction between the negative charges of the cell membrane and the positive charges of the CS groups. Another hypothesis is that the activity is the result of the interaction of the microorganism's DNA with diffuse hydrolysis products that inhibit the synthesis of proteins, RNA and essential nutrients [112].

As for EOs, antimicrobial activity can be explained by the presence of bioactive phytochemicals such as phenols. The mechanism of action of these molecules are numerous. Some phenolic compounds can penetrate the cell membrane and disable its functional and lipophilic properties. These compounds can also alter the permeability of the cell, interfere with the cellular energy generation system (ATP), damage the cytoplasmic membranes and induce cell death upon adhesion to specific receptors [113,114].

Microbes are extremely diverse unicellular organisms including viruses, fungi and bacteria. There are two types of bacteria: Gram-

positive and Gram-negative, as determined by the structure of their membranes [113].

Several researchers believe that EOs are more susceptible to inhibit the growth of Gram-positive bacteria because their lipophilic nature interacts easily with Gram+ cellular membranes. EOs can separate the lipids from the cell membrane of the bacteria and in doing so make the cell more permeable. According to these studies, Gram-negative bacteria are globally less susceptible to the effects of EOs because of their hydrophilic cell walls [112–114]. Table II-4 shows a map of the different CS-templates of EOs against different microorganisms.

Table II-4. Summary of the different microorganisms used to assess the antimicrobial activity of CS-templates of essential oils.

EOS	Template	Microorganism	Application	Ref
Mentha piperita Camellia sinensis	CS nanoparticles encapsulation	*Staphylococcus aureus Escherichia coli*	Nutraceutical, cosmetic and Pharmaceutical	[88]
Syzygium aromaticum	CS-tripolyphosphate nanoparticles encapsulation	*Aspergillus niger*	Agriculture and food industries	[91]
Prunus armeniaca	CS-N-methyl-2-pyrrolidone nanoparticles films	*Bacillus subtilis Escherichia coli*	Bread	[28]
Zataria multiflora **Boiss**	CS coating	*Enterobacteriaceae*	Beef steaks preserved	[38]

		Pseudomonas spp	by modified atmosphere packaged	
Apple peel polyphenols	CS film	*Bacillus cereus* *Escherichia coli* *Salmonella typhimurium* *Staphylococcus aureus*	Food packaging	[103]
Brassica napus oil **α-tocopherol/cinna maldehyde** **α-tocopherol/***Alliu m sativum* **α-tocopherol/cinna maldehyde** **Allium sativum oil**	Gelatin-CS based films that incorporate nanoemulsions	*Pseudomonas aeruginosa* *Listeria monocytogen*	Food packaging	[86]
Rosmarinus officinalis	CS-benzoic acid nanogel encpaulation	*Salmonella typhimurium*	Beef cutlets during storage	[34]
Carum copticum	CS film reinforced with cellulose nanofibers or lignocellulose nanofibers	*Escherichia coli* *B Botrytis cereus*	Active packaging	[51]
Cinnamon verum **Cumbopogon citrates** **Origanum vulgare**	CS film	*Botrytis sp.* *Pilidiella granati* *Penicillium sp*	Food	[74]

Cinnamon verum *Zingiber officinale*	CS-carboxymethyl cellulose films	*Aspergillus niger*	Food packaging	[35]
Zea mays	CS-gelatin films with nano chitin	*Aspergillus niger*	Food packaging	[42]
Myrcia ovata **Cambessedes**	CS coatings	*Pseudomonas aeruginosa Staphylococcus aureus Bacillus cereus Bacillus subtilis Enterococcus faecalis Serratia marcescens Escherichia coli Salmonella enteritidis*	Mangaba fruits	[115]
Coriandrum sativum L.	Microencapsulated CS	*Aeromonas hydrophila Escherichia coli Klebsiella pneumonia Pseudomonas aeruginosa Salmonella typhimurium Yersinia enterocolitica Bacillus cereus Listeriamonocytogenes Candida albicans*	Packaging technology in the food industry	[43]

Satureja hortensis L.	CS nanoparticles	*Escherichia coli Staphylococcus. aureus Listeria monocytogenes*	Packaging	[44]
Eucalyptus globulus	CS film	*Staphylococcus aureus Escherichia coli Pseudomona aeruginosa Klebsiella pneumonia*	Food packaging	[70]
Ziziphora clinopodioides	CS-gelatin film	*Pseudomonas spp. Listeria monocytogenes Shewanella putrefaciens*	Packaging minced rainbow trout	[116]
Lavandula angustifolia red Thymus vulgaris	CS beads	*Botrytis cinerea*	Strawberry	[110]
Origanum vulgare	CS solution	*Listeria. monocytogenes*	Modified atmosphere packaged pork	[117]
Zataria multiflora Cinnamomum zeylanicum	CS coating	*Phytophthora drechsleri*	Cucumber fruit rot	[118]

Thyme vulgaris **Ocimum basilicum**	CS- oleic acid film-forming emulsion	*Aspergillus niger* *Botrytis cinerea* *Rhizopus stolonifer*	Food	[69]
Carum carvi	CS film	*Staphylococcus aureus* *Escherichia coli*	Active packaging	[104]
Carvacrol **Citrus aurantium ssp.** **Citrus reticulata** **Citrusx limon L.**	CS coating containing nanoemulsion	*Escherichia coli* *Salmonella typhimurium*	Green beans	[119]
Thyme vulgaris	CS-benzoic acid nanogel encapsulation	*Aspergillus flavus*	Grape	[78]
Cuminum cyminum	CS-caffeic acid nanogel - encapsulation	*Aspergillus flavus*	Food packaging	[85]
Mentha piperita	CS-cinnamic acid nanogel	*Aspergillus flavus*	Food	[84]
Citrus Limonum **Thymus vulgaris** **Cinnamomum zeylanicum**	CS film	*Escherichia coli* *Staphylococcus aureus*	Active food packaging	[61]
Origanum vulgare	Skin gelatin-CS film	*Escherichia coli* *Staphylococcus aureus* *Bacillus subtilis* *Salmonella enteritidis* *Shiga bacillus*	Food packaging	[120]

Thymus moroderi ***Thymus piperella***	CS edible films	*Listeria innocua* *Serratia marcenscens* *Aeromonas hydrophila* *Achromobacter denitrificans* *Alcaligenes faecalis*	Food	[36]

2.6.1. *Antimicrobial activity of CS-EOs coating and films*

One of the most studied fungi in food is *Aspergillus niger,* that commonly occurs on vegetables. CS has been shown a good antimicrobial activity when used in biomaterials [121], and as such CS-EOs coatings can be thought to show antimicrobial activity. Perdones et al. [37]studied the antifungal effect of CS-films with the addition of basil or thyme oil against *Aspergillus niger*, *Botrytis cinerea* and *Rhizopus stolonifer*. The experiments showed no effect on the inhibition of fungal growth. These same results were obtained by Sahraee et al. [42], who studied the antifungal effect of *A. niger* in gelatin-based nanocomposite films with corn oil: the nanocomposites had no antifungal effect. In these cases, the absence of observed antimicrobial activity may be due to the oil covering the active amino groups that interact with the anionic groups on the surface of the cell, impeding activity and effect on microorganism growth.

However, the lack of antifungal effect is not systematic. Noshirvani et al. [35] used CS-carboxymethyl cellulose films

40

emulsified with oleic acid and with cinnamon or ginger essential oil, which resulted in antifungal activity against *A. niger*. In this case, increasing the concentration of EOs resulted in decreased fungal growth. Comparing the two EOs, it was shown that cinnamon oil has higher antifungal effects. The results reflect a synergistic effect between the oils and the fatty acid, and to the shortening of the chains in the CS fraction.

Other authors such as Priyadarshi et al. [28] studied the effect of CS- (N-methyl-2-pyrrolidone) films with apricot kernel oil (*Prunus armeniaca*) against *Bacillus subtilis* (Gram-positive) and *Escherichia coli* (Gram-negative). Decrease of bacterial growth in both bacteria could be observed on addition of the EOs. Furthermore, it was shown that N-methyl-2-pyrrolidone, which is a known antimicrobial, improved microbial inhibition when included with the oil. N-methyl-2-pyrrolidone help to dissolves the lipids of the cell membrane, provoking its disintegration and, consequently, cell death.

The antimicrobial activities effects of CS-EOs coatings have been the subject of several recent studies. Mojaddar et al. [38] analysed the antimicrobial effect of *Zataria multiflora Boiss* oil and sumac hydroalcoholic extract in CS coatings for beef steaks stored over 20 days. The microorganisms studied were *Pseudomonas spp.*, Lactic acid bacteria, *Enterobacteriaceae* and yeasts: for all less microbial growth was observed with higher concentration of EOs and the extract. In addition, it was demonstrated that the antimicrobial effect was greater when using EOs and extracts together. This synergistic effect was also found by Kakaei et al. [116], with ethanolic red grape see extract and *Ziziphora clinopodioides* oil in a CS-gelatin film

inhibiting *Listeria monocytogenes* growth in minced trout fillet. The synergistic effect between the extracts and EOs is explained by the combination of different mechanisms such as the inhibition of protective enzymes and concurrent alteration of cell walls.

2.6.2. Antimicrobial activity of CS-EOs emulsions and (nano)gels

Hadian et al. [46] studied how to preserve beef cutlets against *Salmonella tryphimurium* during 12 days in refrigeration. *Rosmarinus officinalis* essential oil (REO) was encapsulated in a CS-benzoic acid nanogel. Meat was inoculated by 10^9 CFU *S. typhimurium* / mL, then sprayed with free REO and nanoencapsulated REO. The results showed encapsulation resulted in a greater inhibitory effect as measured by minimum inhibitory concentration (MIC) and minimum bactericidal concentration (MBC). This was explained by the greater accessible surface area of CS particles interacting with the cell wall. In addition, it was also observed that on day 1 of refrigeration, the nanoencapsulation with the highest concentration (2 mg nanoencapsulated REOs / g beef) showed a large decrease in the population of *S. typhimurium* (3.3 log CFU / g) and after 12 days of refrigeration, reduction was maximum with a value of 2.5 log CFU / g.

Severino et al. [119] also evaluated the inhibition of the growth of *S. typhimurium* and *Escherichia coli* in green beans. The antimicrobial effect of modified CS coatings containing nanoemulsions of essential oils (carvacrol, bergmot, lemon and mandarin oil), gamma irradiation treatment, and modified atmosphere packaging (MAP), were examined alone or in combination. Carvacrol showed the highest

antimicrobial inhibition on both microbes, so it was used in the other experiments. In the next step, the behaviour of *E. coli and S. typhimurium* was evaluated against gamma irradiation. In the experiments a synergic effect was observed with the coating under MAP, which increased the radiosensitivity in *E. coli and S. typhimurium* of 1.80-fold and 1.89-fold, respectively. The combination of CS-coating with carvacrol, gamma irradiation treatment and MAP caused the greatest decrease in the population of *E.coli and S.typhimurium* after 7 days of storage.

One of the fungi that most proliferates in food systems is *Aspergillus flavus* and is believed to be the cause of infections in the corneas [78]. These authors studied the antimicrobial activity of thyme oil encapsulated in CS-benzoic acid nanogel against *A. flavus* on grapes during 1 month of storage. In vitro, sealed and unsealed experiments were performed. In the sealed experiments, the MIC of the free oils was 400 mg / L and 300 mg / L for encapsulated oils. In the unsealed experiment, the MICs were much higher. The free oils did not achieve complete inhibition, not even at 1000 mg / L, for the encapsulate MIC was 500 mg / L. This explained by the volatility of the compounds present in EOs. In *in vivo* analysis, *A. flavus* by was inhibited by encapsulates at a concentration around 700 mg / L. Similar results were obtained in the work of Zhaveh et al. [85], *Cuminum cyminum* oil encapsulated in CS-caffeic acid nanogel antimicrobial activity was measured against *A. flavus*. Free oil in unsealed flasks failed to prevent the growth of the fungus, even using a concentration of 1000 mg / L. Under the same conditions, the encapsulates succeeded in inhibiting the growth of *A. flavus* at 950 mg / L, which was much higher than under sealed conditions (350 mg /

L). Encapsulation of the oil in CS-caffeic acid nanogel is nevertheless the best option, with slower evaporation of the oil slow and delayed release of the EO into the medium.

2.6.3. Antimicrobial activity of CS-EOs encapsulations

The application of Crayfish CS microencapsulated with coriander (*Coriandrum sativum L.*) essential oil for its antioxidant properties and antimicrobial activity against *Aeromonas hydrophila, Escherichia coli, Kleb-siella pneumoniae, Pseudomonas aeruginosa, Salmonella typhimurium, Yersinia enterocolitica, Bacillus cereus, Listeria monocytogenes and Candida albicans* was reported by Duman et al. [21]. Although numerous authors have demonstrated the antimicrobial activity of coriander oil [122,123], in this work the authors did not observe any antimicrobial effect. In addition, the effect against microorganisms was greater with the pure crayfish CS than with the microcapsules of CS-coriander oil. This result could be because the microcapsules are covered with an oil without antimicrobial effect and which effectively prevents CS from having an effect.

In the work of Shetta et al. [88] the encapsulation of peppermint (PO) and Green tea (GTO) oils in CS nanoparticles was compared and the antimicrobial activity against *Staphylococcus aureus* (Gram-positive) and *Escherichia coli* (Gram-negative) was studied. Antimicrobial activity was observed for both encapsulated oils, although lower against *E. coli* than against *S. aureus*. MBC values of pure EOs were greater than encapsulated oils against *S. aureus*. This could be because the walls of the Gram-positive bacteria are

hydrophilic while the molecules of the EOs are hydrophobic. Therefore, by encapsulating the EOs in CS-nanoparticles that contain hydrophilic compounds, they can penetrate the bacteria. In the Gram-negative bacteria, the antimicrobial activity depends on the interaction of the lipophilic oil with the bacterial membrane of phospholipids generating a passive permeability of the oil.

CS-nanoparticle encapsulation improved the antifungal activity of clove oil against *Aspergillus niger* [124]. This could be because the encapsulation helps the oil compounds to not evaporate and results in a better inhibitory effect. In 2015, Zhaveh et al. [85] obtained the nearly conclusions. In addition, they found that the organoleptic alterations that the oils can cause are reduced by means of the encapsulation.

3. Conclusion and future perspectives

This chapter compiles information related to the antimicrobial and antioxidant activity of CS-templates namely films, coatings, nanocapsules, nanogels and emulsions of EOs. A special emphasis was addressed to CS active films with *Cinnamon verum, Zingiber officinale, Thymus moroderi and Thymus piperella*; CS-based coatings with *Zataria multiflora, Corum copticum* and *Camelia sinensis;* and emulsions with *Zea mays*. The final bioactive properties of these materials show the potential of CS-EOs materials for different applications in particular in food industry as well as in medicine, agriculture and cosmetics.

Future research should focus on the application of the different CS-templates of EOs for different food matrices and the cytotoxicity of the EOs and final materials.

PART III: GENERAL METHODOLOGY
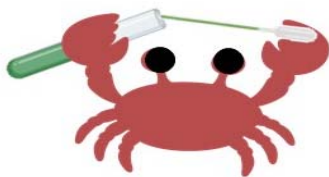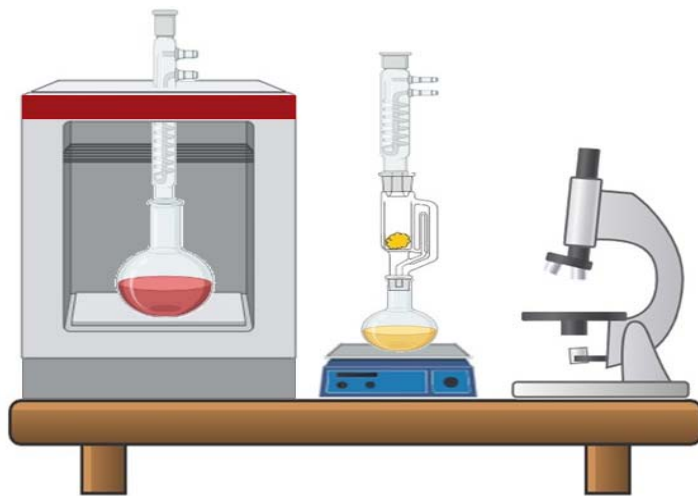
Part III: General methodology

1. Extraction/isolation of raw materials

1.1. Chitin and chitosan extraction

Spider crab (*Maja squinado, Figure III-1*) (see Chapter 3) and lobster (*Homarus gammarus, Figure III-2*) (see Chapter 4) shells waste were provided by a local restaurant - San Sebastian (Spain), and were used to obtain chitosan as previously described by Salaberria et al. [125] with slight modifications. First, chitin was extracted in three steps: The first step was deproteinisation with 1M NaOH, in the second step calcium carbonate was

Figure III-1. Spider crab (Maja squinado).

removed by 1M HCl and in the last step lipids and pigments were removed by acetone following the procedure described by Salaberria et al. [19]. Afterwards, it was dried at 106 °C overnight and grinded. The chitin obtained was then deacetylated to produce chitosan. For this purpose, the chitin powder was treated with a NaOH solution (60

Figure III-2. Lobster (Homarus gammarus).

% w/v) using a CH:NaOH ratio of 1:15 w/v at 130 °C in an oil bath for 4 h under N_2 atmosphere. The CS obtained was filtered and washed. Finally, it was dried in an oven at 106 °C overnight. The degree of N-acetylation was determined by ^{13}C-NMR (equation III-1 in section 2.1.2) and was of 10.00 % for spider crab and of 13.29 % for lobster.

1.2. Nanochitin extraction via Microwave-assisted extraction technique (MAE)

The isolation of nanochitin from yellow lobster (*Cervimunida johni,* Figure III-3), shrimp (*Parapenaeus longirostris,* Figure III-3) and squid pen (*Loligo vulgaris,* Figure III-3) (see Chapter 1) was carried out using the MAE technique. Each chitin powder sample
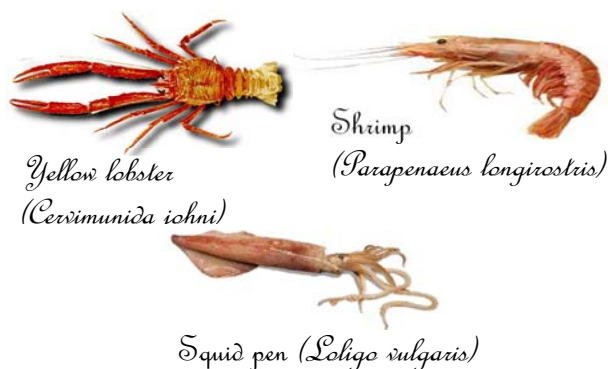
Figure III-3. Yellow lobster (Cervimunida johni), shrimp (Parapenaeus longirostris) and squid pen (Loligo vulgaris).

(1 g) was hydrolysed under vigorous shaking by MAE (Discover system, CEM, USA) (Figure III-4-a). The reaction conditions were adapted from the previously reported protocol Salaberria et al. [19] using a varying HCl concentration from 1 to 3 M with a CH:HCl ratio of 1:30 w/v. MAE conditions employed for time between 10 and 30 min and for power between 50 and 300 W. After isolation, each reaction mixture was stopped by dilution with ice bath and washed twice by filtration. Finally, the reaction mixtures were dialysed with distilled water (regenerated cellulose dialysis tube: MWCO 12-14 kDa) until the pH of the surrounding bath was stable (pH 5). The samples were then stored in the refrigerator at 4 °C until analysis. Three different nanochitin samples were obtained: (i) α-nanochitin from lobster (α-

NCH$_L$), (ii) α-nanochitin from shrimp (α-NCH$_S$), and (iii) β-nanochitin from squid feather (β-NCH$_{Sp}$).
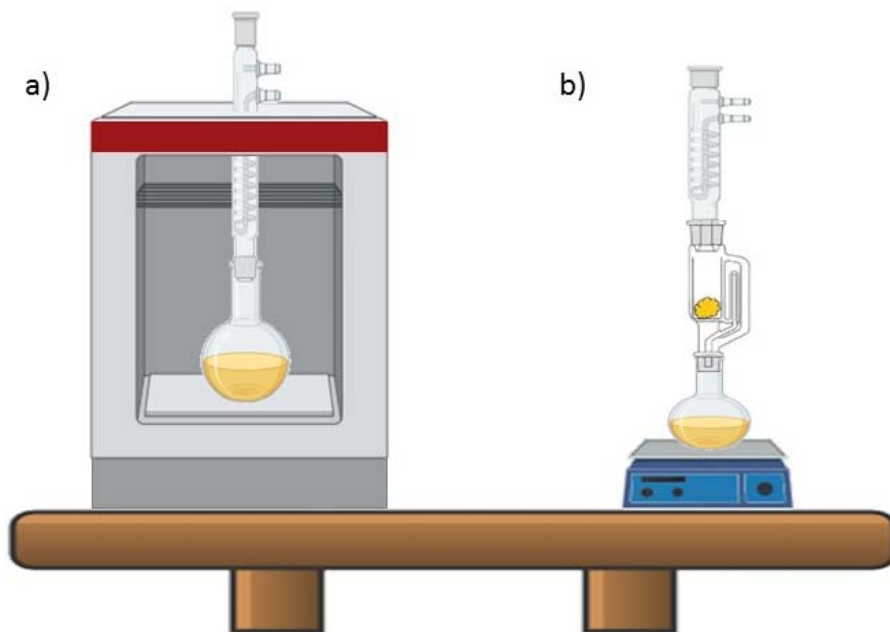
Figure III-4. a) Microwave-assisted extraction technique and b) Soxhlet extraction technique.

1.3. *Curcuma longa* L. extraction via Microwave-assisted extraction technique (MAE)

The MAE technique was used to extract *Curcuma longa* L. oil (Figure III-5) (see Chapter 2) employing an open vessel equipped with a condenser and heated by microwave (Milestone flexiWAVE, Japan), as shown in Figure III-4-a. For the

Figure III-5. Curcuma root (*Curcuma longa L.*).

extraction, the root of *Curcuma longa* L. was first obtained from a local market in Bizkaia, Spain. The root was cleaned with water to

remove possible impurities and dried in an oven at 50.00 ± 0.05 °C. It was then ground (Retsch SM 2000, Haan, Germany) and sieved with a 0.5 x 0.5 mm mesh. The extraction conditions of the experimental design were performed using a range of 1:20-1:5 g/mL (*Curcuma longa* L.:EtOH), power of 150-250 W and a time between 10-30 min. After the extractions, the solvent was removed with a rotary vacuum evaporator at 50ºC. The extraction yield was determined gravimetrically and the optimum point experiment was performed in triplicate.

1.4. *Curcuma longa* L. extraction using Soxhlet approach

Soxhlet extraction (conventional method) (Figure III-4-b) was performed to obtain *Curcuma longa* L. oil (see Chapter 2) following the method of Priyanka et al. [126] with slight modifications. Curcuma root (*Curcuma longa* L.) from India was purchased from a local market in Bizkaia, Spain. For cleaning of impurities, the root was washed in water and dried at 50.00 ± 0.05 °C. The root was then ground with a cutting mill (Retsch SM 2000, Haan, Germany) and sieved (0.5 × 0.5 mm mesh). 5 g of *Curcuma longa* L. powder in 150 mL EtOH at boiling temperature (78 °C) for 6 h was used for the extraction. After that time, the solvent was removed by rotary evaporation at 50 °C until a constant weight was obtained to calculate the extraction yield gravimetrically. Soxhlet extraction was performed in triplicate.

1.5.   Anthocyanin extraction

Anthocyanin was extracted from red cabbage (Brassica oleracea var. capitata f. rubra, Figure III-6) purchased at a market in Gipuzkoa, Spain (see Chapter 4). Red cabbage was washed with distilled water, dried at 50.00 ± 0.05 °C and ground (Retsch SM 2000, Germany). It was then sieved using a 0.5 x 0.5 mm mesh. For extraction, 25 g of powder was used in 500 mL of acidified ethanol (85:15 v/v, EtOH:HCl (1M)) with stirring at 50 °C in the dark

Figure III-6. Red cabbage (Brassica oleracea var. capitata f. rubra).

overnight following the protocol described by Li Y. et al. [127] with slight modifications. Finally, it was filtered and rotavaporated at 45 °C to remove the solvent. The obtained extract was stored in the dark at 4 °C until use.

2. General characterization
2.1.   Chemical and physical structure characterization
2.1.1. Attenuated Total Reflection-Fourier Transform Infrared Radiation (ATR-FTIR)

The ATR-FTIR spectra of samples were determined using a Spectrum Two FTIR spectrometer with a universal attenuated total reflectance accessory (Perkin Elmer Inc., Waltham, MA, USA). The spectra were acquired in a transmittance range of 600 to 4000 cm^{-1} with 64 scans and 4 cm^{-1} resolution.

2.1.2. ^{13}C nuclear magnetic resonance (^{13}C-NMR)

The ^{13}C-NMR spectra of the chitin, nanochitin and chitosan solid samples were obtained with a Bruker Advance III 400WBplus (MHZ) spectrometer (Bruker, USA). The degree of N-acetylation (DA %) was estimated following the method described by Kasaai et al. [128] using the following equation:

$$DA\% = \left[\frac{I_{CH_3}}{\frac{I_{C1}+I_{C2}+I_{C3}+I_{C4}+I_{C5}+I_{C6}}{6}}\right] x \ 100 \qquad (III\text{-}1)$$

where I_{CH_3} indicates the integral of the methyl carbon (CH3) and I_{C_1} to I_{C6} represent the integrals of the carbons of the D-glucopyranosyl ring from C1 to C6.

2.1.3. The X-ray diffraction (XRD)

The XRD spectra of the chitin, nanochitin and chitosan samples were measured by a Philip X'pert Pro diffractometer (Phillips N.V., Amsterdam, The Netherlands) employing Cu-Kα radiation and operating at 40 mA and 40 kV. The angular range of data collection was from 5 to 70° 2θ at room temperature.

The crystallinity index (CI %) of the samples was calculated according to the equation [129]:

$$CI\% = \left[\frac{I_{110}-I_{am}}{I_{110}}\right] x \ 100 \qquad (III\text{-}2)$$

where I_{110} corresponds to the plane 110 which is the plane of maximum intensity and Iam represents the amorphous diffraction which usually appears around 2θ = 12.5°-13.5°.

2.2. Morphology
2.2.1. Atomic force microscopy (AFM)

The AFM technique was used to analyse the morphology and size of the isolated nanochitins. To prepare the samples for analysis, the samples were dispersed in distilled water and subjected to an ultrasonic bath for 5 minutes. Then, a drop of the suspension was placed on a mica dish and a spin coating equipment (Specialty coating systems INC, Spin Coater model P6700 series) was used to remove the water at 2000 rpm for 3 minutes. The AFM images were captured using a Dimension 3100 NanoScope IV (Veeco, USA) at room temperature. The mode used was tapping with a silicon nitride cantilever with a tip radius of 10 nm and a frequency of 1 KHz. For each sample, 10 measurements were taken in random areas and average length and width values were calculated with NanoScope Analysis 1.9 software.

2.3. Thermal properties

Thermogravimetric analysis (TGA) analyses of native chitin, nanochitin samples and nanocomposite films were performed on TGA/SDT 851 Mettler Toledo instrument (Mettler Toledo, New Castle, USA). Approximately 6 mg of each sample was heated from 25 to 800 °C with a temperature ramp of 10 °C/min in nitrogen atmosphere (20 mL/min).

2.4. Gas chromatography and mass spectrometry (GC/MS)

The chemical composition of the essential oils (see Chapter 2 and 5) was characterised by GC/MS technique (GC 7890A, MS 5975C, Agilent, Santa Clara, CA, USA). For this purpose, 0.01 g of essential oil was dissolved in 1 mL of ethyl acetate. The capillary column used for the analysis was HP-5MS (5%-phenyl)-methylpolysiloxane, 30 m × 0.25 mm). The conditions applied were: helium was the carrier gas with a flow rate of 0.7 mL/min; the method used was split/splitless with the split mode (10:1) with an injector temperature of 280 °C. The temperature ramp was started at 50 °C and increased to 120 °C with 10 °C/min increments. At this temperature it was maintained for 5 minutes. In the next stage, the temperature was raised to 280 °C increasing at 10 °C/min and maintained for 8 minutes. In the final step, the temperature was raised to 300 °C with increments of 10 °C/min and kept constant for 2 minutes. The identification of the compounds in the essential oil was carried out with the National Institute of Standards (NIST) Library.

2.5. Total phenolic content (TPC)

The total phenolic content test of the nanocomposite films and *Curcuma longa* L. oil was carried out following the method of Gullón et al. [130] with slight modifications. For both types of samples, 25 mg were dissolved in 3 mL of MeOH. This mixture was centrifuged at 450 rpm for 24 h. After this time 300 μL of each extract was used for analysis. The absorbance was measured at a wavelength of 760 nm with an UV/Vis spectrophotometer (V-630, Jasco, Pfungstadt, Germany) using gallic acid as reference standard. The assay was

performed in triplicate and the results were reported as mg gallic acid equivalents/g sample (mg GAE/g).

2.6. Antioxidant assays

In the antioxidant activity assays, samples were prepared employing 25 mg of sample in 3 mL of MeOH. The sample was then centrifuged at 450 rpm for 24 h and the supernatant was stored for the assays.

2.6.1. DPPH Radical Scavenging Assay

The DPPH (2,2-diphenyl-1-picrylhydrazyl) free radical scavenging assay is a method for measuring antioxidant activity based on the ability of a compound to transfer a hydrogen to the DPPH* radical. This assay was carried out for nanocomposite films and curcuma oil following the method of Gullón et al. [130] with slight modifications. From each sample, 300 µL of supernatant (as previously described) was mixed with 3 mL of a solution of DPPH in MeOH (6×10^{-5} M). After 15 min, the absorbance was measured at a wavelength of 515 nm with an UV/Vis spectrophotometer (Jasco V-630, Pfungstadt, Germany) using Trolox as reference standard. The measurements were performed in triplicate and the results were reported as mg Trolox equivalent/g sample (mg TE/g). In addition, in Chapter 4, the results were expressed as the percentage of DPPH radical scavenging activity following the equation below:

$$DPPH \% = \frac{A_0 - A_S}{A_0} \; x \; 100 \qquad \text{(III-3)}$$

where A_0 corresponds to the absorbance of DPPH of the control and A_S represents the absorbance of the film. Each sample was measured in triplicate.

2.6.2. FRAP Assay

The FRAP assay was used to measure the antioxidant properties of curcuma oil (see Figure 2). This assay is based on measuring the reduction of the compound FeIII-TPTZ (ferric tripyridyltriazine) to the complex FeII-TPTZ (ferrous-tripyridyltriazine) when exposed to an antioxidant compound. This reaction produces a colour change which is measured at a wavelength of 593 nm with a UV/Vis spectrophotometer (Jasco V-630, Pfungstadt, Germany) using Trolox as reference. FRAP reagent (3 mL) was added to 300 µL of the sample supernatant (obtained as described previously). The FRAP reagent solution was prepared by mixing 2.5 mL of 2,4,6-tripyridyl-s-triazine (10 mM), 25 mL of acetate buffer (300 mM) at pH 3.6 in HCl (37 % v/v) and 2.5 mL of $FeCl_3-6H_2O$ (20 mM) in distilled water [130]. Measurements were performed in triplicate and results were expressed as mg Trolox equivalent/g extracted curcuma oil (mg TE/g).

2.6.3. 2,2'-Azino-bis(3-ethylbenzothiazoline-6-sulfonic acid) Assay (ABTS)

The ABTS antioxidant activity assay was applied to curcuma oil following the method described by Gullón et al. [130] with slight modifications (see Chapter 2). This method consists of reacting a solution of $K_2S_2O_8$ (2.45 mM) with a solution of ABTS (7mM) to promote the generation of the ABTS+ radical. Then, phosphate buffer (PBS) (pH = 7.4) was added to this mixture to achieve an absorbance

of 0.7 at a wavelength of 734 nm with an UV/Vis spectrophotometer (Jasco V-630, Pfungstadt, Germany). Once this was achieved, 30 µL of supernatant (obtained as above) and 3 mL of ABTS solution were added. The absorbance of the samples was measured at 734 nm using Trolox as reference. Measurements were performed in triplicate and data were expressed as mg Trolox equivalent/g extracted curcuma oil (mg TE/g).

3. Characterization of nanocomposite films
3.1. Thickness

The thickness of the films was determined with a digital micrometer (Ultra Präzision Messzeuge GmbH, Glattbach, Germany) at six random points on each sample. The accuracy of the instrument is 0.001 mm. Thickness values were expressed in terms of average and standard deviation.

3.2. Moisture content

The moisture content (MC) of the films was determined according to the method described by Priyadarshi et al. [28] with slight modifications.

For this purpose, 3 rectangular portions (1.5 x 3 cm²) were cut from each film. Then, were weighed and dried at 106 ºC (Memmert UN160 plus Twindisp oven, Germany) for 24 h. The MC was calculated using the below equation:

$$MC\ (\%) = \frac{(W_0 - W_1)}{W_1} x100 \tag{III-4}$$

where Wo corresponds to the initial weight of the rectangular portion of the sample (g) and W1 represents the weight after 24 h of drying in the oven (g). The MC was determined in triplicate and the results were calculated as means and their standard deviations.

3.3. Water solubility

The water solubility (WS) of the films was determined by immersion following the method explained by Sahraee et al. [42] with some modifications. For this purpose, 3 rectangular pieces of each sample (1.5 x 3 cm²) were cut and then dried for 3 h at 106 °C (Memmert UN160 plus Twindisp, Germany) until constant weight was obtained. Afterwards, each rectangle was immersed in 50 mL of distilled water under constant stirring for 24 h at 25 ºC. The undissolved piece of the film after immersion was dried at 106 °C for 24 h and weighed. The WS was calculated by equation (III-5):

$$WS\ (\%) = \frac{(W_0 - W_1)}{W_0} x100 \qquad\qquad \text{(III-5)}$$

where Wo corresponds to the constant weight obtained before immersion (g) and W1 corresponds to the weight of the undissolved film after the drying process after 24 h (g). WS was determined in triplicate for each sample and the values for each film were expressed as average and their standard deviations.

3.4. Water contact angle

The water contact angle was used to evaluate the hydrophobicity changes on the surface of the films. For the measurements, the DataPhyscs OCA20 equipment (DataPhysics Instruments GmbH, Filderstadt, Germany) was used at room temperature. A 4 µL drop of

distilled water was applied to the surface of the films. The measurements of the contact angles were obtained with the SCA20 software between 0 and 2 min. For each film, six different measurements were determined.

3.5. Color properties

The color variation of the films was evaluated using a colorimeter (PCE-CSM3, PCE, Spain) according to the CIELAB color scale (see Chapter 3 and 4). The parameters measured were the color difference ΔE^*, L* (lightness), b* (-blue/+yellow) and a*(-green/+red). The ΔE^* parameter was calculated employing the next equation [131]:

$$\Delta E^*=\sqrt{[(\Delta L^*)^2+(\Delta a^*)^2+(\Delta b^*)^2]} \qquad (III-6)$$

Measurements were obtained on 10 random sections of each film and results were expressed as mean and standard deviation.

In Chapter 4, the colour of the films exposed to pH and volatile ammonia variations was evaluated. For each assay, the films were cut into 2 x 4 cm² rectangles and each experiment was performed in triplicate.

a) *Colour of samples treated with volatile ammonia*

This experiment was carried out following the method described by [132] with a slight modification. Each portion of the films was subjected to two different concentrations of ammonia solutions (0.008 mol/L and 0.5 mol/L). For this, 70 mL of each ammonia solution was used in a 500 mL bottle where the film was placed 1 cm above the ammonia solution (Figure III-7). In the closed bottle, the

films were exposed to ammonia vapour for 20 minutes. Finally, the colour parameters were determined.
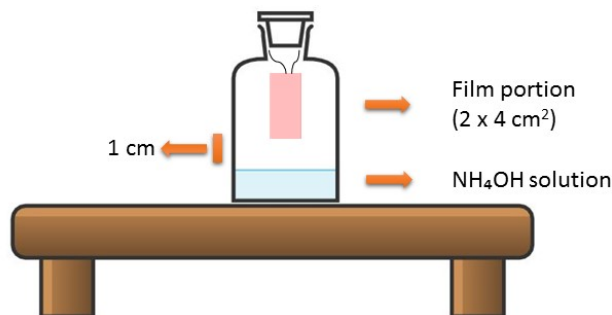
Figure III-7. Film exposed to ammonium gas.

b) *Color of the samples at different pH*

This experiment was performed following the method described by [127] with a slight modification. Portions of the films were immersed in 10 mL of different solutions of pH 2, 4, 6, 8, 8, 10, 12 and 14 (0.1 M HCl and 0.1 M NaOH) for 30 min at 25 °C. Afterwards, they were dried at room temperature and the color parameters were determined.

3.6. Optical properties (transmittance and opacity)

The UV/Vis light barrier properties of the nanocomposite films were carried out by measuring the transmittance with a UV/Vis spectrophotometer (Jasco V-630 UV/VIS spectrophotometer, JASCO, Germany) from 250 to 700 nm.

The opacity was carried out with an UV/Vis spectrophotometer according to the method of [28] with slight differences. Three rectangles of 1 x 4 cm² were cut from each film and were measured

with an absorbance of 600 nm. The following equation was used to determine the opacity values:

$$\text{Opacity} = \frac{\text{Abs}_{600}}{\text{X}} \qquad \text{(III-7)}$$

where Abs 600 corresponds to the absorbance measured at 600 nm and x is the thickness of the average of the three portions of each nanocomposite film (mm).

3.7. Scanning electron microscopy (SEM)

The morphology of the films was determined by scanning electron microscopy (SEM) (Hitachi Ltd. Japan). The samples were prepared by coating with 20 mm gold in high vacuum and scanned at an accelerating voltage of 10 kV. The cross section was measured at 500 x and the surface was scanned at 2 000x - 10 000x magnification.

3.8. Mechanical properties

The mechanical properties of the films were carried out on an Instron 5967 testing machine (Instron, Norwood, MA, USA). At least 8 rectangular pieces of 0.5 cm x 4.5 cm² were cut from each film. The load cell employed was 500 N and the crosshead speed was 3 mm/min. The tensile strength (TS, MPa), Young's modulus (YM, MPa) and elongation (E, %) were determined.

3.9. Cytotoxicity assay

L929 mouse fibroblast cell line was obtained from the Ministry of Health, Turkey, and maintained in DMEM medium supplemented with 10 % (v/v) fetal bovine serum 1 % penicillin/streptomycin at 37 °C in a humidified incubator in an atmosphere of 5 % CO_2. L929 cells

were cultured as a 70 % to 80 % confluence and cells were harvested after trypsinized. In vitro assay was performed to determine the cytotoxic effects of nanocomposite films. The samples were sterilized by placing them under UV light for 40 minutes. Cells were seeded into a 96-well plate at a density of 1 x 104 cell and incubated for 24 h at 37 °C. After the 24 h incubation, the medium was aspired out and L929 cells were supplied with a fresh medium. Then the cells were treated with nanocomposite film samples at a concentration of 8mg/mL and incubated for 24, 48 and 72 h. DMEM was selected as a negative control. The cell viability was evaluated by following the MTT (3- (4, 5-dimethylthiazol-2-yl)-2, 5-diphenyltetrazolium bromide) reduction assay. 20 µL MTT solution (5 mg/mL of stock in DPBS) was added into each well and then incubated for 4 h at 37 °C in an incubator. The culture medium was removed and 100 µL DMSO was added into each well to extract the insoluble formazan crystals within the cells. The plates were shaken for 15 min. The presence of viable cells was demonstrated by purple color due to the formation of formazan crystals. The absorbance was measured at 540 nm using a microplate reader. The results represent the average values of four experiments.

$$\text{Viability (\%)} = \frac{X_{OD}}{X_{OD_0}} x \ 100 \qquad\qquad \text{(III-8)}$$

where X_{OD} represents the mean of optical density of treated cells and X_{OD_0} is the mean of optical density of control cells.

$$\text{Cytotoxicity (\%)} = \text{Viability x 100} \qquad \text{(III-9)}$$

3.10. Antifungal properties

The antifungal activity of the films against *Aspergillus niger* was performed by the agar plate test following the method described by Salaberria et al. [11] with slight modifications (see Chapter 3). *Aspergillus niger* was seeded on potato dextrose agar substrate in sealed petri dishes that were incubated for 72 h at 25 ºC. A spore aliquot was then prepared at a concentration of 1.29 x 10^6 cells/mL dissolved in Ringer's solution. The films were then cut into 1 x 1 cm² squares and placed on the agar. These film portions were inoculated with 40 µL of the *A. niger* suspension under aseptic conditions and incubated at 25 °C for 7 days. After this time, the number of colony forming units per millilitre (CFU/mL) was estimated and the fungal growth inhibition (FGI %) was calculated according to the following equation:

$$FGI \% = \frac{C_g - T_g}{C_g} \; x \; 100 \qquad \qquad \text{(III-10)}$$

where Cg represents the average concentration of the control film and the average concentration of the treated film determined by Tg. Each nanocomposite film was analysed in triplicate.

PART IV: RESULTS AND DISCUSSION

A. Extraction of nanochitin and essential oils
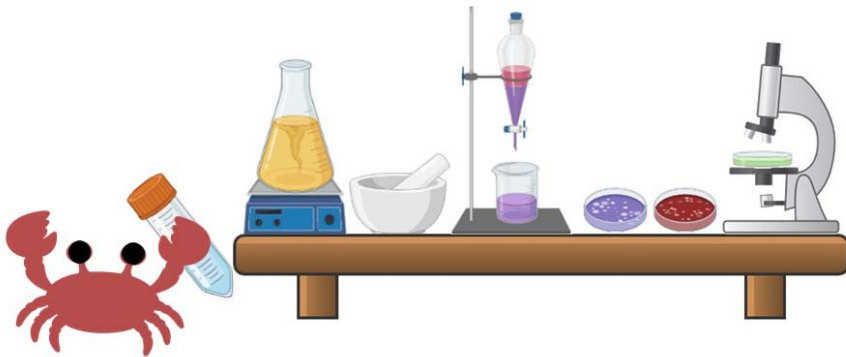
PART IV: RESULTS AND DISCUSSION

A. *Extraction of nanochitin and essential oils*

Chapter 1

Optimization of eco-friendly isolation of nanochitin from different origins by response surface methodology by microwave irradiation

Abstract

The isolation of nanochitin by the conventional acid hydrolysis conditions requires high temperature and acid concentration, time and energy. For this, the aim of this work was to optimise the isolation conditions through an experimental design of Box-Behnken using the surface response methodology with different sources of chitin using the eco-friendly technique of microwave irradiation. The data showed optimal conditions of 1 M HCl, 10.00 min and 124.75 W to obtain lobster nanocrystals; of 1 M HCl, 14.34 min and 50.21 W to obtain shrimp nanocrystals; and 1 M HCl, 29.08 min and 54.08 W to obtain squid pen nanofibres and isolation yields were 85.30, 79.92 and 80.59 %, respectively. The chemical structure, morphology and thermal stability of the ensuing nanochitins were maintained after treatment. Thus, the results showed that nanochitin could be obtained using an eco-friendly approach reducing the time and concentration of HCl.

1. INTRODUCTION

In recent years, the production of fishery by-products has considerably risen causing serious environmental problems due to its high chemical demand for oxygen and presence of fats, pathogens, and others [133]. Nonetheless, because of the high content in proteins, minerals and polysaccharides present in these by-products, it has been observed an increasing interest in their valorisation [133,134].

Among the marine-derived polysaccharides, chitin (CH, poly β-(1-4)-N-acetyl-D-glucosamine), obtained mainly from seafood wastes like shrimp, crab, lobster and squid pen is renewable and abundant, and, in a near future, chitin will become one of the most important organic raw materials [18,135].

Being a supporting material in living organisms, chitin presents a highly-organized micro- and nanofibril structure, which contains crystalline and amorphous domains [10,11,18,22]. Depending on its origin and under controlled extraction conditions, it is possible to isolate chitin microfibrils in the form of nanocrystals (6-60 nm in width and 100-800 nm in length) and nanofibres (10-100 nm in width and many micrometres in length) in the alpha form (α), which is the most common, contains alternate antiparallel chains or beta form (β) that is formed by parallel chains [8,11,22]. Several studies have demonstrated the advantages of their unique properties such as small size, low density, high surface area, good chemical reactivity, biocompatibility, biodegradability, low toxicity, antimicrobial and antioxidant activity, and excellent mechanical performance [27,107]. These qualities generate a high interest in different industrial sectors (e.g. cosmetics, medical and food industries) as functional and reinforcing agents in nanotechnology and materials science [8,136].

For the isolation of nanochitin, from the extracted macroscopic chitin, the 'top-down' strategy is the most common and refers to the isolation of nanostructured crystals or fibrils via chemical or physical methods. For instance, the most popular of conventional methods to isolate chitin nanocrystals is strong acid hydrolysis. On the other hand, chitin nanofibres have been obtained by mechanical approach

or by ultrasonic technique [10,11]. Nonetheless, these treatments require high temperature and long reaction times, which implicates high-energy consumption [24,25]. There is an evident need of new eco-friendly and sustainable alternatives for the extraction of nanochitin.

An alternative methodology could be the microwave-assisted extraction (MAE) irradiation that presents low energy consumption, fast reaction and high production yield. The MAE consists of applying an electromagnetic field to a sample with polar solvents. The electromagnetic waves cause the dipoles of the molecules to try to align themselves with the field and produce frictions and collisions that raise the temperature [137,138]. Some researchers reported the extraction of chitin or chitosan with microwave irradiation technique. For instance, in a study realised by Sagheer et al. [139], the extraction time of α- and β-CH and chitosan decreased from 6-10 h to 10-15 minutes by using microwaves approach. Similarly, El Knidri et al. [135] achieved α-chitin and chitosan from shrimp, reducing the extraction time to 24 minutes by microwave. Also, Nguyen et al. [140] showed an experimental design where the demineralization step was optimized to obtain α-chitin from lobster employing 23 minutes under microwave irradiation. However, to the best of our knowledge, no literature was found related with the isolation of nanochitin by using microwave methodology.

In this context, in the present study, we propose to optimize the isolation conditions of α-chitin nanocrystals from shrimp and yellow lobster and β-chitin nanofibres from squid pen by using the microwaves irradiation methodology through an experimental Box-

Behnken (BBD) design using response surface methodology (RSM). The chemical structure, crystalinity, thermostability and morphology of the nanochitin were also assessed.

2. MATERIALS AND METHODS
2.1. Raw materials and chemicals

Powder α-chitin from shrimp shells (α-CH_S) and powder β-chitin from squid pens (β-CH_{SP}) were kindly supplied by Mahtani Chitosan PVT Ltd., India. Powder α-chitin from yellow lobster *(Cervimunida johni)* shells (α-CH_L) was extracted *in-house* based on our previous works [10,19]. Antarctic Seafood S.A. (Chile) kindly provided the yellow lobster shell wastes. Hydrochloric acid (HCl, 37%, ACS reagent) was purchased from Sigma-Aldrich.

2.2. Experimental design of microwave-assisted isolation of nanochitin
2.2.1. General Experimental Procedure

To obtain nanochitin, 1 g of chitin powder was used at 1-3 M HCl concentration (Table IV-1 and IV-2) using a 1:30 w/v, CH:HCl ratio by the MAE technique (Discover system, CEM, USA) as shown in **PART III**. The samples obtained were: (i) α-nanochitin from lobster (α-NCH_L), (ii) α-nanochitin from shrimp (α-NCH_S), and (iii) β-nanochitin from squid feather (β-NCH_{Sp}).

2.2.2. Experimental design and determination of the optimal isolation conditions

The RSM was used to analyse the effect of HCl concentration (HCl, M), reaction time (t, min) and microwave power (P, W) on the isolation yield of nanochitin: α-NCH_L, α-NCH_S and β-NCH_{SP}. A BBD,

which consists of 15 experiments of which 3 corresponds to the replicates in the central point, was selected for the experimental design and optimization. The experimental design was created and the optimum conditions were predicted with the desirability function of Statgraphics Centurion version XV software (StatPoint Technologies INC., Warrento, VA, USA). Regression analysis function of Microsoft Excel Add-In, USA was employed to fit the experimental data obtained in the experimental design.

In order to adjust the experimental data a second-order polynomial equation was employed as described in Equation IV-1:

$$y_j = \beta_0 + \sum_{i=1}^{k} \beta_i X_i + \sum_{i=1}^{k} \beta_{ii} X_i^2 + \sum \sum_{i<j=1}^{k} \beta_{ij} X_i X_j + \varepsilon \qquad \text{(IV-1)}$$

where K represents the number of factors (3), Y represents the dependent variables: Y_L (%, Yield of α-NCH_L), Y_s (%, Yield of α-NCH_S) and Y_{Sq} (%, Yield of β-NCH_{SP}). β_o, β_i, β_{ii} and β_{ij} represent the regression coefficient calculated from the experimental results employing the least-squares method, X_i and X_j are the dimensionless and normalized independent variables, which present variation ranges from -1 to 1 and ε is the experimental error. The model was validated by evaluating the lack of fit, the coefficient of determination (R^2), significance of the regression coefficients, the F-test value acquired from the analysis of variance (ANOVA).

The experimental variables implicated in the study are outlined in Table IV-1, which includes the fixed and independent variables and their values or range. The dependent variables that correspond to the

nanochitin yields obtained from lobster (Y_L), shrimp (Y_S) and squid pen (Y_{Sq}) are also listed.

The isolation yields (Y) of nanochitins were determined according to the method of Xiao et al. [141] with slight modifications (Equation IV-2):

$$Y \% = \left(\frac{M_2 \; x \; V_1}{M_1 x \; V_2}\right) x \; 100 \qquad \text{(IV-2)}$$

where M_1 is the mass of chitin (g), M_2 is the total mass of the oven dried nanochitin suspension at 105 °C (g), V_1 is the total volume of the suspension obtained (mL), and V_2 (mL) is an aliquot of the suspension that was dried at 105 ºC. The optimum point of each nanochitin was measured three times.

Table IV-1. List of the experimental variables involved in the microwave-assisted isolation of nanochitin.

	Variable	Nomenclature	Units	Value or range
Fixed	CH:HCl	ratio	g/mL	1:30
Independent	HCl concentration	HCl	M	1-3
	Reaction Time	t	min	10-30
	Microwave power	P	W	50-200
Dependents	Nanochitin isolation yield	Y_L Y_S Y_{Sq}	%	-

The chemical structure and crystallinity of the raw materials and the isolated nanochitin were characterised by ATR-FTIR, ^{13}C-NMR and XRD, their morphology was observed by AFM and their thermogravimetric properties by TGA. The techniques are described in **PART III**.

3. RESULTS AND DISCUSSION
3.1. Optimization of the isolation conditions for obtaining nanochitin

Conventional nanochitin isolation involves long and hard hydrolysis conditions, namely, the use of high concentration of HCl and time. These parameters affect the final nanochitin yields and properties, as well as the cost and environmental impact. Thus, it is crucial to find novel sustainable approaches to isolate nanochitin from chitin and optimize its isolation. Herein, the combination of response surface methodology and Box-Behnken design was used in order to optimize the isolation conditions, taking into account the most influential variables in the process (HCl concentration, reaction time and microwave power) to obtain the most interesting nanochitin yields of 3 different chitin origins, using an eco-friendly approach: microwave-assisted irradiation. Microwave irradiation was chosen because of lower energy consumption, shorter reaction times and higher yields. Table IV-1 lists the experimental plan including the fixed variable (CH:HCl ratio), the independent variable (concentration of HCl; t and P) and the dependent variables (nanochitin yields: Y_L, Y_S and Y_{Sq}). A summary of the set of experiments that were designated by the Statgraphics software, as

well as the experimental results obtained for the dependent variables
is shown in Table IV-2.

Table IV-2. Box-Behnken experimental design with operational conditions expressed in terms of dimensional and dimensionless independent variables HCl (HCl concentration, M) (X_1); t (time, min) (X_2); P (power, W) (X_3) and experimental responses obtained for dependent variables (nanochitin yield: Y_L, Y_S and Y_{Sq}).

	Independent Variables			Normalized Variables			Dependent Variables		
Experiments	HCl (M)	t (min)	P (W)	X_1	X_2	X_3	Y_L	Y_S	Y_{Sq}
1	3	20	50	1	0	-1	83.71	75.03	68.57
2	2	20	125	0	0	0	85.47	71.03	73.30
3	1	20	50	-1	0	-1	88.42	77.85	76.60
4	2	10	50	0	-1	-1	87.73	78.61	71.91
5	1	30	125	-1	1	0	89.33	68.62	74.72
6	1	10	125	-1	-1	0	90.56	76.55	76.35

7	3	10	125	1	-1	0	88.25	49.71	70.98
8	2	30	50	0	1	-1	84.84	61.80	70.86
9	3	30	125	1	1	0	83.33	56.09	47.77
10	2	20	125	0	0	0	85.86	70.55	70.49
11	1	20	200	-1	0	1	89.20	76.53	74.10
12	2	10	200	0	-1	1	86.76	74.56	72.32
13	3	20	200	1	0	1	82.98	64.50	51.27
14	2	30	200	0	1	1	85.04	57.60	54.35
15	2	20	125	0	0	0	86.22	72.47	70.58

The determination coefficient R^2 indicates the validity of the design by explaining the total variations of the model [130,142]. Thus, as can be seen in Table IV-3, the determination coefficients R^2 obtained for nanochitin from lobster (α-NCH$_L$) and from squid pen (β-NCH$_{Sp}$) were 0.9802 and 0.9905 respectively, indicating that only 0.0198 % and 0.0095 % of the total variations remain unexplained with the selected model. These values indicate that the selected model is adequate to represent the relationships between the selected variables. In addition, Fisher's F-test evaluates the model's predictive goodness. The samples from α-NCH$_L$ and β-NCH$_{Sp}$ showed F-experimental (27.5041 and 58.0143, respectively) higher than the F-critical values for 9 degrees of freedom. This confirms that the model is statistically relevant. On the other hand, in the case of nanochitin from shrimp α-NCH$_S$, although R^2 and F values (0.8122 and 2.4024, respectively) were significantly lower, can be considered suitable to validate the model.

Table IV-3. Regression coefficients and statistical parameters.

Coefficients	Y_L	Y_S	Y_{Sq}
b_0	85.85	71.35	71.46
b_1	-2.41[a]	-6.78[a]	-7.90[a]
b_2	-1.35[a]	-4.42	-5.48[a]
b_3	-0.09	-2.51	-4.49[a]
b_{12}	-0.92[a]	3.58	-5.40[a]
b_{13}	-0.38	-2.30	-3.70[a]
b_{23}	0.29	-0.04	-4.23[a]
b_{11}	1.00[a]	-1.64	-1.86[c]
b_{22}	1.02[a]	-6.97[c]	-2.14[b]
b_{33}	-0.77[b]	3.76	-1.96[c]
R^2	0.9802	0.8122	0.9905
F-exp	27.5041	2.4024	58.0143
F-critical	0.0009	0.1736	0.0002
Significance level (%)	99.90	82.64	99.98

F-crítical for 9 degrees of freedom.
[a]Significant coefficients at the 99% confidence level
[b]Significant coefficients at the 95% confidence level
[c]Significant coefficients at the 90% confidence level

It was shown that the isolation yields are dependent of the source of chitin (Table IV-2). Therefore, the yield ranged from 82.98 % (exp. 13) to 90.56 % (exp. 6) for α-NCH$_L$, from 49.71 % (exp. 7) to 78.61 % (exp. 4) for α-NCH$_S$, and from 47.77 % (exp. 9) to 76.6 % (exp. 3) for β-NCH$_{Sp}$. Also, the regression coefficients summarised in Table IV-3 showed different behaviour depending on the feedstock. For instance, in the case of β-NCH$_{Sp}$, the independent variables that showed more influence in the isolation yield were the HCl concentration (X_1) and the time (X_2) as well as the interaction between both and their quadratic effect. The quadratic effect of power (X_3^2) also demonstrated influence with a 95 % confidence interval. In the case of α-NCH$_S$, only two variables were significantly relevant (>90%), the linear effect of temperature and the quadratic effect of time An

explanation for this could be the low adjustment showed by the design (R^2=82.64 %). Finally, for α-NCH$_S$, all independent variables, as well as the interaction between them and their quadratic effects influenced the isolation yield.

3.2. Isolation Yield

The interaction between the independent variables and their influence on the α-NCH$_L$, α-NCH$_S$ and β-NCH$_{Sp}$ isolation yields are shown in Figure IV- 1.

Figure IV-1-1 displays the influence of the independent variables time (X_2) and power (X_3) on the samples yield when the HCl concentration was set to the midpoint value (X_1=0). This figure shows that time had a significant influence on the obtained nanochitin yield, the latter increase with the decrease of the reaction time. Nonetheless, due to the different contributions of the quadratic coefficients of time in the regression equation (see Table IV-3), two different behaviours are differentiated between the samples: (1) in α-NCH$_L$ sample (Figure IV- 1-1a) a slight decrease in yield is observed as the time reduces to a minimum, after which a decrease in reaction time leads to an increase in yield, this is explained by the positive contribution of the quadratic coefficient of time; and (2) in α-NCH$_S$ (Figure IV-1-1b) and β-NCH$_{Sp}$ (Figure IV-1-1c) samples, the opposite effect is observed due to the negative contribution of this coefficient meaning that the yield increased to a maximum as the reaction time decreased, after which a diminution in time decreased the yield. This behaviour was most pronounced for chitin shrimp feedstock (Figure 1-1b). Interestingly, the data indicated that power (P, W) does not

show a major influence on the isolation yield of α-NCH_L and α-NCH_S samples; however, for the β-NCH_{Sp} sample the results indicated that an increase in power dramatically decrease the yield. Only in this case the independent variable power shows influence on the model (Table IV-3).

The independent variable X_3 exhibit the same behaviour in Figure IV-1-2, in which the influence of the HCl concentration and power when the time value was fixed at a middle point value (X_2=0) is displayed. In this case, it should be noted that a reduction on the HCl concentration increased the obtained isolation yield in all samples. In addition, the lowest yield in all three cases was obtained when the HCl concentration and the microwave power were at their maximum levels. However, while in the case of α-NCH_L (Figure IV-1-2a) at high HCl concentration a drop in the power does not have a relevant influence in the obtained nanochitin yield, in the case of α-NCH_S (Figure IV-1- 2b) and β-NCH_{Sp} (Figure IV-1-2c) the yield was increased substantially by decreasing the power.

Finally, the relationship between the independent variables that most influence the model, time and HCl concentration, by keeping the power at the midpoint (X_3=0) is represented in Figure IV-1-3. This figure showed that a decrease in the HCl concentration together with low reaction times have a positive effect on obtaining nanoforms. Nonetheless, slight differences can be noticed among the three samples. On the one hand, in the case of α-NCH_L (Figure IV-1-3a) the yield decreases when the reaction time is reduced, but due to the positive contribution of the quadratic coefficient of time the trend changes and the yield increases, obtaining the maximum yield with

minimum HCl concentration and reaction time. Nevertheless, for α-NCH$_S$ and β-NCH$_{Sp}$, Figures IV-3b and 1-3c, respectively, in which the contribution of the quadratic coefficient of time is negative, the tendency is just the opposite. This means that the yield first rises as the time goes down to a maximum and afterwards it decreases.

Lobster (α-NCH$_L$)   Shrimp (α-NCH$_S$)   Squid pen (β-NCH$_{Sp}$)

86
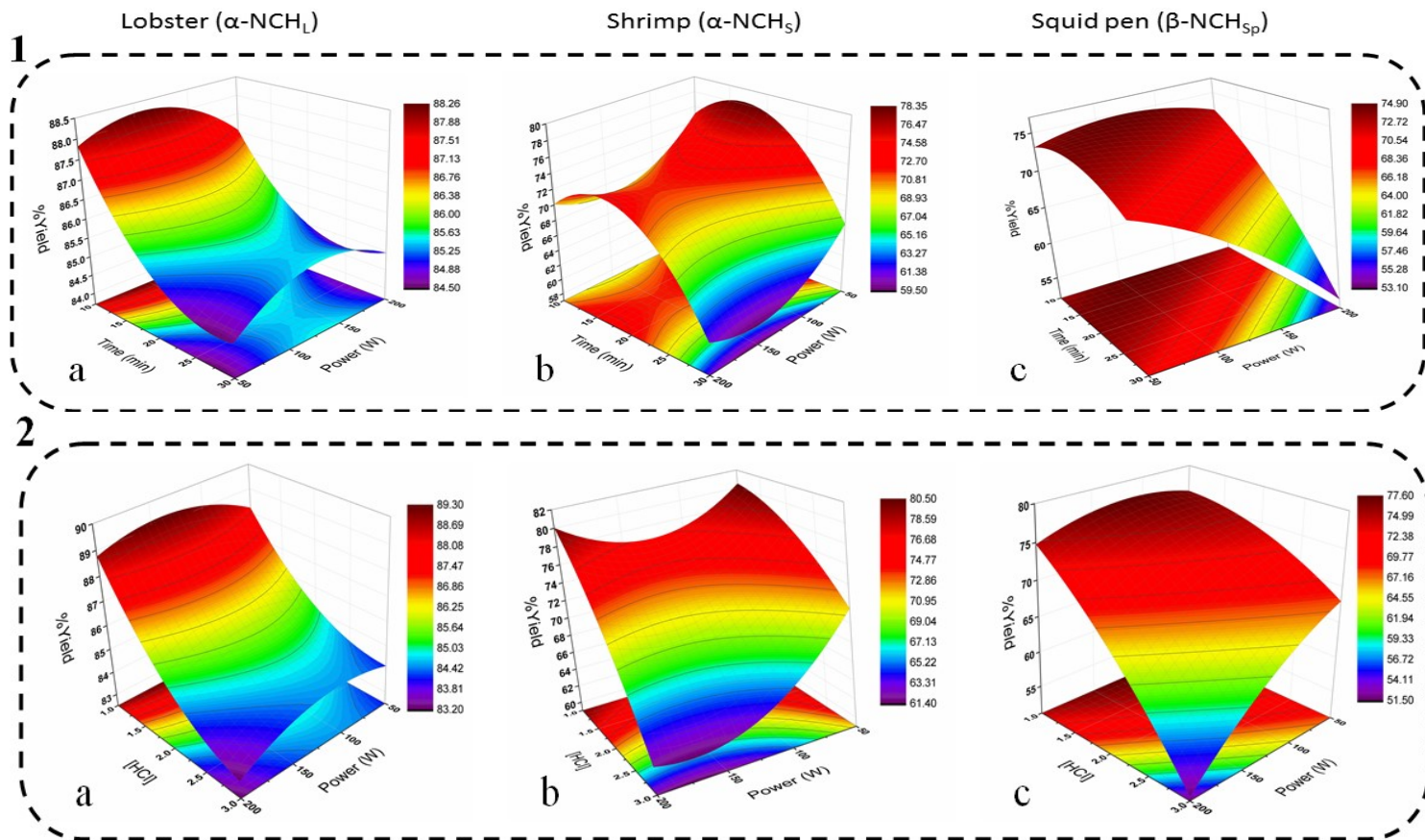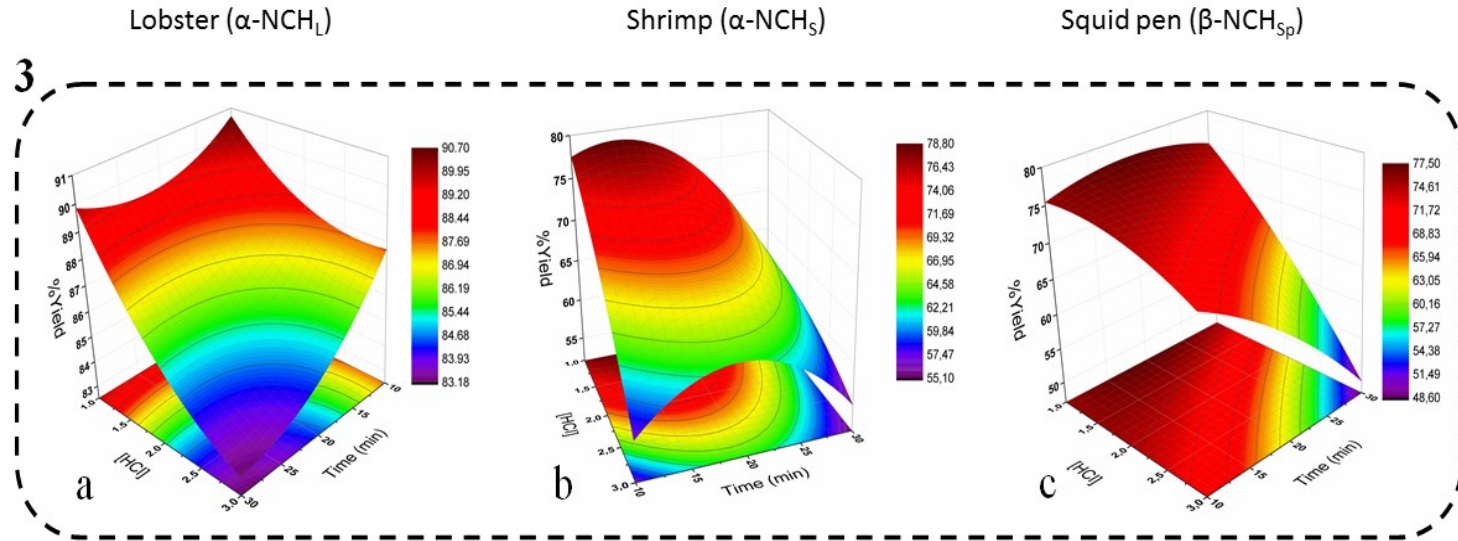
Figure IV-1. Isolation yield as a function of: 1) time (t) and power (P) at a fixed HCl concentration (HCl) (X₁=0); 2) HCl concentration (HCl) and power (P) as a fixed time (X₂=0); 3) time (t) and HCl concentration (HCl) at a fixed power (P) (X₃) for: a) α-NCH$_L$, b) α-NCH$_S$ and c) β- NCH$_{Sp}$.

3.3. Optimization of isolation conditions and validation of the model

The aim of the optimisation was to determine the optimal conditions for maximising the isolation yield of nanochitin from different chitin sources used in this study. Therefore, the dimensionless and dimensional values of the independent variables obtained through Statgraphics Centurion XV software are summarized in Table IV-4.

A triplicate of the experiments was performed to validate the model under optimal conditions. A comparison was made between the obtained results and the theoretical ones (Table IV-4). The experimental results are in agreement with those predicted by the software, which validates the selected design (Box-Behnken).

Table IV-4. Dimensionless and dimensional values of the optimal point of the system and predicted and experimental values at optimum conditions of the nanochitin isolation. The yields experimental values were average ± standard deviation from three replications (n=3).

	Optimal point							
	Dimensionless			Dimensional			Yield %	
	X_1	X_2	X_3	HCl (M)	t (min)	P (W)	Predict value	Experimental value
α-NCH$_L$	-1	-1	-0.0034	1	10.00	124.75	90.69	85.30 ± 0.37
α-NCH$_S$	-1	-0.5660	-0.9972	1	14.34	50.21	82.72	79.92 ± 0.24
β-NCH$_{Sp}$	-1	0.9082	-0.9456	1	29.08	54.08	78.27	80.59 ± 0.11

Authors such as Yuan et al., who studied the isolation of nanocrystals from crab shells, obtained similar yields. In this study, different isolation yields between 78 - 87.5 % were obtained by ultrasonic treatment among 1 and 3 h [143]. Other authors such as Arakari et al. [144] showed lower isolation yields (55-60%) when acid hydrolysis with 3M HCl at 100 ºC was performed during 3 h for the isolation of crab nanocrystals. Other authors showed that the isolation yield of nanochitin is usually in the range of 40 to 86 % and for the CHNF is between 75-84 % depending on the reaction time and the source of chitin [145–147]. These results demonstrated that similar yields to traditional methods could be obtained by reducing the reaction time using the microwave technique.

3.4. Characterization of the ensuing Nanochitin
3.4.1. Chemical structure and crystallinity

The chemical structure of the samples was assessed by ATR-FTIR and by ^{13}C-NMR (Figure IV-2 and IV-3).

As shown in Figure IV-2, there were no changes in the ATR-FTIR spectra when the raw chitin samples and the isolated nanochitin samples were compared.

α-CH bands from lobster and shrimp and their corresponding α-NCH$_L$, α-NCH$_S$ showed similar bands around at 3438 cm^{-1} and 3260 cm^{-1} corresponding to the O-H and N-H stretching vibrations. The amide II and amide III were observed around 1554 cm^{-1} and 1309 cm^{-1}, respectively [148,149].

Regarding the FTIR spectra of β-CH and β-NCH$_{Sp}$, they displayed similar absorption bands. For both, it was observed the band at 3278

cm^{-1} and 2875 cm^{-1} corresponding to the O-H and C-H stretching vibration; the peaks at around 1549 cm^{-1} corresponding to amide II; the bands at 1374 cm^{-1} and 1308 cm^{-1} assigned to the stretching band of C-H of methyl groups; and the peak at 1027 cm^{-1} corresponding to C-O stretching [121,150].

Interestingly, it was observed a difference between the α- and β-structures in the amide I band. In the α- chitin structure spectrum, two disticted bands were observed around 1654 cm^{-1} and 1621 cm^{-1} that have been assigned to the single H-bonded and double H-bonded, respectively; whereas for the β- structure an unique single band was observed at around 1631 cm^{-1} [121,149].
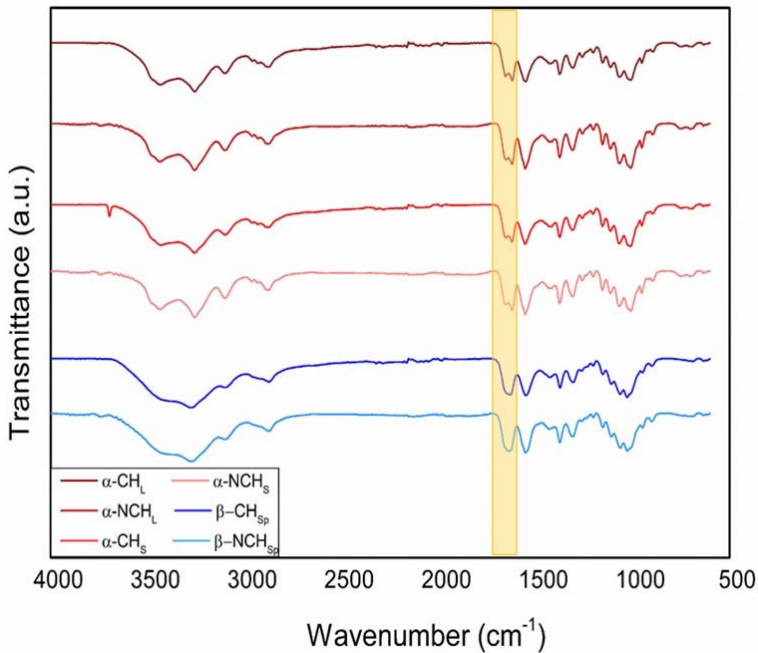
Figure IV-2. ATR-FTIR spectra of the different samples.

Figure IV-3 shows the ^{13}C-NMR spectra of α-NCH$_L$ and α-NCH$_S$, β-NCH$_{Sp}$. In all samples, the methyl group (CH3) was observed around 23 ppm and carbonyl group (C=O) at 173 ppm. The signals between 58-100 ppm were attributed to the carbon atoms of D-glucopyranosyl ring, where the peaks located at 104, 82, 61 and 55 ppm were assigned to C1, C4, C6 and C2, respectively, for all samples. The chemical shifts of C5 and C3 of α-NCH$_L$ and α-NCH$_S$ appeared as a doublet at 75 and 73 ppm because of the different configurations; nonetheless, the peaks of C3 and C5 (C5/C3) of β-NCH$_{Sp}$ sample merged into single resonance at 75 ppm, which is typical of beta-chitin structures [18,151]. Interestingly, in the present solid-state ^{13}C NMR spectra, there are no protein peaks (C–O: 180 ppm; C–N: 55 ppm).

The values determined by Equation 1 (section 2.1.2. in Part III), showed that α-NCH$_L$ and α-NCH$_S$ have a DA equal to 90 and 91%, respectively, and 88% for β-NCH$_{Sp}$. These results are in accordance with previous works about nanochitin isolated from different sources [125,152,153].
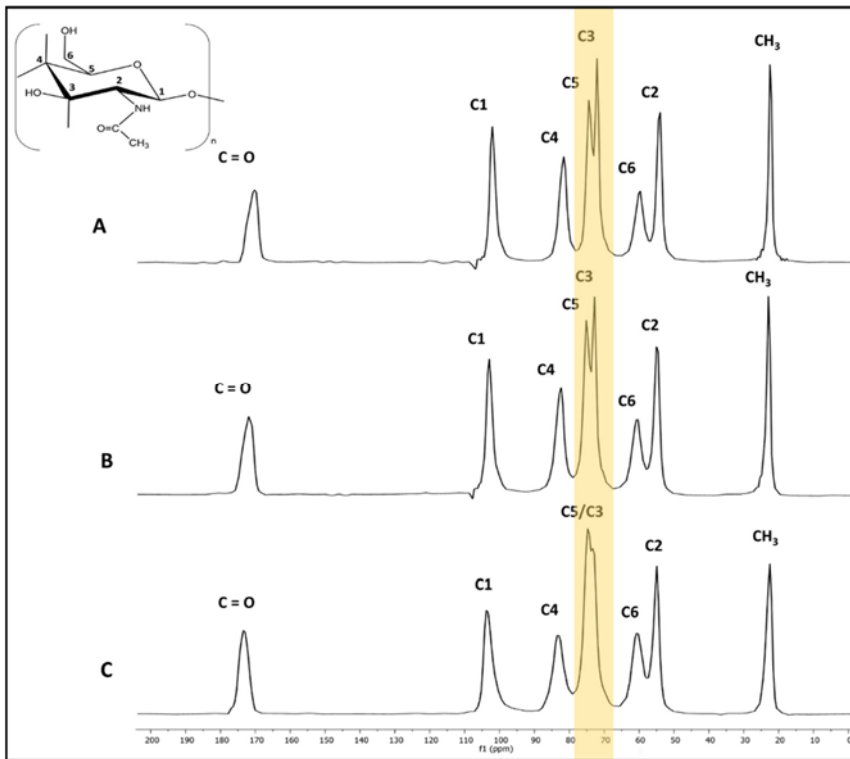
Figure IV-3. ¹³C-NMR spectra of: A) α-NCH$_L$, B) α-NCH$_S$ and C) β-NCH$_{Sp.}$

The XRD patterns of α-CH and α-NCH from lobster and shrimp and β-CH and β-NCH$_{Sp}$ were employed for study their crystal structure (Figure IV-4).
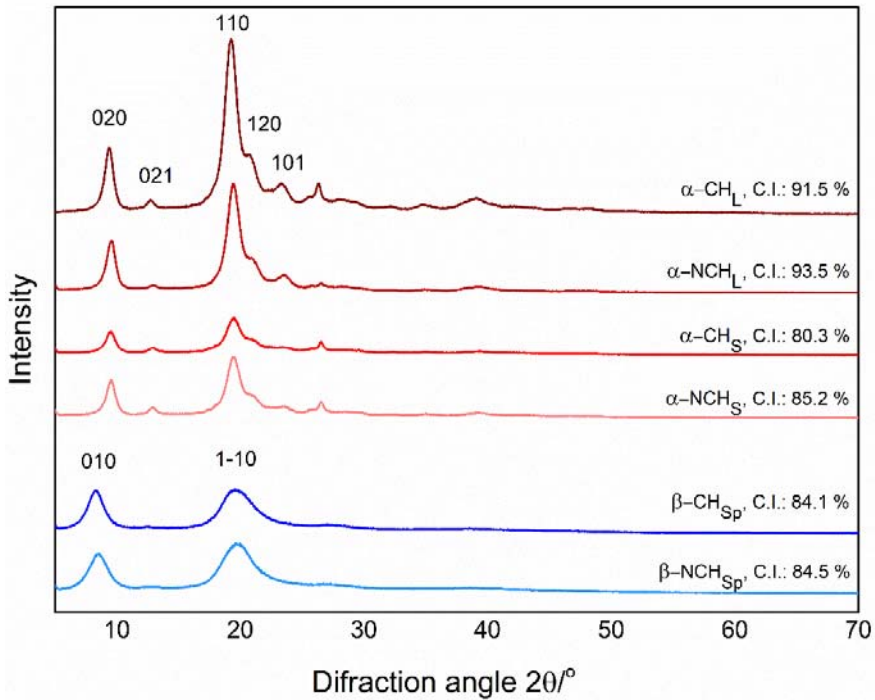
Figure IV-4. XRD patterns and crystallinity index (C. I. %, [139]) of α-CH_L, α-NCH_L, α-

CH_S, α-NCH_S, β-CH_Sp and β-NCH_Sp.

All the XRD patterns of shrimp and lobster were very similar. The diffractograms exhibited the typical diffraction pattern of both α-NCH (lobster and shrimp) in which 5 crystalline reflection were observed between the ranges 5-40 in 2θ. α-NCH$_L$ and α-NCH$_S$ demonstrated two narrow and strong crystalline peaks at 9.5 and 19.5° in the 2θ angles indexed as (020) and (110) planes. A smaller crystalline peak corresponding to the amorphous domains was observed at around 13° (021). Its low value was due to the amorphous part of the chitin has been removed under acid hydrolysis when obtaining the nanocrystals [22]. The other two peaks that were observed were 20.9° (120) and 23.4° (101) with a similar result as the one reported by [19].

94

On the other hand, the β-CH and β-NCH$_{Sp}$ diffraction patterns were similar and exhibited two peaks wider than in α-CH and α -CHNC samples. These peaks appeared around 9.30˚ and 19.30˚ which corresponding with (010) and (1-10) planes [20].

The crystallinity index (C.I. %) of each samples was calculated by [139] (Equation III-2 in Part III) and is shown in Figure IV-3-a. The higher C.I. % values of the chitin nanocrystals and nanofibres compared with their respective chitin is related to the amorphous part which was removed.

The C.I. % of α-NCH$_L$ (93.5 %) and α-NCH$_S$ (85.2 %) showed very similar results compared to the ones obtained by different studies such as Salaberria et al. (chitin nanocrystals from lobster 90%) and Goodrich et al. (chitin nanocrystals from shrimp 84.0 %), which were carried out using acid hydrolysis treatment [19,154].

Regarding the C.I. % results for β-CH and β-NCH$_{Sp}$ values of 84.1% and 84.5% were obtained, respectively. A similar behaviour was reported by Wu et al. [155] using mechanical approaches.

The difference between the peak's shapes in diffraction patterns and the C.I. % values demonstrates that the alpha structure is more crystalline polymorph since its antiparallel chains are more compacted [139].

3.4.2. Thermostability

The chitins and the nanochitins thermograms profiles (thermogravimetric analysis (TGA) and derivate (dTGA)) are displayed in Figure IV-5.
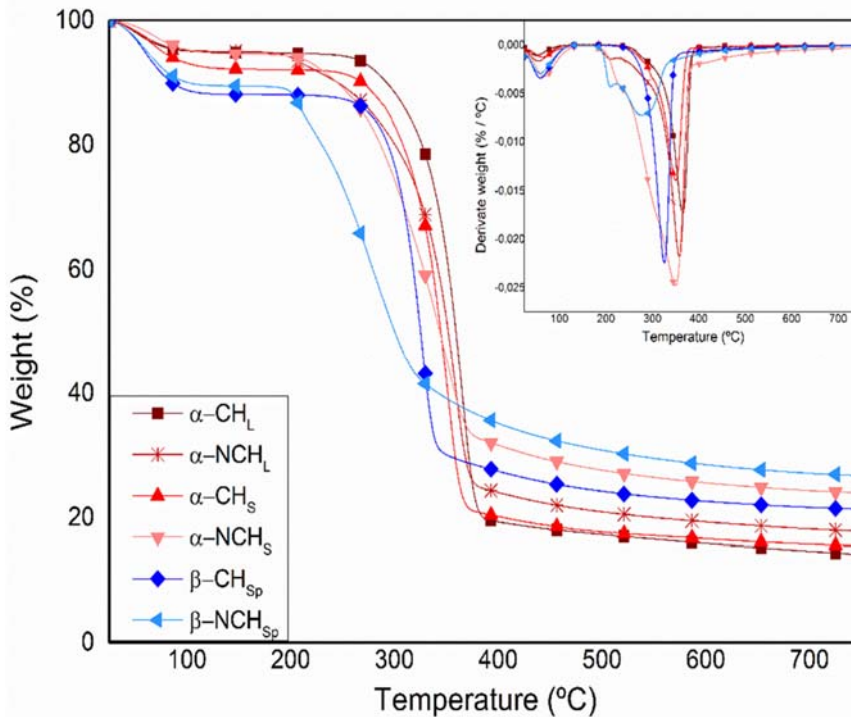
Figure VI- 5. TGA and dTGA curves of α-CH$_L$, α-NCH$_L$, α-CH$_S$, α-NCH$_S$, β-CH$_{Sp}$ and β-NCH$_{Sp..}$

The first mass loss observed in both TGA and dTGA profiles of all samples at about 100 °C was assigned to the water evaporation and corresponds to a weight loss of 5-8 wt % for the α- chitin and around 10 wt% for the β- chitin [148]. The second mass loss, also observed in all samples, was attributed to the degradation of the chitin biopolymer corresponding to the degradation and dehydration of the polysaccharide structure and decomposition of the acetylated and deacetylated units of chitin polymer [148,152,156]. The dTGA profile (Figure IV-3-b) showed the maximum degradation temperature around 350 °C and mass losses between 70 and 80 wt% for all samples with α-structure [152,157]. In contrast, lower maximum temperatures

were observed for the samples of β-CH (329 °C) and β-NCH$_{Sp}$ (281 °C) with mass losses of 60 and 70 wt%, respectively [158]. This difference between the two chitins polymorphs is due to the fact that β-structure contains slightly packed chains that require less heat for degradation [139,156].

Finally, TGA profiles demonstrated that the trend of nanocrystals and nanofibres samples were less thermostable than their respective native chitins. The same remark was done by Shankar et al. [121], regarding the isolation of chitin nanocrystals from crab shells by the acid hydrolysis employing HCl during 3 h.

3.4.3. *Morphology of the obtained nanochitin*

The morphology and dimensions of nanochitin samples were analysed by AFM (Figure IV-6). As expected, the α-NCH$_L$ and α-NCH$_S$ showed characteristic rod-like morphology. Interestingly, α-NCH$_L$ exhibited shorter lengths and widths (average of 314.74 ± 62.50 nm in lengths and 41.62 ± 10.92 nm in width) than α-NCH$_S$ (average of 386.12 ± 47.49 nm and 42.16 ± 4.62 nm in width). Similar results were reported by Phongying et al. [146] that obtained shrimp nanocrystals with lengths of 200-560 nm and diameters of 18-40 nm and Salaberria et al. [19], that get lobster nanocrystals with lengths of 300 nm and diameters of 60 nm after acid hydrolysis. The aspect ratio (L/d) of α-NCH$_L$ and α-NCH$_S$ was of 7 and 9, respectively. Similar results were reported by Yuan et al. [143] that obtained chitin nanocrystals with eutectic acid solvents (choline chloride and organic acids, such as citric, malonic, and lactic acid) with aspect ratios between 5 and 8.

On the other hand, the β-NCH$_{Sp}$ samples exhibited long and fibrillar morphology with length superior to 900 nm and average diameter of 19.82 ± 1.16 nm. Nata et al. [159] demonstrated the same morphology and size for nanofibers isolated from squid pen using mechanical treatment. As expected, the aspect ratio for the β-NCH$_{Sp}$ was much higher, with a value greater than 45.
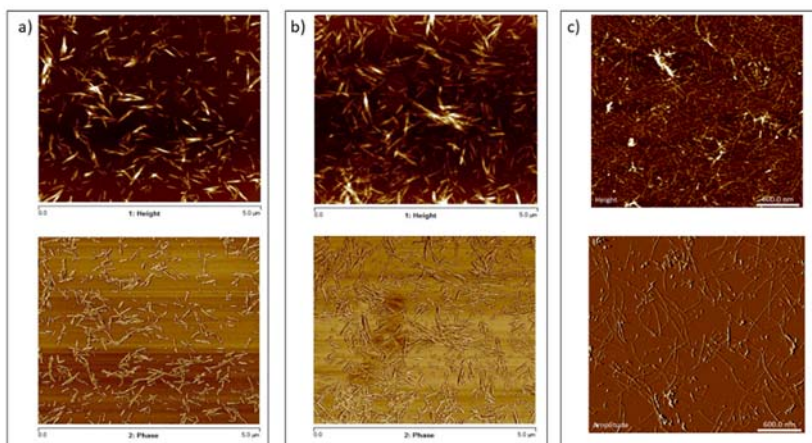
Figure IV- 6. Atomic force microscopy images in height (top) and phase (down) of a) α- NCH$_L$, b) α- NCH$_S$ and c) β-NCH$_{Sp}$.

4. CONCLUSIONS

The isolation of α-NCH$_L$, α-NCH$_S$ and β-NCH$_{Sp}$ was optimized by microwave-assisted extraction technique using the Box-Behnken design. The optimal isolation conditions were for α-NCH$_L$ of 1M HCl concentration, 10 min and 124.75 W; for α-NCH$_S$ 1 M, 14.34 min and 50.21 W and for β-NCH$_{Sp}$ 1M, 29.08 min and 54.08 W. The predicted values of the optimal yield isolation values were in accordance with the experimental results, being 85.30, 79.92 and 80.59 % for α-NCH$_L$,

α-NCH$_S$ and β-NCH$_{Sp}$, respectively. The characterisation of the samples demonstrated that chitin nanocrystals and nanofibers were successfully isolated. Moreover, the samples showed high C.I. % values and morphology similar to those obtained by conventional methods, such as acid hydrolysis, TEMPO-mediated oxidation or mechanical treatments. In addition, the reaction time was considerable reduced, with microwave-assisted extraction. Depending of the chitin source, the time can be reduced from 90-180 min using conventional chemical acid hydrolysis to 10-30 min and the HCl concentration can be decresed from 3M to 1M using microwave-assisted extraction.

Overall, the obtained data showed that nanocrystals and nanofibres could be obtained from different chitin sources by using an eco-friendly alternative like microwave irradiation technique. Such nanochitin samples could be used in different nanotechnologies and nanomaterials namely hydrogels, foams, porous scaffolds and polymeric nanocomposites.

PART IV: **RESULTS AND DISCUSSION**

A.*Extraction of nanochitin and essential oils*

Chapter 2

Microwave-assisted extraction of Curcuma longa L. oil: Optimization, chemical structure and composition, antioxidant activity and comparison with conventional Soxhlet extraction

Abstract

The curcuma root (*Curcuma longa* L.) is a very important plant in gastronomy and medicine for its unique properties namely antiseptic, anti-inflammatory, antimicrobial and antioxidant. Conventional methods for the extraction of curcuma oil require long extraction times and high temperatures that can degrade the substances. Therefore, the objectives of the present study were: (i) first, to optimize the extraction yield of curcuma oil by applying a Box-Behnken experimental design using surface response methodology to the Microwave-Assisted Extraction (MAE) technique (the independent variables studied were reaction time (10 - 30 min), microwave power (150 - 200 W) and quantity of ratio (w/v) (curcuma powder/ethanol, (1:20-1:5)); and, (ii) second, to assess the Total Phenolic Content and their antioxidant activity of the oil (at the optimum conditions point) and compare with the conventional Soxhlet technique. The optimum conditions for the MAE were found to be 29.99 min, 160 W and 1:20 w/v to obtain an optimum yield of 10.32 %. Interestingly, the oil extracted by Microwave-Assisted Extraction showed higher total phenolic content and better antioxidant properties than the oil extracted with conventional Soxhlet technique. Thus, it was demonstrated that the method applied for extraction influences the final properties of the extracted *Curcuma longa* L. oil**.**

1. INTRODUCTION

The curcuma or turmeric root (*Curcuma longa* L.) is an herbaceous plant belongs to *Zingiberaceae* family. The cultivation is widespread in tropical and subtropical regions, especially in Asia, being India and China the greatest producers [160–162]. Turmeric is known since antiquity and is of great importance worldwide in different applications namely in gastronomy as a condiment, in the textile industry as a dye and in medicine as anti-inflammatory [163,164], anti-cancer [165], or in the treatment of Alzheimer's disease [166,167]. It is also used as antiseptic [161], antioxidant [168], antiviral [169], antimicrobial [163,164], as well as insect repellent [170,171].

This is mainly due to the presence of the oleoresins of turmeric, which are a mixture of curcuminoids and essential oils. Curcuminoids are yellow pigments whose main compounds are curcumin (70-75%), demethoxycurcumin (10-20%) and bisdemethoxycurcumin (5-10%) and represent 2-9% of active components in turmeric [161,172,173]. Essential oils, that represent 3-5% of active compounds, are aromatic, volatile liquids with ar-turmerone as major compound which is a class of sesquiterpenoid cyclic ketones [162,172,174].

Due to their great importance in several applications, different extraction approaches have been developed. These compounds are usually extracted by steam distillation, hydrotrope, hot and cold percoxation, sohxlet and alkaline solution, which are known as conventional methods [161,175,176]. Nevertheless, these methods request high energy, temperature and solvent consumption, in addition to long reaction times leading consequently to the degradation of many compounds and low yields [161,177]. Therefore,

eco-friendly alternatives including ultrasound assisted extraction, supercritical fluids mainly through supercritical carbon dioxide and microwave assisted extraction (MAE) have been studied [126,176,178,179].

Among them, MAE technique has proven to be a good alternative for the extraction of bioactive compounds from plants due to the low energy and solvent consumption, short reaction times and high extraction yields. In 2011, Wakte and co-authors compered the efficiency of different extraction techniques, including MAE, Soxhlet, ultra-sonic and supercritical CO_2 assisted extraction in terms of yield. In this work, they demonstrated that MAE technique was more efficient for the curcumin extraction from powdered *C. longa* rhizomes [176].

For the purpose of optimizing complex experimental processes with many factors, response surface methodology (RSM) is a useful multivariate technique. The RSM is a mixture of statistical and mathematical modelling techniques, evaluating the effect of several independent variables with a view to determine the optimal value for the desired product. This methodology is very useful since the regression equations of the variables under study are obtained, as well as the responses in the desired ranges. In addition, the relationships between the dependent and independent variables can be observed by the use of contour plots [180].

Herein, we go a step further: first, by optimizing the MAE conditions using response surface methodology. In addition, a Box-Behnken design (BBD) is employed to investigate the effects of the microwave power, ratio w/v *Curcuma longa* L. powder/EtOH, and

extraction time; and second, by comparing the yield, total phenolic content and the antioxidant properties of *Curcuma longa* L. oil extracted by MAE and Soxhlet.

2. MATERIALS AND METHODS

The pre-treatment of *Curcuma longa* L. root is explained in **PART III** and the reagents are shown in Appendix B.

2.1. Extraction of *Curcuma longa* L. oil

2.1.1. *Microwave-assisted extraction (MAE) - experimental design*

2.1.1.1. *General experimental procedure*

The MAE extraction of *Curcuma longa* L. oil was carried out as described in **PART III**. The conditions of the experimental design are shown in Tables IV-5 and IV-6. The extraction yield was calculated gravimetrically and the optimum point was performed in triplicate.

2.1.1.2. *Experimental design and determination of the optimal extraction conditions*

RSM was applied to analyse the effect of the reaction time (t, min), the microwave power (P, W) and ratio w/v (*Curcuma longa* L./EtOH) (R, g/mL) on the extraction yield (Y). For the experimental design and optimisation, a BBD was used, consisting of 15 experiments of which 3 correspond to the replicates in the central point. The experimental design was prepared and the optimal conditions were predicted with the desirability function of the Statgraphics Centurion version XV software (StatPoint Technologies INC., Warrento, VA, USA).

Table IV-5 shows the experimental variables (independents and dependents) used in the design and their values or range.

Table IV-5. List of the experimental variables involved in the microwave-assisted extraction of Curcuma longa L. oil.

Variables		Nomenclature	Units	Value or range
Independents	Reaction Time Microwave	t	min	10-30
	Power	P	W	150-250
	Ratio w/v (*Curcuma longa* L./EtOH)	R	g/mL	1:20-1:5
Dependent	Curcuma oil yield	Y	%	-

The regression analysis function of Microsoft Excel Add-In (USA) was implemented to adjust the experimental data obtained in the experimental design. To adjust the experimental data, a second order polynomial equation was employed:

$$y_j = \beta_0 + \sum_{i=1}^{k} \beta_i X_i + \sum_{i=1}^{k} \beta_{ii} X_i^2 + \sum \sum_{i<j=1}^{k} \beta_{ij} X_i X_j + \varepsilon \qquad \text{(IV-3)}$$

where Y is the dependent variable *Curcuma longa* L. oil yield (%), K corresponds to the number of factors (3), ε is the experimental error, β_0, β_i, β_{ii} and β_{ij} indicate the regression coefficient estimated from the experimental results by the method of minimum squares, and Xi and

Xj are the dimensionless ones and indicate the standardised independent variables (variation range from -1 to 1).

The model was validated by evaluating the lack of fit, the coefficient of determination (R^2), the importance of the regression coefficients, the value of the F test using analysis of variance (ANOVA).

2.1.2. Soxhlet extraction

The Soxhlet extraction (conventional method) was done following [126] method with slight modifications. For the extraction, 5 g of *Curcuma longa* L. powder were put in 150 mL of EtOH at boiling temperature (78 °C) for 6 h. After extraction, the solvent was then removed using rotary vacuum evaporator at 50 ºC until a constant weight in order to obtain the extraction yield gravimetrically. The experiments were done in triplicate.

2.2. Characterization of the *Curcuma longa* L. oil

The *Curcuma longa* L. oil samples obtained by MAE in the optimum point and by Soxhlet extraction were characterized in terms of chemical structure and composition (ATR-FTIR, GC/MS) as well as their total phenolic content and antioxidant properties (DPPH, FRAP and ABTS) for 24 h. The methodology was describe in **PART III**.

2.3. Statistical analysis

The statistical analysis was performed using IBM SPSS software (Version 24, Inc. Chicago, IL, USA). One-way analysis of variance (ANOVA) was used to validate the experimental design and to study

the differences between the MAE and Soxhlet extraction for each analysed parameter. The values of the significant differences were identified by Duncan's multiple range test and significance was accepted at α= 0.05. The results were shown as mean ± SD (standard deviation) by performing 3 measurements for each analysis.

3. RESULTS AND DISCUSSION
3.1. MAE based experimental design
3.1.1. *Optimization of the Curcuma longa L. oil extraction*

Conventional methods to extract *Curcuma longa* L. oil require long reaction time and high-energy consumption. These conditions often cause degradation of the extracted compounds and low yields. Therefore, it is important to use other extraction techniques, in particular MAE and optimize the extraction conditions to obtain better yields while maintaining the quality of the extracted samples. For this purpose, a BBD with the RSM was used to optimise the extraction yield of *Curcuma longa* L. oil. In the present study, the independent variables were the reaction time (t, min), the microwave power (P, W) and the ratio w/v (R, g/mL). The dependent variable was the yield of the extracted *Curcuma longa* L. oil (Table IV-5).

Table IV-6 lists the experiments randomly determined by Statgraphics Centurion software and the experimental results of the extraction yield (dependent variable).

Table IV-6. Box-Behnken experimental design and operational conditions represented in accordance of dimensional and dimensionless independent variables t (time, min) (X_1); P (power, W) (X_2); R (ratio w/v, g/mL) (X_3) and experimental response (extraction yield by microwave-assisted extraction, $Y_{C\text{-}MAE}$).

Experiments	Independent Variables			Normalized Variables			Extraction yield
	t (min)	P (W)	R (g/mL)	X_1	X_2	X_3	$Y_{C\text{-}MAE}$ %
1	20	200	1:8	0	0	0	9.50
2	30	150	1:8	1	-1	0	8.59
3	30	200	1:5	1	0	1	4.00
4	10	150	1:8	-1	-1	0	5.58
5	30	250	1:8	1	1	0	6.92
6	10	200	1:5	-1	0	1	7.06
7	10	200	1:20	-1	0	-1	7.41
8	20	250	1:20	0	1	-1	4.48
9	20	200	1:8	0	0	0	9.35
10	10	250	1:8	-1	1	0	6.12
11	20	150	1:20	0	-1	-1	10.84
12	20	250	1:5	0	1	1	3.03
13	30	200	1:20	1	0	-1	9.27
14	20	200	1:8	0	0	0	9.47
15	20	150	1:5	0	-1	1	6.77

The validation of the model was determined by the regression coefficient (R^2) explaining the total variations of the model and was reinforced by Fisher's F-test obtained by ANOVA [181]. As showed in Table IV-7, the value of R^2 was 0.82, which means that only 0.18% of the total variances are not explained by the selected model. Regarding Fisher's F-test, the high F values confirm a good fit of the model considering that the experimental F (2.55) was higher than the critical F (0.16) with 9 degrees of freedom. This indicates that the values obtained for the proposed model are appropriate to describe the interactions between the different variables selected.

Concerning the regression coefficients, the variables microwave power, ratio w/v (*Curcuma longa* L. powder/EtOH) and the quadratic of power significantly influenced the oil extraction yield (Table IV-7). Power and ratio w/v *(Curcuma longa* L./EtOH) showed an influence with a confidence interval of 95 %, while in the case of quadratic power it was 90 %. Through the obtained regression coefficients, the second-degree polynomial equation for the extraction yield has been calculated as shown below:

$$Y_{C\text{-}MAE}\ \% = 9.44 + 0.32X_1 - 1.40X_2 - 1.39X_3 - 0.99X_1{}^2 - 0.55X_1X_2 -$$
$$1.23X_1X_3 - 1.65X_2{}^2 + 0.66X_2X_3 - 1.51X_3{}^2 \qquad\qquad (IV\text{-}4)$$

Table IV-7. Regression coefficients and statistical parameters of the optimization of Curcuma longa L. oil extraction by MAE.

Coefficients	$Y_{C\text{-}MAE}$
b_0	9.44
b_1	0.32
b_2	-1.40[a]
b_3	-1.39[a]
b_{12}	-0.55
b_{13}	-1.23
b_{23}	0.66
b_{11}	-0.99
b_{22}	-1.65[b]
b_{33}	-1.51
R^2	0.82
F-exp	2.55
F-critical	0.16
Significance level (%)	84.24

F-critical for 9 degrees of freedom.
[a]Significant coefficients at the 95% confidence level.
[b]Significant coefficients at the 90% confidence level.

3.1.2. *Effect of independent variables on extraction yield response*

As shown in Table IV-7 the extraction yields of *Curcuma longa* L. oils were found to be in the range of 3.03 % (exp.12) and 10.84 % (exp. 11).

The surface plot (Figure IV-7- A), B) and C)) presents the interactions between the independent variables (t, P and R) and the extraction yield of *Curcuma longa* L. oil by MAE ($Y_{C\text{-}MAE}$).

Figure IV-7-A shows the influence of the independent variables microwave power (X_2) and ratio w/v (*Curcuma longa* L. powder/EtOH) on the extraction yield for a fixed extraction time at a mean value ($X_1=0$). This surface plot shows how the extraction yield increases when P (X_2) and R (X_3) decrease. In this design, the extraction yield reaches a maximum when microwave power (X_2) is around 155 W and ratio w/v approximately 1:20. However, these parameters rise above these values when yield decreases which reaffirms the negative quadratic effect of P^2 (Table IV-7). As listed in Table IV-7, these two independent variables have an influence on the model.

Figure IV-7-B displays the extraction yield as a function of time (X_1) and ratio w/v (*Curcuma longa* L. powder/EtOH) ($X3$) keeping the microwave power constant at a midpoint value ($X2=0$). The progressive decrease of ratio w/v and the increase of extraction time resulted in a positive effect on the extraction yield of *Curcuma longa* L. oil. The extraction yield obtained a maximum value at around 10 %,

when high reaction times and a minimum amount of *Curcuma longa* L. powder were used.

Figure IV-7-C presents the response surface for extraction yield as a dependence of reaction time (X_1) and microwave power (X_2) for a fixed value of ratio w/v (*Curcuma longa* L. powder/EtOH) ($X_3 = 0$). This curve discloses a highest extraction yield when the extraction time increases and the microwave power is decreases. This trend is explained by the linear and quadratic negative contribution of power (Table IV-7).
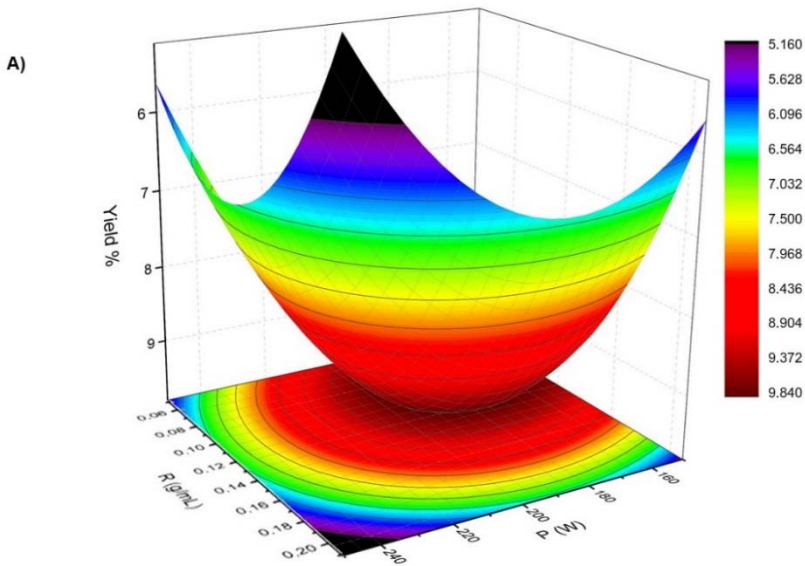
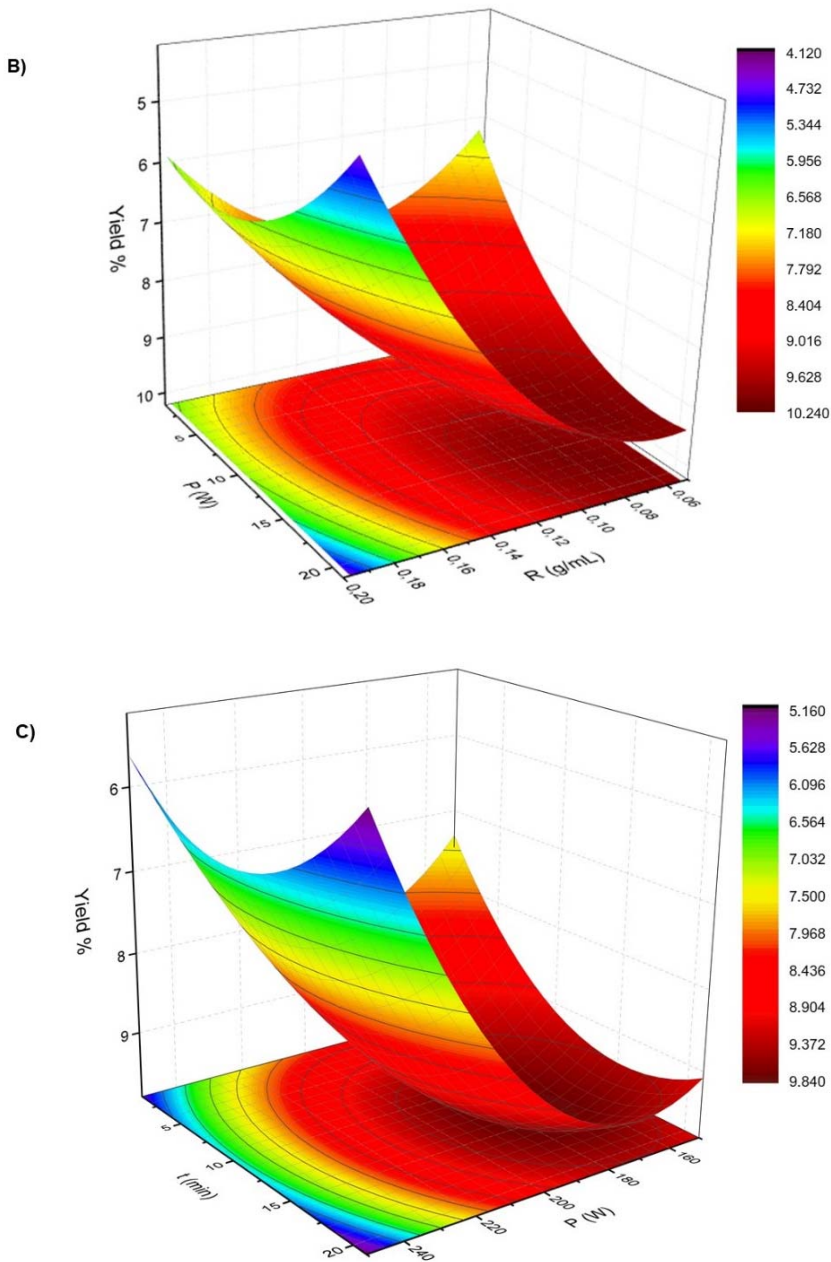*Figure IV-7. Curcuma longa L.* oil extraction yield as a function of: A) P (power, W) and R (ratio w/v, *Curcuma longa L.* powder/EtOH, g/mL) at a fixed t (time, min, $X_1=0$); B) t (time, min) and R (ratio w/v, ratio *Curcuma longa L.* powder/EtOH, g/mL) at a fixed P (power, W, $X_2=0$); C) t (time, min) and P (power, W) at a fixed R (ratio w/v, ratio *Curcuma longa L.* powder/EtOH, g/mL, $X_3=0$).

3.2. Comparison of MAE and Soxhlet extraction yields

The objective of the BBD was to optimize the different extraction conditions *i.e.* extraction time, microwave power and *Curcuma longa* L. powder to obtain the maximum extraction yield of *Curcuma longa* L. oil. The expected optimum point values were calculated using Statgraphics Centurion XV software and experimentally verified in triplicate in order to validate the model (Table IV-8).

Table IV-8. The dimensionless and dimensional optimum points and the predicted and experimental extraction yield by microwave-assisted extraction (Y_{C-MAE}) and the extraction yield by the Soxhlet method (Y_{C-S}). The experimental extraction yields were mean ± standard deviation of three replications (n=3).

	MAE					Soxhlet
X_1 (t, min)	X_2 (P, W)	X_3 (R, g/mL)	Y % (predict value)	Y_{C-MAE} % (experimental value)	Y_{C-S} % (experimental value)
0.99 (29.99)	-0.79 (160.41)	-0.99 (5.00)	10.92	10.32 ± 0.69	8.44 ± 0.17

As listed in Table IV-8, the optimum extraction yield obtained experimentally was 10.32 ± 0.69 %, while the predicted extraction yield calculated by the software was of 10.92 %. The proximity of these two values confirms the validation of this BBD. This optimum extraction yield of 10.32 ± 0.69 % was attained using 1:20 g/mL ratio of

Curcuma longa L./EtOH for 30 min and with a microwave power of 160 W.

From the Soxhlet extraction technique, an yield value of 8.44 ± 0.17 % was obtained (Table IV-8) using 5g of *Curcuma longa* L. in 150 mL ethanol for 6 h. Vijayan et al., obtained similar *Curcuma aromatica* extraction yield (7.48%) by using the same extraction technique and solvent [182]. Priyanka et al., observed lower extraction yields of *Curcuma longa* (5.95 %) using non-polar solvents like n-hexane for 24 h [28].

Comparing the MAE with the conventional Soxhlet technique (Table IV-8), the first technique showed better extraction yield of *Curcuma longa* L. oil together with a reduction of the extraction time (from 6 h with Soxhlet method to 30 min with MAE) and lower energy consumption. Wakte and co-authors, compared different techniques such as ultra-sound, Soxhlet, supercritical CO_2 and MAE, they have observed high extraction yields of curcuminoid compounds with shorter times using the MAE technique [176].

In the next sections, the chemical structure and composition of the *Curcuma longa* L. oil obtained by the two techniques are assessed and compared as well as the amount of total phenolic content and antioxidant properties.

3.3. Characterization of the extracted *Curcuma longa* L. oil

3.3.1. *Chemical structure and composition*

Figure IV-8 displays the ATR-FTIR spectra of *Curcuma longa* L. oils obtained by MAE and Soxhlet methods. The two samples

exhibited identical spectra showing that similar compounds were obtained by both methods. The two samples showed a broad band around 3340 cm^{-1} corresponding to O-H stretching. The -CH$_3$ and -CH$_2$ stretching vibrations were observed around 2967 and 2925 cm^{-1}, respectively [183,184]. The peak around 1680 cm^{-1} was attributed to C=O vibrations [184] and the peaks at 1624 cm^{-1} and 1600 cm^{-1} were assigned to the aromatic ring stretching (C=C) and to a mixture of C=C and C=O stretching, respectively [126,183,184]. The band at around 1430 cm^{-1} was ascribed to CH$_2$ bending, while the peak around 1377 cm^{-1} was assigned to CH$_3$ bending indicating the presence of curcuminoids [126]. The band observed near to 1034 cm^{-1} was attributed to C-OH stretching vibration [183]. The small peaks appearing around 879 cm^{-1} and 814 cm^{-1} were assigned to C-O vibrations and C-H vibrations out of the plane of the aromatic ring. These two peaks are important considering that they are characteristic of the species *Curcuma longa* L. [183,184].
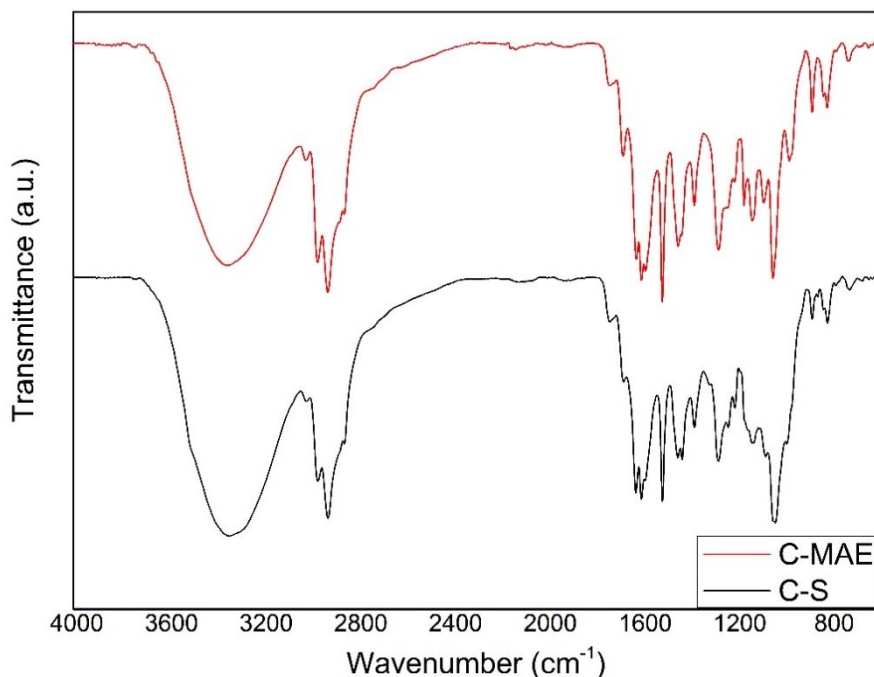
Figure IV-8. ATR-FTIR spectra of the Curcuma longa L. oil extracted with microwave-assisted extraction (C-MAE) and Soxhlet extraction method (C-S).

Table IV-9 summarizes the volatile components of *Curcuma longa* L. oil extracted by MAE and Soxhlet methods. The identification of the compounds was done by using the NIST library and the stat-of-the-art in this domain. Interestingly, the same compounds were obtained in almost the same proportions for both techniques. The main components obtained were Ar-turmerone (33.78 % MAE and 37.08 % Soxhlet), turmerone (20.12 % MAE and 18.15 % Soxhlet) and β-turmerone, known as curlone (20.05 % MAE and 19.22 % Soxhlet). These data were comparable to those reported before in the literature using different extraction techniques such as hydrodistillation,

different supercritical fluids and especially the use of CO_2 with co-solvents [126,162,177,185].

Table IV-9. Curcuma longa L. oil composition evaluated by GC/MS.

Component	MAE		Soxhlet	
	A (%)	RT (min)	A (%)	RT (min)
α-curcumene	0.55	18.8991	0.92	18.8993
Zingiberene	0.35	19.1652	0.54	19.1654
β-sesquiphellandrene	0.65	19.7682	0.95	19.7684
Ar-Tumerol	0.74	20.859	0.84	20.8592
p-cymene	1.52	21.329	1.48	21.3293
Zingiberenol	0.26	21.7725	0.32	21.6929
3-Ethyl-n-methylaniline	0.51	21.8434	0.44	21.8436
Ar-turmerone	33.78	22.3933	37.08	22.3935
Tumerone	20.12	22.4553	18.15	22.4555
Bisacurol	0.57	22.7657	0.25	22.7482
β-tumerone	20.05	22.9786	19.22	22.9788
(Z)-α-atlatone	0.52	23.1471	0.50	23.1473
(6R, 7R)-bisabolone	0.96	23.6437	1.00	23.6439
(E)-α-atlatone	3.01	24.0516	2.38	24.0519
(O)-Paradol	0.66	24.6902	0.94	25.6861
2-cyclohenen-1-on,6-[(1S)-1,5-dimethyl-3-oxo-4-hexen-1-yl]-3-*methyl*-(6S)	0.68	25.8697	0.67	25.8699

A: Area; RT: retention time; MAE: Microwave-Assisted Extraction; S: Soxhlet.

3.3.2. Total phenolic content and antioxidant activity

Table IV-10 shows the TPC and antioxidant activity data of the *Curcuma longa* L. oils obtained at the optimum point of the experimental design with the MAE and with the conventional Soxhlet extraction.

Interestingly, these data show that at the optimal point with MAE technique, higher phenolic compound content were obtained when compared with the Soxhlet method: 232.75 ± 0.31 and 140.72 ± 0.42 mg GAE/g *Curcuma longa* L. extracted oil for MAE and Soxhlet, respectively. These results were higher than those obtained by de Carvalho and co-authors (5018 mg GAE/100 g), that extracted *Curcuma longa* L. oil by supercritical fluid method with CO_2 and EtOH as co-solvent [186]. Patil et al., obtained similar values for turmeric extraction by using the Soxhlet method (143.67 mg GAE/g) [187].

The lower TPC with Soxhlet may be due to: (i) the long exposure (6 h) of the sample to high temperatures (solvent boiling temperature) and consequently degradation of the sample [188]; and (ii) the different of MAE and Soxhlet process; *i.e.*, the electromagnetic field generated in the MAE method induced high pressures leading to the cell walls disruption allowing a better diffusion of the substances [189,190]. Similar trends were reported by Sánchez-Reinoso and co-authors, that used the MAE and Soxhlet extraction method for the extraction of Sacha Inchi shell extracts [189]. Also, Pan et al., observed the same fact when extracting oil from *Osmanthus fragans* flower using MAE with deep eutectic solvents and reflux extraction with ethanol [191].

Table IV-10. Results of total phenolic content (TPC) and antioxidant activity (DPPH, FRAP and ABTS assays) of the Curcuma longa L. oil extraction by MAE (microwave-assisted extraction technique) and Soxhlet. Values were mean ± standard deviation (n=3). Superscript letters represent significant differences (Duncan's test, $p < 0.05$) between each assay with the two extraction methods.

	MAE	Soxhlet
TPC (mg GAE/g)	232.75 ± 0.31[a]	140.72 ± 0.42[b]
DPPH (mg TE/g)	64.71 ± 0.49[a]	49.00 ± 0.33[b]
FRAP (mg TE/g)	255.66 ± 0.24[a]	73.37 ± 0.18[b]
ABTS (mg TE/g)	79.82 ± 0.03[b]	71.42 ± 0.04[a]

GAE: gallic acid equivalents; TE: Trolox equivalent.

The antioxidant activity results from a synergy among the different phenolic compounds. Because the *Curcuma longa* L. antioxidant activity results from different mechanisms, in the present study, three methods were employed (DPPH, FRAP and ABTS) to compare the two extraction methods.

Among the three techniques, DPPH showed the lowest antioxidant activity. Similar results were observed previously, in the extraction of *Curcuma longa* oil by Soxhlet *vs.* supercritical fluids with CO_2 and ethanol [186]. Like previously observed in oil extracted from seeds and flowers [186,189], with the FRAP assay a considerable difference was detected in the antioxidant activity between the samples extracted by MAE (255.66 ± 0.24 mg GAE/g) and Soxhlet (73.37 ± 0.18 mg GAE/g) (Table IV-10). Finally, ABTS method is considered excellent for the evaluation of the antioxidant activity of several substances and can be applied to both liposoluble and

hydrosoluble compounds. The results obtained for the ABTS test with MAE and Soxhlet, even if quite similar, showed a significant difference $p < 0.05$ between both techniques. Other authors showed lower values of ABTS in the extraction of *Curcuma longa* using supercritical fluids CO_2 and ethanol [186] compared with our data.

The differences in the values between the antioxidant assays could be due to the different mechanisms involved. The DPPH assay measures the ability of a substance to donate a hydrogen to the DPPH* free radical, whereas the FRAP method is based on the measurement of the reduction of the ferric ion-TPTZ complex. In the ABTS assay, the activity is based on the capacity of the *Curcuma longa L.* oil to decrease the amount of $ABTS^{\bullet+}$ cation radical preformed in the solution. This reducing capacity of *Curcuma longa* L. oil is an important indicator of their antioxidant capacity [191].

Taking into account the obtained data, it can be concluded that the MAE technique allows having samples with higher TPC and this phenolic extract exhibited higher antioxidant properties comparing with traditional methods.

4. CONCLUSIONS

The optimization of the extraction yield of *Curcuma longa* L. oil was carried out by Microwave-Assisted Extraction using the Box-Behnken experimental design with response surface methodology. The optimum conditions for the extraction were 29.99 min, 160 W and a ratio of 1:20 g/mL, *Curcuma longa* L./EtOH and the yield of extracted oil was 10.32 ± 0.69 %. This yield value was higher than that obtained by the conventional Soxhlet method (8.44 ± 0.17 %).

It was also concluded that the treatments applied for the extraction of the *Curcuma longa* L. oil influenced the amount of Total Phenolic Content and their antioxidant activity. The data revealed higher phenolic content and higher antioxidant activity (with the three applied assays: DPPH, ABTS and FRAP) in *Curcuma longa* L. oil when it was extracted using the MAE method.

Therefore, these results demonstrated that MAE is a viable and more environmentally friendly method for the extraction of *Curcuma longa* L. oil.

B. Materials development
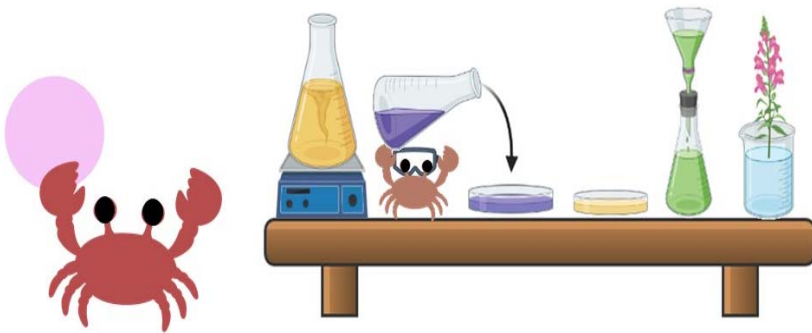
PART IV: RESULTS AND DISCUSSION

B.Materials development

Chapter 3

Effect of deterpenated Origanum majorana L. essential oil on the physicochemical and biological properties of chitosan/ β-chitin nanofibres nanocomposite films

Abstract

In this work, the effect of three deterpenated fractions from *Origanum majorana* L. essential oil on the physicochemical, mechanical and biological properties of chitosan/ β-chitin nanofibres-based nanocomposite films was investigated. In general, the incorporation of *Origanum majorana* L. original essential oil or its deterpenated fractions increases the opacity of the nanocomposite films and gives them a yellowish color. The water solubility decreases from 58 % for chitosan/ β-chitin nanofibres nanocomposite film to around 32 % for the nanocomposite films modified with original essential oil or its deterpenated fractions. Regarding the thermal stability no major changes were observed, and the mechanical properties decreased. Interestingly, data shows differences on the biological properties of the materials depending on the incorporated deterpenated fraction of *Origanum majorana* L. essential oil. The nanocomposite films prepared with the deterpenated fractions with high concentration of oxygenated terpene derivatives show the best antifungal activity against *Aspergillus niger*, with a fungal growth inhibition of around 85.90 %. Nonetheless, the only nanocomposite film that does not presents cytotoxicity on the viability of L929 fibroblast cells after 48 and 72h is the one prepared with the fraction presenting the higher terpenic hydrocarbon content (87.92%). These results suggest that the composition of the deterpenated fraction plays an important role in determining the biological properties of the nanocomposite films.

1. INTRODUCTION

Essential oils (EOs) are plants' secondary metabolites, composed of a mixture of low molecular weight and volatile compounds which can be extracted from different parts of the plant including barks, roots, seeds, flowers and leaves [54,115]. Nowadays, EOs have shown a particular interest in the development of bioactive materials because of their intrinsic properties namely antioxidant and antimicrobial activities [115,192].

EOs are mainly composed of terpenes and terpenoids, which are responsible for their biological activity, and are largely used in packaging, medicine, food and cosmetics sectors. The minor group of the EOs are terpenoids (oxygenated terpene derivatives). They are composed of alcohols, ketones and aldehydes, and are responsible for the organoleptic characteristics of essential oils. Terpenoids contribute to the protection of plants against insects, herbivores, fungal diseases and infestations [193,194]. On the other hand, the terpenes (simple hydrocarbons molecules) contribute to the flavor, fragrance, and color of plants. These compounds can easily degrade into undesirable compounds under the influence of light, heat or oxygen, among others decreasing the quality and its market value. For this reason, is important carried out a deterpenation of the essential oils to separate the terpenes from the oxygenated terpene derivatives (terpenoids) to improve the stability and the bioactive properties of EOs [195]. Deterpenation has been done using different methods namely vacuum distillation, solvent extraction, membrane technologies and extraction with ionic liquids [193–199].

Among the EOs, the one which is extracted from the *Origanum majorana L.* plant is one of the most promising due to its excellent antioxidant, antimicrobial, antifungal and antiparasitic properties and, consequently, high economic and industrial importance. *Origanum majorana L.* belongs to the *Lamiaceae* family and is distributed in all Mediterranean region and Asia. It has been used since ancient times for food as a condiment and spice. Recently, Ben Salha and co-workers, performed the deterpenation of the *Origanum majorana* L. EO and showed that the deterpenated fractions presented low antioxidant activity, but a good inhibition against *Aspergillus niger* [200].

These unique properties make EOs excellent candidates for several industrial sectors like packaging, medicine, food and cosmetics [192,201]. To limit their instability and preserve their bioactivity, EOs and/or their fractions need to be encapsulated/incorporated in a matrix, in particular polymeric matrices for the development of multifunctional materials [192,201]. Among the bio-based matrices, chitosan-based matrices can be potential candidates for the incorporation of EOs as already demonstrated with *Carum copticum, Thymus moroderi, Thymus piperella* and *Cinnamon verum* essential oils [36,37,107]. Chitosan (poly-β-(1/4)-N-acetyl-D-glucosamine, CS) is a cationic polymer obtained from the deacetylation of the chitin, which is mainly extracted from the exoskeleton of crustaceans. CS presents a great interest for the food industry and packaging application because of its intrinsic properties namely low toxicity, biocompatibility, biodegradability and bioactive activity [125,202]. However, as chitosan has limited mechanical properties, the incorporation of nanofibres

like nanocellulose, lignocellulose nanofibres and chitin nanofibers and nanocrystals are often required to reinforce the matrix [10,203]. In our previous studies, we have shown the improvement of the biological and mechanical properties of bio-based matrices by the incorporation of nanochitin [11,136,192,204–206].

In this context, the objective of this research is to assess the effect of different *Origanum majorana* L. deterpenated oil fractions on the final properties, in particular antifungal activity and cell viability, on chitosan/β-chitin nanofibres nanocomposite films.

2. MATERIALS AND METHODS
2.1. Materials

The reagents used are shown in Appendix B.

β-chitin powder (from squid pen) was supplied by Mahtani Chitosan PVT Ltd., India. β-chitin nanofibres (β-CHNF) were isolated *in-house* by acid hydrolysis using the MAE (Discover system, CEM, USA) under the following conditions: 1M of HCl for 29.08 min at 79.08 W (optimum point obtained in **Chapter 1**).

Spider crab shells wastes Crab shell waste was used to extract CS. The method followed is explained in **PART III**.

The essential oil (EO) and the 3 deterpenated fractions (F1, F2 and F3) of *Origanum majorana* L. (OM) were extracted by reduced pressure steam distillation as a function of boiling temperature. F1 and OM contained higher percentages of total terpenes hydrocarbons 87.92 % and 50.70 %, respectively; and 12.05 % and 47.36 %, respectively of total oxygenated terpene derivatives. On the other hand, the deterpenated fractions F2 and F3 were composed of 12.90 %

and 8.98 % of total terpenes hydrocarbons, respectively; and 85.06 % and 88.86 % of total oxygenated terpene derivatives, respectively, as previously describe [200].

2.2.   Preparation of nanocomposite films

CS (1 % w/v) was dissolved in acetic acid solution (1 % v/v) overnight with stirring, and the solution was then filtered to remove potential impurities. Afterwards, 0.16 % v/v glycerol (CS-based) was added to chitosan solution as a plasticizer and the mixture was stirred for 5 min at 14 600 rpm at room temperature using an Ultra-Turrax (Heidolph Silent Crusher M., Germany). After that, Tween 20 (0.016 % v/v, CS-based) was added as an emulsifier to assist essential oil dispersion in the film-forming solutions. Then, oil fractions (0.2 5 % v/v F1, F2 and F3, CS-based) and essential oil (0.25 %v/v OM, CS-based) were added and mixed at 14 600 rpm for 10 min. Finally, β-CHNF (0.5 %w/v, CS-based) was added to each solution and mixed for 10 min at 14 600 rpm. All suspensions were degassed to remove the air bubbles. The films were prepared by casting-method overnight at 30 ºC using 50 mm diameter Petri dishes. The nanocomposites were kept in a conditioning cabinet at 50 ± 5 % relative humidity and 25 °C before used. A control film was prepared without the addition of *Origanum majorana* L. essential oil or deterpenated fractions. Table IV-11 shows the samples identification and composition.

Table IV-11. Identification and composition of the nanocomposite films.

Samples	Samples identification	β-CHNF (% w/v)*	Fractions and essential oil (% v/v)*
Chitosan + β-CHNF	CSNF	0.5	-
Chitosan + β-CHNF + F1	CSNF-F1	0.5	0.25
Chitosan + β-CHNF + F2	CSNF-F2	0.5	0.25
Chitosan + β-CHNF + F3	CSNF-F3	0.5	0.25
Chitosan + β-CHNF +OM	CSNF-OM	0.5	0.25

% v/v and % w/v, chitosan (CS) based

The nanocomposite films were characterized in terms of physicochemical, morphology, thermogravimetric analysis and mechanical properties as well as biological properties such as antifungal and cytotoxicity assays. The techniques employed are described in **PART III**.

2.3. Statistical analysis

The statistical analysis was carried out using a one-way analysis of variance (ANOVA) by SPSS Statistical software (Version 24, Inc. Chicago, IL, USA). The significant difference values were calculated by Duncan's multiple range test. Results are given as mean ± standard deviation and p values < 0.05 were statistically significant.

3. RESULTS AND DISCUSSION

3.1. Physicochemical characterization

Figure IV-9 shows the general aspect of the nanocomposite films. All samples are homogeneous, translucent and with a slightly yellowish tone (Table IV-12 & 13). The incorporation of the OM and its fractions slightly affected the thickness of the films ($p < 0.05$), as listed in Table IV-2. This could be due to the increase of the density as a result of the formation of intramolecular interactions between β-CHNF, CS and essential oil [207].
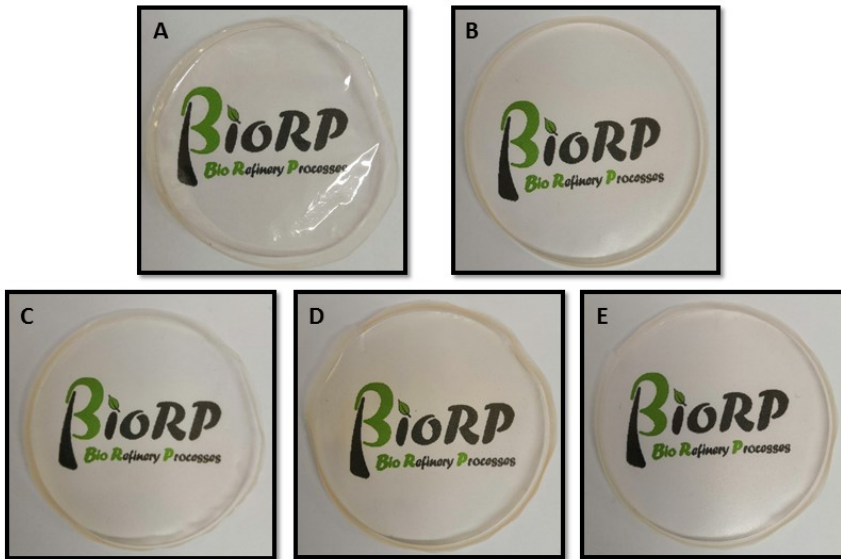

Figure IV-9. The general appearance of the films. A) CSNF; B) CSNF-F1; C) CSNF-F2; D) CSNF-F3; E) CSNF-OM.

Table IV-12. Thickness and color parameter of the nanocomposite films.

Samples	Thickness (μm)	ΔE	L*	b*	a*
CSNF	41.33 ± 1.97[a]	1.73 ± 0.56[a]	91.83 ± 0.69[a]	6.02 ± 0.69[a]	1.23 ± 0.11[a]
CSNF-F1	45.00 ± 3.03[b]	6.68 ± 1.05[b]	90.20 ± 0.23[a]	11.02 ± 0.51[b]	1.35 ± 0.12[a]
CSNF-F2	41.83 ± 5.34[a]	2.21 ± 1.05[a]	91.95 ± 0.47[b]	6.84 ± 1.07[a]	0.91 ± 0.06[b]
CSNF-F3	44.33 ± 4.41[bc]	2.85 ± 2.21[a]	91.42 ± 1.12[a]	7.13 ± 2.09[a]	1.23 ± 0.36[a]
CSNF-OM	42.83 ± 5.19[c]	1.94 ± 0.83[a]	91.97 ± 0.33[b]	6.56 ± 0.83[a]	0.94 ± 0.05[b]

The values were average ± standard deviation (thickness n = 6; color parameter n = 10). Different letters in the same column depict significant differences between samples (Duncan`s test, $p < 0.05$).

3.1.1. Color properties

The color parameters of the nanocomposite films were also assessed, the data listed in Table IV-12 show an L* (lightness/darkness) of around 90 for all samples. Similar results were obtained by Bonilla et al. using chitosan/gelatin as matrix and eugenol and ginger oil [100]. The a* parameter of all films was quite similar with a value of around 1 and with a positive sign, indicating a tendency toward reddish color ($p < 0.05$). The yellowness effect given by parameter b*, was also very similar for all the films, except for the CSNF-F1 films (11.02 ± 0.51) ($p < 0.05$). The yellowish color is attributed to the color of the oils themselves [100,208]. Consequently, the total color (ΔE) of the films was different for the CSNF-F1 film, resulting in a film with more color. In general, the films with OM and its fractions

showed higher values of total color ($p < 0.05$). This tendency was also observed in previous studies using chitosan films with eucalyptus extract [209] and with apple peel extracts [103].

3.1.2. *Transmittance and opacity*

The opacity of the nanocomposite films was calculated by using equation III-7 (see **PART III**) taking into account the absorbance at 600 nm and the thickness (Table IV-13). As expected, the lowest opacity value was observed for the CSNF film with a value of 4.76 ± 0.42. The opacity increased with the incorporation of OM and its fractions. The nanocomposite films with the deterpenated fractions showed the highest opacity (7.47 ± 0.77 for CSNF-F2 and 7.90 ± 0.35 for CSNF-F3). These values were observed in accordance with the transmittance of the films (Figure IV-10). Notably, it was observed that films with essential oils showed higher opacity [95,100,192].

Table IV-13. MC (moisture content), WS (water solubility) and opacity of nanocomposite films.

Samples	MC %	WS %	Opacity
CSNF	54.98 ± 2.48[a]	57.87 ± 4.78[a]	4.76 ± 0.42[a]
CSNF-F1	40.41 ± 7.96[b]	32.53 ± 1.30[b]	7.08 ± 0.78[b]
CSNF-F2	45.20 ± 9.03[b]	34.56 ± 3.07[b]	7.47 ± 0.77[b]
CSNF-F3	53.79 ± 1.48[b]	49.27 ± 3.60[b]	7.90 ± 0.35[b]
CSNF-OM	42.72 ± 7.45[b]	32.37 ± 4.87[b]	6.61 ± 0.53[b]

The values were mean ± standard deviation (MC, WS and opacity n = 3). Different letters in the same column indicate significant differences between nanocomposite films (Duncan`s test, $p < 0.05$).

The transmittance of the films was assessed from 700 to 250 nm (Figure IV-10). The films with OM or fractions presented transmittances around 35 and 50 % in the visible light region. Interestingly, in the ultraviolet region, the transmittance of all films was recorded as below 20% (350-250 nm), and CSNF-F1 nanocomposite film blocks UV light in the range of 300-250 nm. CSNF-F1 nanocomposite film presents a higher percentage of terpenes. Similar results were reported by Sahraee et al. [42], who employed corn oil in gelatin films incorporated with nanochitin. Wu et al. [120] also showed that the rising concentration of oregano oil in chitosan films decreased the transmittance almost completely in the UV range.
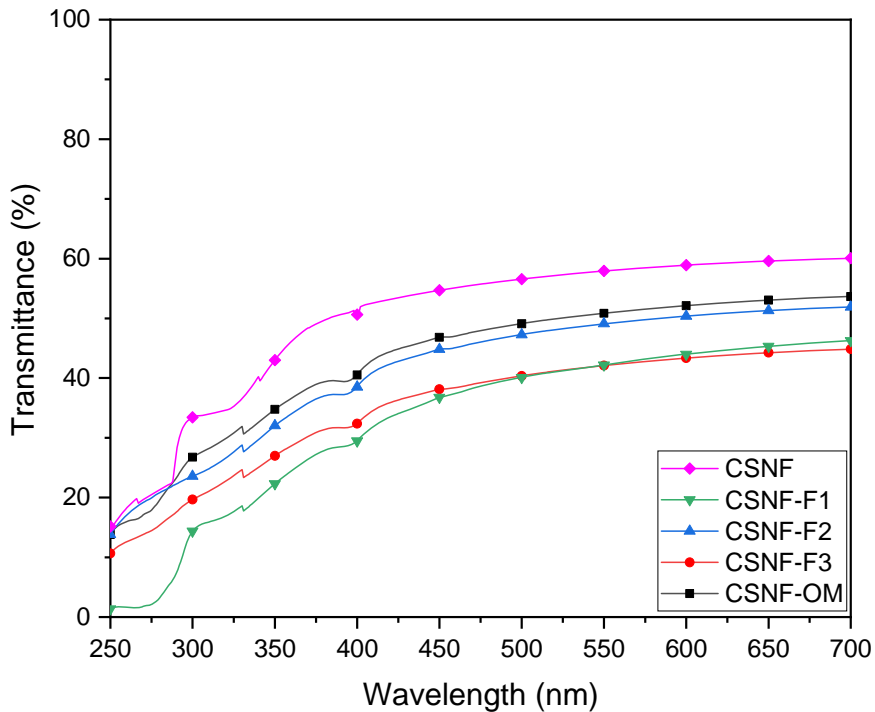

Figure IV-10. UV-Vis spectra (700- 250 nm) of the nanocomposites films.

3.1.3. *Moisture content and water solubility*

The effect of the incorporation of the deterpenated fractions of *Origanum majorana L.* essential oil on the moisture content, solubility and hydrophobicity of chitosan/ β-chitin nanofibres nanocomposite films, were also assessed. The moisture content of the nanocomposite films is listed in Table IV-13. As expected, the addition of the essential oil resulted in a decrease in the moisture content, and no significant differences were observed between the films with fractions or essential oil ($p > 0.05$). Similar results were also observed by Fernández-Marín et al. [192], who added oregano essential oil and chitin nanocrystals to poly(vinyl alcohol) films, and other authors demonstrated this tendency when they combined chitosan, olive oil and cellulose nanocrystals [210]. Regarding the water solubility behavior of the samples, it was observed that the addition of the OM and its fractions to the CS/chitin nanofibres matrix decreased the water solubility Table IV-13. As for the moisture content, it was observed that films containing essential oils did not show significant differences between them ($p > 0.05$).

3.1.4. *ATR-FTIR*

The chemical structure of the nanocomposite films was analyzed by ATR-FTIR (Figure IV-11). All nanocomposite films exhibited the typical chitosan bands at 1640 and 1540 cm^{-1} corresponding to amide I and amide II, respectively [121,150,151]. The band around 1405 cm^{-1} was observed in all films and was attributed to C-H stretching vibration [211]. A difference was observed in the band appearing at 1377 cm^{-1} in the films CSNF-F1, CSNF-F2, CSNF-F3, CSNF-OM, which

was attributed to the C-N stretching of the bioactive compounds of the essential oils [212,213]. Another remarkable difference was noticed between the films with and without oil. In CSNF films, two bands appeared around 1065 and 1021 cm^{-1} which were assigned to C-O bending secondary and primary O-H groups, respectively [151]. While in the films with oil and fractions a single band appeared around 1030 cm^{-1} corresponding to C-OH stretching vibration [213].
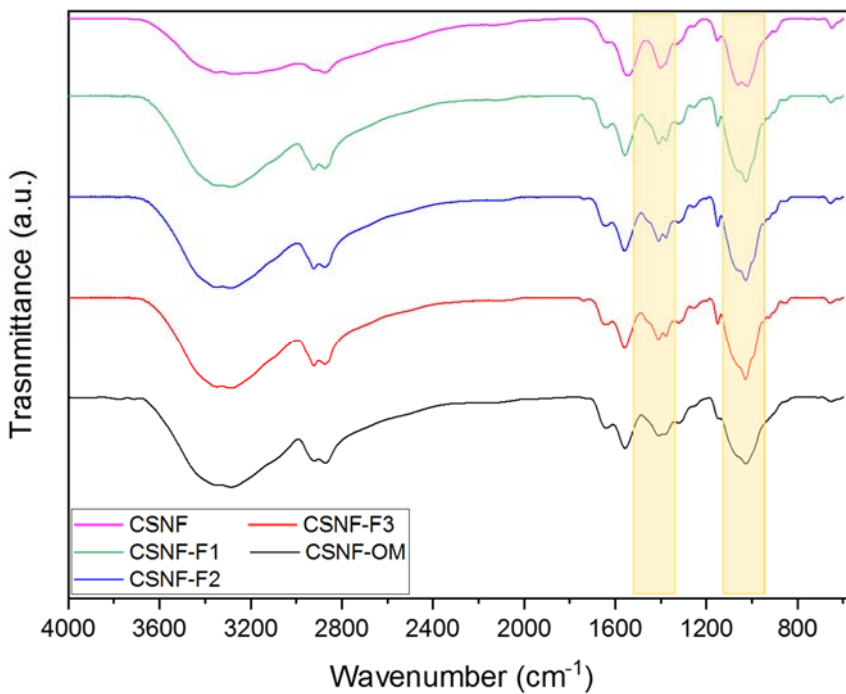

Figure IV-11. ATR-FTIR spectra of the nanocomposite films.

3.1.5. Water contact angle

The hydrophilic/hydrophobic behavior of nanocomposite films was studied using the water contact angle technique. In general, angles above 90º indicate a hydrophobic surface while angles below

60º indicate a hydrophilic surface [214,215]. Figure IV-12 shows the contact angle values for all samples for 0 and 120 seconds. As expected, the CSNF film demonstrated an hydrophilic behavior, with an initial contact angle of around 85°, which were attributed to the surface rigidity of the film (Figure IV-13), that quickly fell to characteristic values of chitin and chitosan (54.9º at 120 s, Figure IV-12) [216]. The incorporation of OM essential oil and its fractions showed a different behavior; the starting contact angles were around 80º and the drop was maintained stable over time (from 0 to 120 s, Figure IV-12). This fact is due to the presence of polyphenolic groups in the oils [202,215,217]. For instance, CSNF-F1 and CSNF-OM films demonstrated a contact angle loss of 1.6 and 1.15º, respectively, showing the effect of the hydrophobic behavior of the oils.
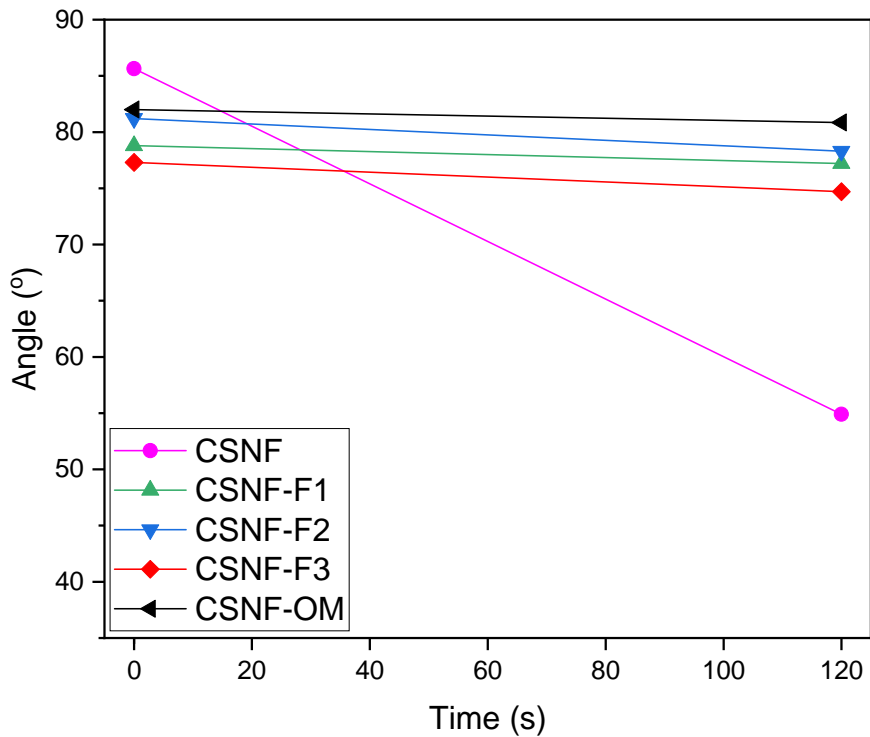
Figure IV-12. The water contact angle of nanocomposite films.

3.2. **Morphology**

Scanning electron microscope (SEM) analysis was employed to assess the morphology of the nanocomposites films. Figure IV-13 shows the cross-section and the surface images of all nanocomposite films. The presence of the chitin nanofibers in all samples was confirmed by both cross-section and the surface SEM images (Figure IV-13 A, B, C, D and E). In general, the nanocomposite films exhibited a homogeneous morphology with a rough surface. As shown by the cross-section images, the addition of the deterpenated fractions of *Origanum majorana L.* essential oil, promoted films more compact (dense), probably resulting in the establishment of strong interactions

138

between the EOs molecules and the chitosan chains and chitin nanofibers. It was also observed the presence of dots at the surface of the matrices with deterpenated fractions of *Origanum majorana* L. essential oil (Figure IV-13 C and D), as observed previously by Valizadeh et al. after the incorporation of EOs on chitosan and carboxymethyl cellulose matrices which could be due to emulsified drops of essential oil [218]. These results are also consistent with the results obtained by Khan et al. in their cellulose nanocrystals reinforced chitosan films [219].
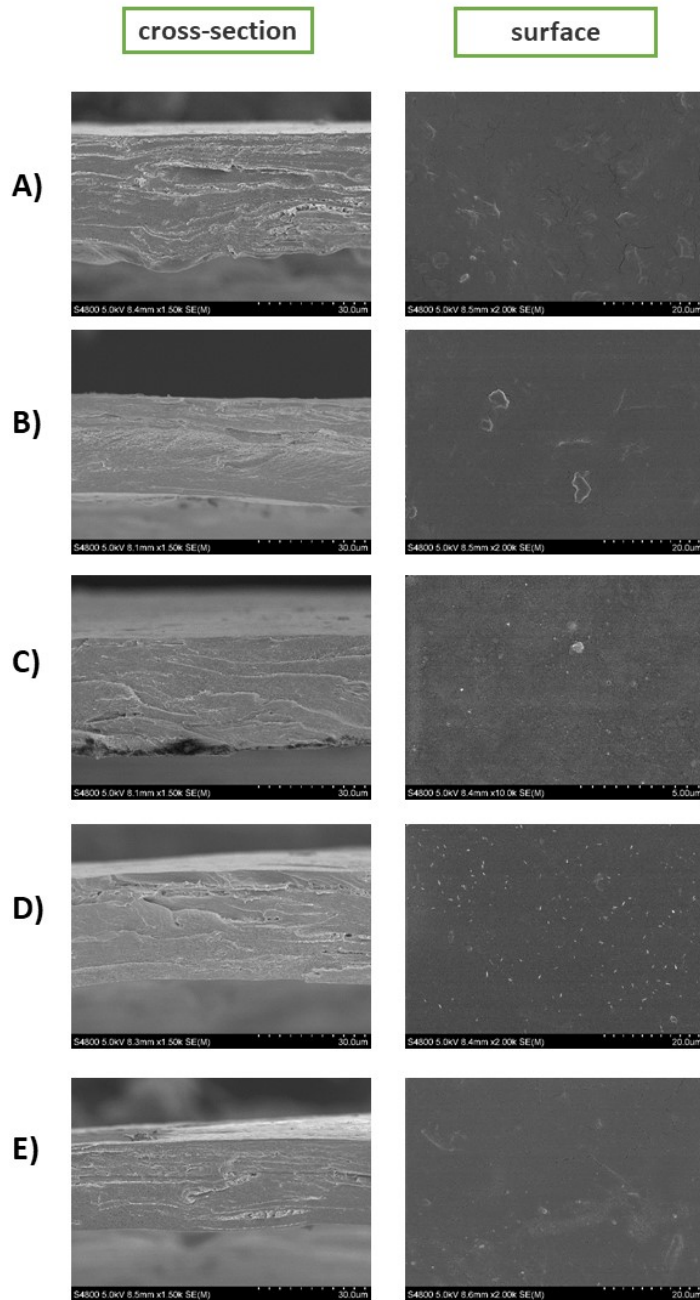
Figure IV-13. Cross-section and Surface images of scanning electron microscopy of A) CSNF; B) CSNF-F1; C) CSNF-F2; D) CSNF-F3; E) CSNF-OM films.

3.3. Thermogravimetric analysis and mechanical properties

The influence of the introduction of the deterpenated fractions of *Origanum majorana* L. essential oil on the thermal stability and mechanical properties of chitosan/ β-chitin nanofibres nanocomposite films were also investigated by TGA and tension tests, respectively.

The onset thermal decomposition and the temperature of a maximum of mass loss have been determined from TGA and derivative TGA (dTGA) curves (Figure IV-14). TGA and dTGA of the CSNF sample displayed five main degradation steps. The first step occurred bellow 100 °C and was attributed to the acetic acid and water evaporation. In the second step the onset temperature was 150 °C with a maximum degradation at 200 °C and was assigned to the decomposition of the major of Tween 20 molecules and loss of some glycerol molecules. The maximum degradation temperatures at 330 and 350 °C (third and fourth steps) were attributed to chitosan and nanochitin degradation, respectively [35,101,220]. The small decomposition step between 425 and 500 °C was ascribed to the remaining Tween 20 molecules [35,220]. As can be observed by the TGA and dTGA curves, the main difference between samples containing the EO fractions and the CSNF matrix was observed in the second degradation step. This step is larger and presents the main loss of compounds. The onset temperature starts at around 150 °C and the maximum degradation temperature was observed at 240 °C. This consequent loss was mainly attributed to the loss of the low molecular weight molecules of the EOs, and also to the Tween 20 and glycerol

molecules loss. Interestingly, the CSNF-F1 film showed to be the least thermostable material. The second degradation step displayed an onset temperature of 100 °C and a maximum degradation temperature of around 150 °C. The maximum degradation temperature of chitosan and nanochitin was 250 and 300 °C, respectively.
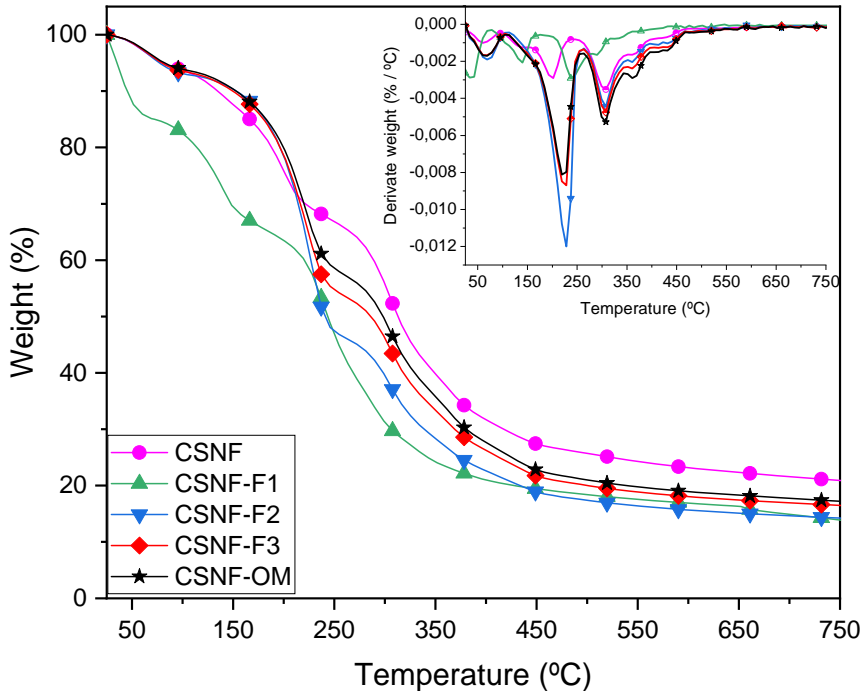
Figure IV-14. TGA and dTGA curves of the nanocomposite films.

The results of the mechanical properties (TS, tensile strength; YM, Young´s Modulus and E, Elongation) are shown in Table IV-14. In general, the incorporation of OM and its different fractions on the CSNF matrix caused a significant decrease in the TS and YM ($p < 0.05$). This trend was also observed by Ardekani et al. [221] when incorporating 10% *Zataria multiflora* oil and mats nanofibres in a

chitosan and poly(vinyl alcohol) matrix. Mohammadi et al. [222] obtained similar results in their whey protein films with cinnamon oil and chitosan nanofibres. The elongation (E %) was also affected by the addition of OM oil and its fractions. These values increased significantly (p < 0.05) in CSNF-F1, CSNF-F2, CSNF-F3 and CSNF-OM films. Essential oils act as plasticizers because they reduce the intermolecular forces in the chitosan network allowing mobility in the chains and enhancing the flexibility of the film [68,100,103].

Table IV- 14. Mechanical properties of the films. (TS: tensile strength, MPa; YM: Young´s modulus, MPa; E: elongation, %).

Samples	TS (MPa)	YM (MPa)	E %
CSNF	15.25 ± 1.86[a]	328.25 ± 18.67[a]	44.87 ± 8.12[a]
CSNF-F1	17.88 ± 5.32[b]	310.98 ± 61.05[b]	64.40 ± 14.64[b]
CSNF-F2	11.52 ± 3.97[bc]	77.09 ± 11.77[c]	67.92 ± 33.13[b]
CSNF-F3	12.20 ± 3.56[c]	153.39 ± 48.92[d]	46.90 ± 15.01[ac]
CSNF-OM	11.49 ± 3.27[bc]	133.89 ± 33.38[d]	50.66 ± 12.62[bc]

The values represent average ± standard deviation (n = 8). Superscript letters in the same column indicate significant differences among the films (Duncan's test, p < 0.05).

3.4. Antifungal properties

The effect of the incorporation of the different fractions and OM essential oil in the CSNF films on the antifungal activity against *Aspergillus niger* was analyzed (Figure IV-15). This fungus was chosen because is one of the main contaminants of food, especially fruits and vegetables, thus important for packaging applications.

As already reported by Salaberria et al., the nanocomposites prepared with nanochitin present significant inhibitory activity in CS matrices (around 64.4 %; Figure IV-15) [125]. Moreover, when OM essential oil

or its fractions were added into the nanocomposite films it was observed an increase of the antifungal activity. The nanocomposite films prepared with the deterpenated fractions CSNF-F2 and CSNF-F3 exhibited higher FGI % than the other oil-based films, 85.49 % and 85.90 %, respectively. The major compounds in the fractions of these films were oxygenated terpenes derivatives (terpenoids) consisting of polar terpenes and alcohols, which have been shown to have a negative effect on fungal growth, as previously demonstrated [200,223]. CSNF-OM also showed good activity against *Aspergillus niger*. The CSNF-F1 nanocomposite films, showed a FGI (%) of around 72 % that is lower compared with the films prepared with the deterpenated fractions, because its major compounds were hydrocarbonated terpenes such as γ-terpinene, α-terpinene or β-pinene, which are usually less effective against *A. niger*, as previously verified [200,224].

The mechanism of the oils against fungi could be justified by the penetration or interaction of these compounds in the cell membrane affecting the fungi functions, like respiratory inhibition and thus causing cell death [35,192].
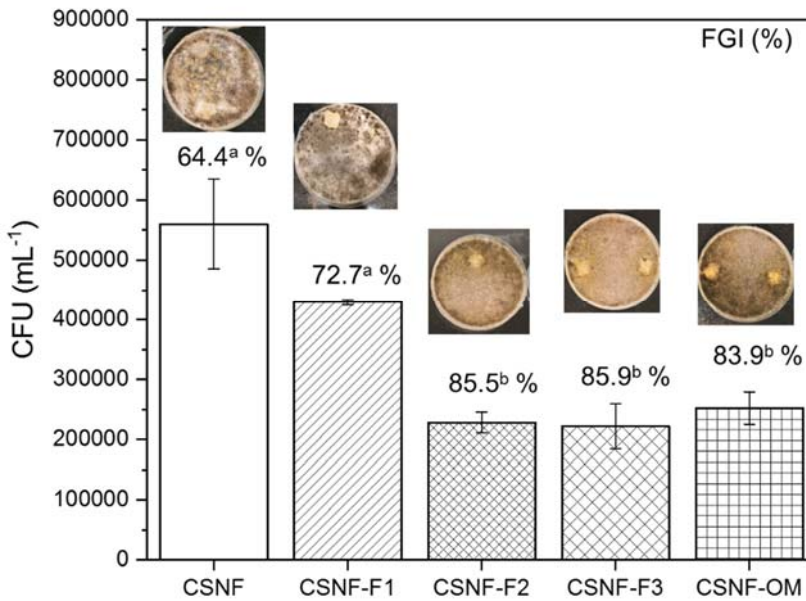
Figure IV-15. *Antifungal activity against Aspergillus niger of the nanocomposite films respect to control only with fungi: CSNF, CSNF-F1, CSNF-F2, CSNF-F3 and CSNF-OM and their appearance after 7 days of incubation. The value above each bar corresponds to the fungal growth inhibition (FGI, %). The error bar represents to the standard deviation (n = 3). Superscript letters in the FGI % data indicate significant differences among the films (Duncan's test, p < 0.05).*

3.5. Cytotoxicity assay

The cell viability of the nanocomposite films on the growth of L929 murine fibroblast cells was analysed by MTT assay at different incubation times (24, 48 and 72 h, Figure IV-16). According to the standard method ISO 10993-5, the samples with a cell viability ratio below 70% are considered cytotoxic. As expected, the CSNF nanocomposite films are non cytotoxic, as previously demonstrated [136,204]. The analyzes carried out to assess the cytotoxic activity of the obtained nanocomposite films prepared with the different EO

fractions have shown that these extracts have different effects on the tested cell line. Interestingly, CSNF-F1 nanocomposite films *i.e.*, revealed no toxic effects on the viability of L929 fibroblast cells after 48 and 72h. On the other hand, the film samples CSNF-F2, CSNF-F3, and CSNF-OM showed cytotoxic effects on the viability of L929 fibroblast cells. This can be ascribed to the high concentration of terpenoids molecules of the deterpenated *Origanum majorana* L. essential oil that may cause the internal cell damage leading to cell death [225]. Also, the samples may have the potential to damage the cell membrane after interaction with intracellular substances inside the cell.
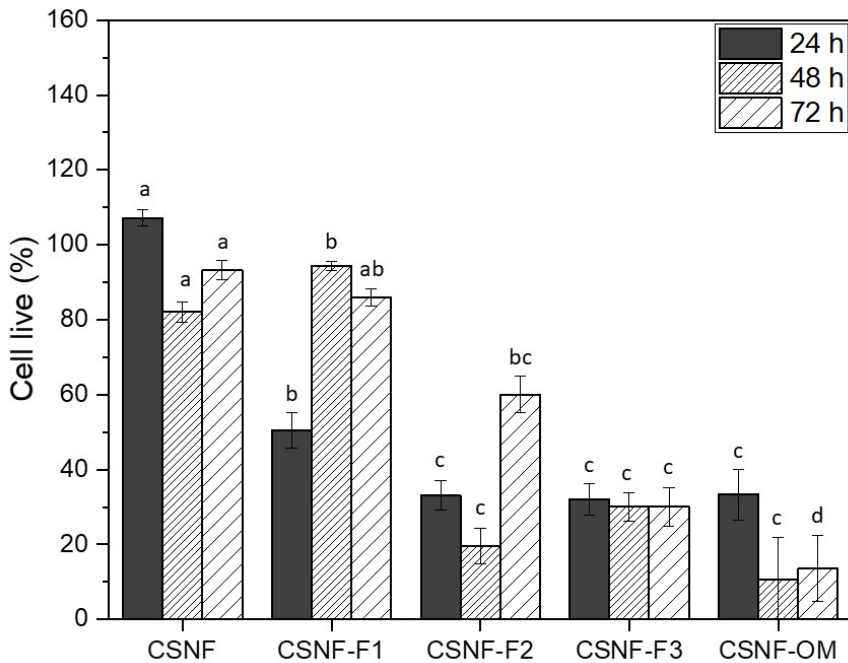

Figure IV-16. Cell viability of the nanocomposite films. Error bar corresponds to standard deviation (n = 4). Letters in the same color bars denote significant differences among the different films and the same treatment time (Duncan's test, p < 0.05).

4. CONCLUSIONS

In this work, the effect of three deterpenated *Origanum majorana* L. essential oil fractions on the physicochemical, mechanical and biological properties of chitosan/ β-chitin nanofibres nanocomposite films were investigated. The presence of the original essential oil or of its deterpenated fractions increased the opacity, give them a yellowish color and improved the hydrophobicity of the nanocomposite films.

The data showed that the proportion of terpenes hydrocarbons or oxygenated terpenes derivatives in the oil fractions influences the biological properties of the materials. The nanocomposite films prepared with oxygenated terpene derivatives showed the best antifungal activity against *Aspergillus niger*, presenting a FGI of 85.49 % for CSNF-F2 and of 85.90 % for CSNF-F3. Nonetheless, these materials presented cytotoxic properties on the studied L929 fibroblast cells, with a cell viability inferior at 30 %. On the other hand, the nanocomposite films prepared with terpenes hydrocarbons (CSNF-F1), showed no cytotoxicity on the viability of L929 fibroblast cells after 48 and 72 h, with a cell viability of around 90 %. Therefore, these findings suggest that these nanocomposite films present a good potential for packaging or medical and pharmaceutical sectors.

Chapter 4
Halocromic and antioxidant capacity of smart pH- and volatile ammonia-sensitive chitosan/chitin nanocrystals nanocomposite films prepared with curcuma oil and anthocyanins

Abstract

Curcuma longa L. essential oil and anthocyanin extracts contain bioactive compounds such as antioxidant properties and their pigments are able to change colour when exposed to different pH or ammonium gas. In this context, the objective of the present work was to develop pH-sensitive intelligent films by adding curcuma oil and anthocyanin extracts to a chitosan matrix reinforced with alpha-chitin nanocrystals. The incorporation of curcuma oil, anthocyanins and nanocrystals enhanced the mechanical properties and hydrophobicity. In addition, it decreased water solubility and moisture content. The films showed almost total blocking against UV/Vis light at wavelengths below 550 nm and good antioxidant properties. The films were sensitive to colour change when exposed to ammonia gas and different pH solutions, with greater variations with the increase of the concentrations of curcuma oil. Hence, these results revealed the potential of these films as intelligent food packaging applications.

1. INTRODUCTION

Food packaging has an important role in storage, transport and especially regarding food spoilage delay [226]. Thus, it has been observed a growing interest into improving packaging to prevent food deterioration caused by light, moisture, oxygen or the proliferation of microorganisms [227]. In this context, lately, smart packaging containing an indicator (thermal, leakage, water or gas permeability indicators) to quickly inform the consumer about the quality status of the food, has generated a great interest in food industry [228–230]. For instance, pH-sensitive films containing colorimetric indicators were developed for the detection of the decomposition of the food, especially meat and fish , release basic volatile organic amines [227,229,231–233].

Natural compounds, which are safe for human health and the environment, biodegradable, non-toxic and with antimicrobial and antioxidant properties, have been used as alternative to the synthetic indicators. Examples of these natural indicators are pigments extracted from plants such as anthocyanins and curcuma oil extracted from curcuma or turmeric root (*Curcuma longa* L.). Anthocyanins, are water soluble pigments and can be extracted from different sources as purple potato, blackberry, roselle, purple onion peel, red cabbage or black chokeberry among others. They present excellent antimicrobial, antioxidant and pH-sensitive properties [127,132,226,227,232,234,235]. Curcuma oil has as major compound, curcumin, a yellow pigment that is pH-sensitive (halochromic) due to its enol and keto tautomeric forms [173]. Moreover, this oil, can be used as a bioactive agent since its properties include antimicrobial and antioxidant properties

[164,236]. Recently, it was also shown that mixing different pigments improves the range of color change as well as antioxidant properties [237,238].

Therefore, different matrices including k-carrageenan, starch and chitosan among others have been used in order to immobilise and apply anthocyanins or/and curcuma oil in food packaging [237,239–241]. For instance, H. Zhi Chen et al. [237] investigated the behaviour of mixing curcumin and anthocyanins in a matrix of starch, poly(vinyl alcohol) and glycerol to test the pH change on the freshness of fish. Among these matrices, chitosan (poly-β-(1-4)-N-acetyl-D-glucosamine, CS), which is obtained from the deacetylation of chitin, has been largely used for food packaging because of its unique properties such as non-toxicity, biocompatibility, biodegradability, excellent film-forming properties [11,239]. However, CS films have disadvantages including low UV light barrier and limited mechanical properties. Thus, nanocrystals or nanofibres from cellulose or chitin have been incorporated as reinforcing agents [5,8,10,134,136,203,204,242] . In particular, chitin nanocrystals (CHNC) have attracted the interest of the scientific community due to their excellent properties such as antimicrobial, small size, low toxicity and biocompatibility [5,10,243]. In this sense, Wu et al., [235] developed pH-sensitive smart films with red cabbage anthocyanins using a matrix of oxidized chitin nanocrystals and Konjac glucomannan.

The present work presents the development of smart multifunctional materials based on chitosan/chitin nanocrystals nanocomposite films and curcuma oil and anthocyanins as pH- and volatile ammonia-sensitive agents. The aim was to obtain final

materials with halocromic and antioxidant capacity for the monitoring of food packaging.

2. MATERIALS AND METHODS

The reagents employed are shown in Appendix B.

For the development of this work, the methodology described in **PART III** was followed. CS was extracted from lobster (Homarus gammarus) and anthocyanin was obtained from red cabbage. Using the MAE technique, alpha-chitin nanocrystal (α-CHNC) was isolated from yellow lobster (Cervimunida johni) (optimum point: 10 min, 124.75 W and 1 M HCl- **Chapter 1**) and *Curcuma longa* L. oil was also extracted (29.99 min, 160 W and 1:20 w/v (curcuma powder: EtOH)- **Chapter 2**).

2.1. Preparation of biocomposite films

To prepare the nanocomposite films, CS (1 % w/v) was dissolved in a solution of acetic acid (1 % v/v) under stirring for 24 h. After, to this solution, glycerol 0.2 % v/v (Cs based) was added as plasticiser and mixed at 15 000 rpm using an Ultra-Turrax (Heidolph Silent Crusher M., Germany) for 10 min at 25ºC. Then, the α-CHNC (0.5 % w/v) were added and mixed at 15 000 rpm for 10 min. Afterwards, 5 different bioactive nanocomposite film samples were prepared by adding or curcuma oil (C) or anthocyanin extract (A), in addition 3 different mixtures of both extracts (see Table IV-15). To prepare the bioactive nanocomposite films, two 2 g/L dilutions were prepared by using or curcuma oil or anthocyanin extract in ethanol, and the nanocomposite films were made by adding 1 % v/v of C solution or A

extract with respect to the CS. The 3 mixtures were prepared by using: (i) 8 % v/v C and 1 % v/v A; (ii) 1 % v/v C and 8 % v/v A; and (iii) 1 % v/v C and 1 % v/v A, all concentration are reported with respect to CS. The suspensions were mixed by using an Ultra-Turrax at 15 000 rpm for 10 min and degassed to remove bubbles. The nanocomposite films were prepared by the solvent-casting technique by using 50 mm diameter Petri dishes at 30 °C for 24 h. CS/chitin nanocrystals nanocomposite films without the extracts were prepared as controls. Before the characterisation, the samples were stored in a climatic chamber at 25 °C with a relative humidity of 50 ± 5%. The identification and composition of the nanocomposite films are shown in Table IV-15.

Table IV-15. Identification and composition of nanocomposite films.

Sample code	α-CHNC (% w/v)	C (% v/v)	A (% v/v)	C:A (% v/v)
CSNC	0.5	-	-	-
CSNC-C	0.5	1	-	-
CSNC-A	0.5	-	1	-
CSNC-CA(8:1)	0.5	8	1	8:1
CSNC-CA(1:8)	0.5	1	8	1:8
CSNC-CA(1:1)	0.5	1	1	1:1

α-CHNC: alpha-chitin nanocrystals; C: curcuma oil; A: anthocyanin extract; % w/v or % v/v based on chitosan.

The nanocomposite films were characterised in terms of physico-chemical, structural, thermal and mechanical properties. In addition, the total phenolic content and antioxidant properties (DPPH) were measured at 24 h. The techniques used are detailed in **PART III**.

2.2. Statistical analysis

A one-way analysis of variance (ANOVA) statistical test was performed using SPSS software (version 24, Inc. Chicago, IL, USA). Significant difference values were obtained by Duncan's multiple range test. The results were expressed as average and standard deviation. P-values < 0.05 were statistically significant.

3. RESULTS AND DISCUSSION
3.1. Thickness and appearance

The general aspect of food packaging and its optical properties like color, opacity and transmittance are a very important factor for both consumer acceptance and food protection against photodegradation [228,244]. Figure IV-17 displays the general aspect of the final nanocomposite films. As shown in Figures IV-17, the samples are translucent and homogeneous and the nanocomposite films with bioactive agent's exhibit yellowish, orange and brownish colours (see also Figure IV-18, Table IV-18 and section 3.6.).
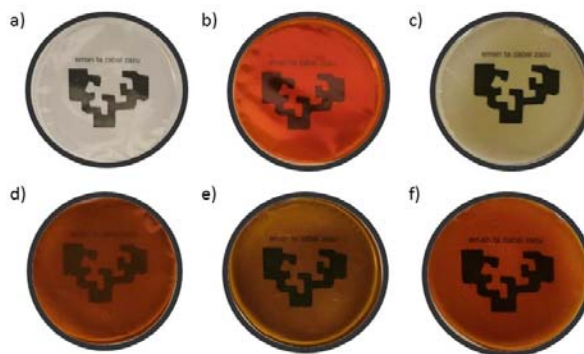

Figure IV-17. Photographs showing the general aspect of the films. a) CSNC; b) CSNC-C; c) CSNC-A; d) CSNC-CA(8:1); e) CSNC-CA(1:8); f) CSNC-CA(1:1).

As defined before, the opacity (Table IV-16) of the films was measured at 600 nm (Figure IV-18) and taking in account the thickness of the samples (Table IV-16). As expected, it was observed that the CSNC nanocomposite film (control) showed the lowest value (4.18 ± 0.20). Higher opacities were observed in the films with prepared with a mixture of curcuma oil and anthocyanin, exhibiting the greatest value when the proportion of curcuma was higher (CSNC-CA(8:1): 29.39 ± 2.10). This may be due to the absorption of some of the light by the mixture of its chromophores and also agrees with the data observed in Figure IV-18 for transmittance [228].

Table IV-16. Th (thickness), MC (moisture content), WS (water solubility) and opacity of the films.

Samples	Th (µm)	MC %	WS %	Opacity
CSNC	49.67 ± 2.07[a]	41.73 ± 0.69[a]	48.50 ± 1.08[a]	4.18 ± 0.20[ab]
CSNC-C	58.67 ± 2.16[b]	22.88 ± 1.28[b]	29.46 ± 0.97[b]	6.81 ± 0.56[b]
CSNC-A	49.00 ± 1.79[a]	34.20 ± 1.37[c]	41.88 ± 0.88[c]	6.73 ± 2.76[b]
CSNC-CA(8:1)	49.83 ± 2.64[a]	25.39 ± 1.35[d]	31.44 ± 0.86[c]	29.39 ± 2.10[c]
CSNC-CA(1:8)	47.17 ± 1.33[c]	32.49 ± 1.61[c]	38.85 ± 0.92[d]	18.67 ± 0.73[d]
CSNC-CA(1:1)	47.50 ± 3.94[c]	27.78 ± 1.35[e]	35.57 ± 1.64[e]	6.28 ± 0.98[b]

Values are expressed as mean ± standard deviation (thickness n = 6; moisture content, water solubility and opacity n = 3). Different letters in the same column denote significant differences between films (Duncan's test, $p < 0.05$).

Figure IV-18 shows the transmittance of the nanocomposite films from 250 to 750 nm (UV-Vis light). As expected, the incorporation of curcuma oil and anthocyanin into the nanocomposite films decrease

their transmittance; and, interestingly, the spectra profile differ depending the kind of additive or mixture. All films containing curcuma oil showed a drastic decrease in transmittance around 500 nm, showing to be a great barrier against UV radiation, probably due to the presence of phenolic compounds [242]. The CSNC-CA(8:1) and CSNC-CA(1:8) nanocomposite films exhibited very low transmittance in the visible region and a total blocking in the UV region.
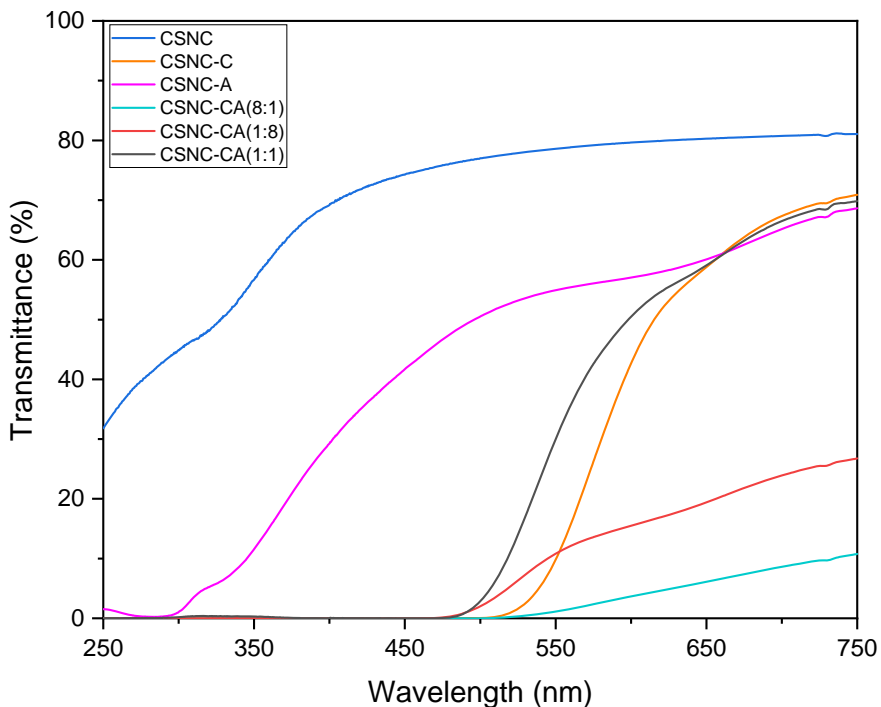

Figure IV-18. Transmittance from 750 to 250 nm of nanocomposite films.

3.2. Moisture content and water solubility

For food packaging films, another important characteristic is their behaviour towards moisture and water.

Table IV-16 shows the water solubility (WS) data of the biocomposite films. The addition of curcuma oil and anthocyanins improved the WS properties ($p < 0.05$). However, the incorporation of anthocyanin, due to its hydrophilic nature, showed slightly higher values than in the films with higher curcuma oil content. This was confirmed in the CSNC-C film, which showed the lowest WS value. This is mainly due to the fact that most of the compounds in the oil have hydrophobic properties [242].

The moisture content values are listed in Table IV-16. The data revealed that the presence of curcuma oil and anthocyanins decrease the MC of the samples. Other authors, who added essential oils and nanofibres in chitosan films, or purple-fleshed sweet potato extract also observed the same behaviour [210,231]. Both films with anthocyanin extracts and curcuma oil significantly decreased the MC values since they can form bonds with the hydroxyl or amino groups of CS preventing their interaction with water [30,239]. It was also observed that the films with the highest curcuma oil content (CSNC and CSNC-CA(8:1)) showed the lowest values, possibly due to their high content of non-polar compounds [245].

3.3. Water contact angle

The water contact angle technique evaluates the hydrophilic or hydrophobic behaviour of the materials. Films with angles greater than 90° are considered hydrophobic [215]. To assess the hydrophilic or hydrophobic character of the nanocomposite films, the contact angle was measured at 0 s and 120 s after to depose a water drop at the surface of the films. The data displayed in Figure IV-19 are in accordance with the data obtained by the water sensitive tests

described before. In other words, the addition of curcuma oil improved their hydrophobic properties as they exhibited angles greater than 90º (t = 0). The films CSNC-C and CSNC-CA(8:1) exhibited lower contact angle loss ($\Delta\alpha$ = 1.3 and 1.9, respectively) after the 120 s as this oil contains non-polar compounds revealing its hydrophobic nature [246]. The films prepared with anthocyanins (CSNC-A; CSNC-CA(1:8) and CSNC-CA(1:1)) showed a decrease in the contact angle after 120 s. This is explained by the fact that they contain a large number of hydroxyl groups which can form hydrogen bonds with water, thus demonstrating their affinity for water [227].
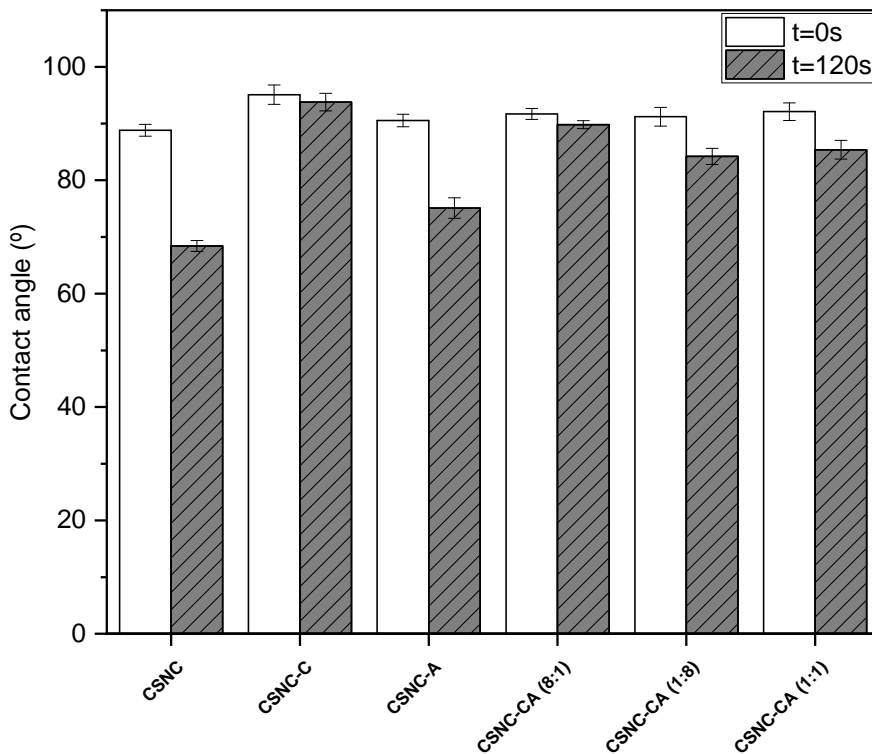

Figure IV-19. Water contact angle of the nanocomposite films at 0 and 120 seconds.

3.4. Mechanical properties

Because of the handling, transport and storage of packaging material for food, another important characteristic of these materials is their mechanical properties [247]. The mechanical properties of the nanocomposite films are shown in Table IV-17.

Table IV-17. Mechanical properties of the nanocomposite films: TS (tensile strength, MPa), YM (Young´s modulus, MPa) and E (elongation, %).

Samples	TS (MPa)	YM (MPa)	E (%)
CSNC	19.52 ± 4.92[a]	31.31 ± 1.29[a]	29.79 ± 9.91[a]
CSNC-C	26.94 ± 2.87[b]	36.04 ± 3.13[b]	27.52 ± 8.14[b]
CSNC-A	28.92 ± 1.46[c]	52.67 ± 4.83[c]	18.76 ± 1.17[c]
CSNC-CA(8:1)	24.80 ± 1.89[d]	46.99 ± 7.11[d]	32.62 ± 4.73[d]
CSNC-CA(1:8)	30.55 ± 3.55[e]	63.94 ± 9.07[e]	21.45 ± 1.92[e]
CSNC-CA(1:1)	25.42 ± 2.29[bd]	34.01 ± 1.46[b]	15.44 ± 7.54[f]

Values are mean ± standard deviation (n = 6). The superscript letters in the same column denote significant differences among the nanocomposite films (Duncan's test, $p < 0.05$).

In general, the addition of curcuma oil and anthocyanins significantly improved the breaking resistance. It was also observed that both CSNC-A and CSNC-CA(1:8) films, which contain the highest proportion of anthocyanins, exhibited the highest TS values. This may be due to the formation of a more stable interactions between CS chains and CHNC and the other additives into the film [248,249]. The YM follows the same trend found for the TS parameter. The incorporation of curcuma oil, anthocyanin extract and their mixture increased the YM, showing the highest value in the CSNC-CA(1:8) nanocomposite film with 63.94 ± 9.07 MPa. These results are probably

due to the adhesion between the matrix and the anthocyanin extract at the interface since both are hydrophilic [250,251]. On the other hand, significant decrease in E% occurred with the addition of the bioactive compounds. This behavior was also found by authors such as Zhou X. et al., [252] in their study based on konjac glucomannan and camellia oil films with the addition of carrageenan, anthocyanin extracts and curcumin. Li Y. et al., [127] reported this trend in chitosan films reinforced with deacetylated chitin nanofibers and purple potato extraction by increasing the concentration of nanofibers. These results may be due to the interactions formed by the extracts and the matrix, which impedes the CS-CS interaction reducing the flexibility of the film [249,250,252]. Overall, the mixture of anthocyanins and curcuma oil improved the mechanical properties which is in agreement with the results obtained by Zhou X. et al. [252].

3.5. TGA

The influence of the introduction of anthocyanins and curcuma oil on the CSCN nanocomposite films was evaluated by thermogravimetric analysis. The TGA and the derivative dTG curves are shown in Figure IV-20. En general, all nanocomposite films displayed profiles with 3 main degradation steps. The first step of degradation occurred below 100 ºC and was due to the evaporation of water and acetic acid residue [229]. In the second step, the onset temperatures were between 125 and 150 °C with a maximum degradation between 200 and 225 °C and were assigned to the loss of the low molecular weight molecules of the anthocyanins and curcuma oil and glycerol molecules [101,228]. The third step was observed between 275-325 °C and were attributed to the chitosan and

nanochitin degradation. In addition, some degradation of curcuma oil and anthocyanin extracts can also occur in this step [220,229]. In general, the results indicated that the addition of curcuma oil and anthocyanin extract exhibited lower thermal stability than the pure CSNC nanocomposite films. This type of behaviour has also been observed by other authors such as Silva-Pereira M. C. et al., [253] who studied CS and corn starch films by adding red cabbage extract.
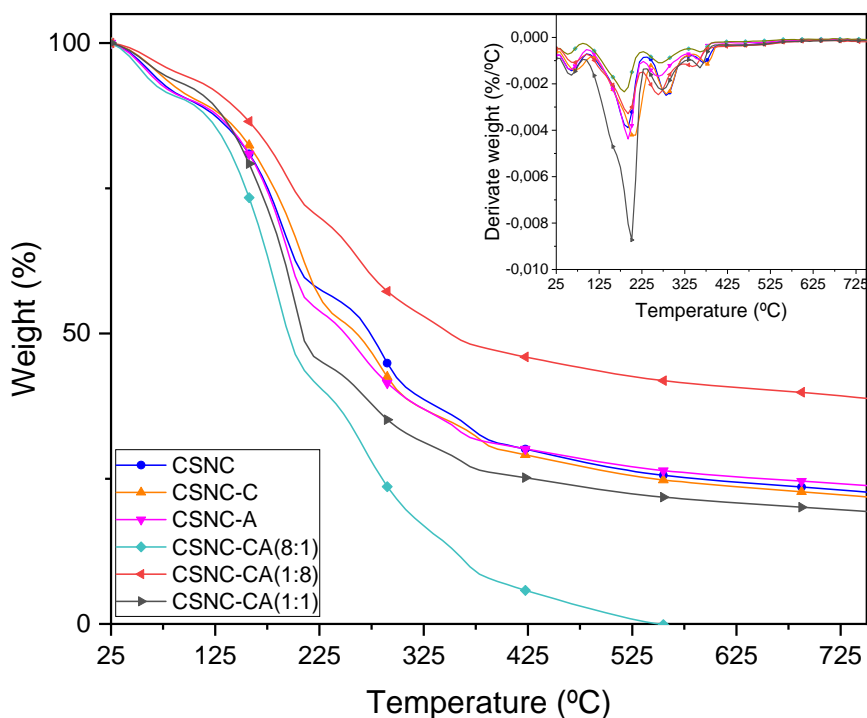

Figure IV-20. TGA and dTG profiles of the nanocomposite films.

3.6. pH- and volatile ammonia-sensitivity

As mentioned before, in order to evaluate the halochromic capacity of the samples, the films were first exposed to pH-variations

and volatile ammonia and then their color was measured. The colors of the untreated films was also measured and used as control.

3.6.1. Color of untreated films

The color parameters (ΔE, L^*, b^* and a^*) of the untreated films are shown in Table IV-18. In the L^* parameter it can be seen that the CSNC films showed values close to 90 so they tend to lightness ($p > 0.05$). While the films containing the bioactive agents are darker than the control CSNC film. In the parameter a^*, which indicates -green/+red, it was observed that all films trended towards red as they have a positive sign. The parameter a^* increased due to the influence of curcuma oil ($p < 0.05$). These results are in agreement with those obtained previously in films prepared with poly(vinyl alcohol), curcumin and grapefruit seed extract [250]. The same trend was observed for the parameter b^* (-blue/+yellow). The films with the bioactive compounds showed a tendency to yellow. The CSNC-C film showed the highest values of a^* and b^* parameters being 32.66 ± 0.11 and 46.37 ± 1.98, respectively. The mixture of both parameters was reflected in the appearance of the film shown in Table IV-18. The addition of curcuma oil and anthocyanin extract significantly ($p < 0.05$) affected the total color difference (ΔE) of the films.

Table IV-18. Color parameters of normal untreated nanocomposite films.

The values were average ± standard deviation (n= 10). In the analysis of the normal color of the films: the superscript letters in the same column indicate the significant differences between each parameter and the films (Duncan's test, $p < 0.05$).

Normal color of the films					
Samples	ΔE	L*	a*	b*	Appearance
CSNC	0.92 ± 0.16[b]	93.85 ± 0.28[a]	0.20 ± 0.03[a]	-0.75 ± 0.19[b]	
CSNC-C	71.15 ± 0.57[c]	56.54 ± 0.46[b]	32.66 ± 0.11[b]	46.37 ± 1.98[c]	
CSNC-A	24.96 ± 0.77[d]	72.36 ± 0.77[c]	1.15 ± 0.13[c]	12.23 ± 0.44[d]	
CSNC-CA(8:1)	59.52 ± 0.25[e]	43.93 ± 0.25[d]	21.19 ± 0.61[d]	24.10 ± 0.53[e]	
CSNC-CA(1:8)	58.71 ± 0.13[f]	44.06 ± 0.45[d]	16.32 ± 0.11[e]	26.04 ± 0.75[f]	
CSNC-CA(1:1)	65.65 ± 0.46[g]	47.21 ± 0.96[e]	32.64 ± 0.33[b]	31.87 ± 1.58[g]	

3.6.2. *Color of the samples treated with volatile ammonia*

The sensitivity of the films to ammonium gases was assessed by color variation at two different concentrations: 0.08 mol/L and 0.5 mol/L (Table IV-19). This experiment is useful because simulates the films sensitivity to volatile compounds generated in the meat decomposition. The mechanism that possibly occurs is that ammonia gas diffuses through the film matrix and is hydrolysed generating hydroxyl ions producing an alkaline environment for the film [254,255]. This causes that the anthocyanin and curcumin pigments, change the structure and consequently the color [173,255]. In all films the data showed positive values of a* and b* parameters indicating that the colors were going to reds and yellows.

In the CSNC-C film, it was observed that increasing the ammonium concentration increased the parameter a* and decreased b* ($p < 0.05$) in comparison with the untreated film, so that the tendency of the film color was red and less yellow. As for the CSNC-A film, a considerable increase in a* and b* was observed, which could be observed by the changing of the color from yellow to brown. Furthermore, no significant difference was observed regarding the change of ammonia concentrations ($p > 0.05$). In the CSNC-CA(8:1) and CSNC-CA(1:8) films the L* and a* parameters are similar while a greater change in the b* parameter was observed. The highest b* values were found in the CSNC-CA(1:8) film, which contains a higher amount of anthocyanin and therefore tends to yellow. Regarding the CSNC-CA(1:1) film, no significant differences were observed in the parameters ΔE* ,L*, a* and b* when they were subjected to the two

ammonia concentrations (p > 0.05). However, it was observed that the b* parameter was somewhat higher and tended more strongly to yellow color when exposed to higher ammonium concentration. In general, all films demonstrated sensitivity to ammonia gas exposure and no significant difference was observed between the two concentrations. These results demonstrated that the films could be employed for food packaging as indicators of food degradation.

Table IV-19. *Color parameters of nanocomposite films treated with volatile ammonia.*

The values were average ± standard deviation (n= 10). In the color analysis of films exposed to ammonia gas: the letters superscript in the same column represent the significant differences between the two different concentrations of ammonia gas and each parameter of each film (Duncan's test, p < 0.05).

Color of films exposed to ammonia gases					
	ΔE	L*	a*	b*	Appearance
CSNC-C					
0.08 mol/L NH₃	68.66 ± 0.97[a]	47.74 ± 0.23[a]	35.58 ± 0.37[a]	35.77 ± 1.18[a]	
0.5 mol/L NH3	70.86 ± 0.95[a]	42.88 ± 1.33[b]	40.70 ± 0.86[b]	27.82 ± 1.22[b]	
CSNC-A					
0.08 mol/L NH₃	42.08 ± 1.90[a]	68.55 ± 0.16[a]	11.08 ± 0.37[a]	31.47 ± 2.23[a]	
0.5 mol/L NH3	48.73 ± 0.99[b]	64.44 ± 1.32[b]	14.77 ± 0.69[a]	35.67 ± 0.49[a]	
CSNC-CA(8:1)					
0.08 mol/L NH₃	63.80 ± 0.11[a]	34.78 ± 1.23[a]	22.76 ± 2.11[a]	10.40 ± 1.44[a]	
0.5 mol/L NH3	61.02 ± 0.04[a]	40.77 ± 1.06[b]	24.21 ± 1.27[a]	18.60 ± 1.32[b]	

CSNC-CA(1:8)					
0.08 mol/L NH$_3$	62.12 ± 0.13[a]	42.52 ± 0.07[a]	22.20 ± 0.35[a]	27.39 ± 0.66[a]	
0.5 mol/L NH3	66.47 ± 1.78[a]	40.89 ± 2.16[a]	32.01 ± 1.45[b]	24.60 ± 1.65[a]	
CSNC-CA(1:1)					
0.08 mol/L NH$_3$	65.82 ± 0.65[a]	43.57 ± 0.30[a]	34.34 ± 0.28[a]	25.27 ± 0.70[a]	
0.5 mol/L NH3	68.28 ± 0.47[a]	46.08 ± 1.11[a]	36.46 ± 0.19[a]	32.37 ± 2.21[a]	

3.6.3. Color of the samples at different pH

The films were exposed to different pH dilutions and their halocromic capacity is shown in Table IV-20. The color of the CSNC-C film became darker (L*), redder (a*) and less yellowish (b*) as the pH became more basic. This is because the pigment curcumin changes structure to the enol form predominantly at basic pH [237]. In the CSNC-A film, it showed at pH = 2 a reddish color due to its a* parameter (35.23 ± 0.45) and the change of the anthocyanin structure to the flavylium form [239,256]. At pH = 4, a drop in the a* value was observed which contributed to the film appearing more yellowish. Between pH = 6-10 no significant changes between the parameters were found and a dark greenish color was observed. This resulted in no visible change in color with the naked eye. From pH = 12 an increasing b* and L* value was noticed which resulted in a bright yellowish color. This color trend was also observed by Yong H. et al. [239] in their analysis of chitosan films with purple-fleshed sweet potato extract. As for the films with mixed curcumin oil and anthocyanin, the perceived colors were more similar to those of curcuma oil. Similar results were observed in the study of Chen H. et

al. [237], who mixed curcumin and anthocyanins in the matrix of starch, poly(vinyl alcohol) and glycerol. In general, all films regardless of pH exhibited a tendency towards dark shades, with L* values being less than 50. In addition, most of them were observed to have ΔE values between 60-70. The CSNC-CA(8:1) film revealed orange to reddish tones due to the higher proportion of curcuma oil. These results are reflected by the increase of parameter a* and the decrease of b* as the pH becomes more basic. As for the CSNC-CA(1:8) film, it was found that the a* parameter gradually increased as the pH approached 14. In the colors of these films, the major presence of the anthocyanin extract was observed. Between pH = 2-8 the b* values were higher than the a* values, which was reflected in yellowish-brownish colors. When the pH becomes more basic, between 10-12, the films turned more yellow due to the increase of b*. It is worth noting that at pH =14 the film showed a dark red color due to the drastic increase of the a* parameter (32.812 ± 0.83). Finally, the colors observed in the CSNC-CA(1:1) film varied from yellow to reddish-orange. Between pH= 4-6, the film redness (a* values) increased while the yellowness (b* values) decreased. On the other hand, a color change to brown tones was obtained between pH = 8-12 showing similar a* and b* values. Finally, it is important to underline that at pH = 14 the a* value rose significantly which gave an orange color to the film.

Table IV-20. Color parameters of films in pH solutions (2-14).

The values represents average ± standard deviation (n= 10). The different superscript letters denote the significant differences of each

film between each parameter at the different pH.

Color of films exposed to different pH						
Samples	pH	ΔE	L*	a*	b*	Appearance
CSNC-C	2	49.79 ± 0.99[a]	53.69 ± 2.50[a]	29.39 ± 3.34[a]	40.02 ± 3.16[a]	
	4	41.79 ± 0.42[b]	45.04 ± 0.93[b]	36.25 ± 0.475[b]	20.80 ± 0.01[b]	
	6	47.43 ± 0.34[c]	49.09 ± 0.18[c]	33.46 ± 0.10[c]	33.62 ± 0.39[c]	
	8	44.4 ± 3.56[d]	44.33 ± 1.68[b]	37.78 ± 1.80[b]	26.26 ± 0.37[d]	
	10	39.08 ± 0.57[d]	41.59 ± 0.98[d]	35.10 ± 0.35[d]	17.18 ± 0.56[e]	
	12	37.39 ± 1.29[d]	40.25 ± 0.59[d]	34.28 ± 0.86[d]	14.91 ± 1.24[e]	
	14	48.71 ± 0.71[a]	39.62 ± 0.48[e]	44.35 ± 0.67[e]	20.12 ± 0.26[b]	
CSNC-A	2	64.65 ± 0.45[ab]	50.43 ± 1.14[a]	35.23 ± 0.45[a]	32.45 ± 1.09[a]	
	4	48.65 ± 1.20[b]	56.91 ± 1.49[b]	12.93 ± 0.30[b]	28.18 ± 0.11[b]	

	6	53.82 ± 0.47^a	47.79 ± 0.62^c	7.02 ± 0.11^c	24.63 ± 0.15^c
	8	53.73 ± 3.24^a	46.80 ± 4.70^c	6.00 ± 0.10^{cd}	23.11 ± 1.29^c
	10	53.48 ± 0.76^a	47.53 ± 1.70^c	6.27 ± 0.21^c	23.59 ± 1.50^c
	12	45.00 ± 0.31^c	60.68 ± 0.52^b	4.84 ± 0.72^d	28.07 ± 0.94^d
	14	32.44 ± 0.12^d	81.90 ± 0.15^d	6.10 ± 0.09^{cd}	34.01 ± 0.13^d
	2	57.76 ± 0.13^a	45.56 ± 0.06^a	19.72 ± 0.11^{ab}	24.08 ± 0.27^a
	4	58.75 ± 0.18^{ab}	41.81 ± 0.36^{bc}	15.40 ± 0.24^a	22.78 ± 1.56^b
	6	62.34 ± 0.37^{ab}	40.11 ± 0.51^{bc}	24.16 ± 0.83^{cd}	17.41 ± 1.65^b
CSNC-CA(8: 1)	**8**	60.08 ± 0.22^{bc}	40.76 ± 0.42^b	22.23 ± 0.16^{bc}	17.16 ± 0.28^b
	10	64.06 ± 0.64^c	40.62 ± 0.96^{ab}	25.10 ± 0.10^d	20.46 ± 0.38^a
	12	61.90 ± 0.26^{ab}	37.43 ± 0.40^b	22.31 ± 0.18^{ab}	13.17 ± 0.23^c
	14	68.06 ± 0.13^d	33.15 ± 0.33^c	27.56 ± 0.91^d	9.52 ± 0.37^d

169

	2	61.23 ± 0.35[a]	45.93 ± 0.02[a]	19.29 ± 0.05[a]	30.77 ± 0.22[a]	
	4	62.76 ± 0.31[a]	39.50 ±0.06[ab]	19.17 ± 0.40[ab]	22.09 ± 0.30[a]	
	6	58.83 ± 0.64[a]	43.27 ±0.47[cd]	18.20 ± 0.45[b]	23.48 ± 2.13[a]	
CSNC-CA(1:8)	**8**	60.35 ± 0.50[a]	44.25 ± 0.19[cd]	20.45 ± 0.37[c]	27.09 ± 0.46[a]	
	10	61.74 ± 0.97[b]	49.86 ± 3.50[e]	21.53 ± 0.40[c]	35.48 ± 2.90[b]	
	12	61.20 ± 0.25[a]	44.16 ± 1.29[d]	22.95 ± 0.15[c]	27.22 ± 1.82[a]	
	14	68.50 ± 0.50[a]	36.05 ± 0.25[a]	32.812 ± 0.83[d]	16.45 ± 1.19[a]	
	2	65.60 ± 0.19[a]	54.99 ± 0.51[a]	23.46 ± 0.08[a]	45.59 ± 0.66[a]	
CSNC-CA(1: 1)	**4**	66.78 ± 0.21[b]	39.99 ± 0.23[b]	31.29 ± 0.36[b]	21.46 ± 0.42[b]	
	6	66.06 ± 0.77[c]	41.35 ± 1.01[c]	34.35 ± 0.28[b]	20.24 ± 0.53[b]	
	8	61.24 ± 0.28[d]	43.86 ± 0.52[d]	22.02 ± 0.06[c]	27.15 ± 0.25[c]	

10	62.97 ± 1.24^d	42.81 ± 0.65^d	22.62 ± 0.36^c	26.79 ± 1.30^d	
12	64.08 ± 1.52^d	41.85 ± 0.57^{cd}	22.85 ± 0.64^c	27.33 ± 1.85^e	
14	75.40 ± 0.13^e	44.62 ± 0.11^d	46.51 ± 0.03^d	30.97 ± 0.08^f	

Interestingly, the color parameters of nanocomposite films prepared with the mixture of CSNC-CA(8:1) showed to be similar after their basic pH (10-12) exposure and volatile ammonia treatment. Thus, these color changes at different pH could be useful as an indicator in food packaging.

3.7. Total phenolic content and antioxidant activity

The antioxidant activity of the nanocomposite films is very important to prevent food oxidation and hence to extend the quality of the product. This was one of the motivations to add curcuma oil into the nanocomposite films with anthocyanins. In this work, first the total phenolic content (TPC) was assessed and then, the antioxidant properties were evaluated by DPPH free radical scavenging activity assay. The TPC assay determines the amount of total phenolic compounds contained in the samples, which are responsible of the antioxidant activity. The DPPH assay evaluates the substance capability of donating H to the free radical DPPH* [201,247]. The TPC and DPPH scavenging activity data are listed in Table IV-21.

Table IV-21. Values of total phenolic content (TPC, mg GAE/g film) and antioxidant activity (DPPH assay, radical scavenging activity %) of the films. Results were average ± standard deviation (n = 3). The superscript letters in the same column indicate significant differences (Duncan's test, p < 0.05) between each sample.

Samples	TPC (mg GAE/ g film)	DPPH %
CSNC	7.93 ± 2.48[a]	18.46 ± 0.03[a]
CSNC-C	110.27 ± 1.94[b]	71.01 ± 0.64[b]
CSNC-A	17.96 ± 0.42[c]	69.41 ± 0.02[b]
CSNC-CA(8:1)	168.73 ± 1.18[d]	76.10 ± 1.79[c]
CSNC-CA(1:8)	119.56 ± 1.27[b]	71.27 ± 1.65[d]
CSNC-CA(1:1)	65.45 ± 1.27[e]	69.44 ± 1.67[b]

Regarding the TPC, it was observed that the nanocomposite film prepared with curcuma oil (CSNC-C) exhibited higher TPC values than the CSNC nanocomposite films and those prepared with anthocyanins (CSNC-A) ($p < 0.05$). Interestingly, the nanocomposite films prepared with the mixture of both bioactive compounds presented the higher TPC values, being the CSNC-CA(8:1) film the one that showed the highest value.

These results were in agreement with those obtained by the DPPH assay to assess the antioxidant activity. In other words, it was observed that the mixture of curcuma oil and anthocyanin extract enhanced the antioxidant activity of the final CSNC nanocomposite films ($p < 0.05$). This could be explained by the fact that both curcuma oil and anthocyanins contain phenolic compounds with the ability to donate hydrogen atoms [242,250]. As expected, the CSNC-CA(8:1) film, which was prepared with the higher proportion of curcuma oil, showed the highest DPPH % value (76.10 ± 1.79 %) [186,236]. Therefore, the data revealed that these films could be used as film packaging to prevent food oxidation.

4. CONCLUSIONS

The aim of this study was to develop smart multifunctional materials based on chitosan/chtitin nanocrystals nanocomposite films and curcuma oil and anthocyanins as pH- and volatile ammonia-sensitive agents. In general, the addition of curcuma oil and anthocyanin extract decreased the moisture content and water solubility of the nanocomposite films and improved their UV-Vis light barrier and mechanical properties. The halocromic and

antioxidant properties of the films were assessed, and it was observed that the final materials are multifunctional since they are at the same time pH- and volatile ammonia-sensitive and present antioxidant properties. In general, the films with the bioactive compounds were sensible to the color change generated by the exposure to ammonium gas, and no significant differences were observed between the different concentrations used. As for the exposure to different pH solutions (2-14), changes were found in all the films with bioactive agents with greater changes in films with a higher percentage of curcuma oil (CSNC-C and CSNC-CA(8:1)). Interestingly, the nanocomposite film prepared with the mixture of CA(8:1) presented the best conditions for food preservation by presenting a great barrier to UV light, excellent antioxidant properties and halocromic capacity to both pH- and volatile ammonia changes. These results demonstrated that the use of the mixture of curcuma oil and anthocyanin extract in chitosan/chitin nanocrystals nanocomposite films could be applied to the food industry due to their food quality sensors capacity and biodegradability.

Part IV: **RESULTS AND DISCUSSION**

B.Materials development

Chapter 5

Using α-chitin nanocrystals to improve the final properties of poly (vinyl alcohol) films with Origanum vulgare essential oil

Abstract

In the present work, nanocomposite films based on poly(vinyl alcohol) (PVA) containing different amounts of Origanum vulgare essential oil (OEO, 0, 0.5, 1, 1.5 and 2 % v/v) were reinforced with 0.5 % (w/v) of alpha chitin nanocrystals (α-CHNC, from shrimp and from lobster) and prepared by solvent casting. Another set of films was prepared without α -CHNC to assess the effect of the nanocrystals on the final properties of the films. The obtained nanocomposite films were homogeneous and showed better thermal stability and mechanical properties. After exposure the nanocomposite films to ultraviolet radiation, the obtained data revealed that the presence of α-CHNC into the materials has a retarding effect on their loss of mechanical properties. It was also shown that the antioxidant activity and the total phenolic content of the materials increased with the augmentation of OEO and with the antioxidant release time. Interestingly, the nanocomposite films made of chitin nanocrystals from shrimp showed better total phenolic content than the unfilled films and the nanocomposite films made of chitin nanocrystals from lobster over the first 48 h. Henceforward, this study demonstrated the potential of the nanocomposite films based on PVA, OEO and reinforced with α-CHNC for active food-packaging applications.

1. INTRODUCTION

One of the big challenges for our society in this century is to decrease the enormous amount of non-biodegradable plastics waste. Every year, 150 million tons of plastic waste are estimated to reach the oceans [6].

To replace part of these non-biodegradable plastics for biodegradable and/or 'bioplastics', *i.e.* plastics prepared from renewable resources (biopolymers), in recent years, many by-products from both agricultural and marine companies have gained interest in different industry sectors such as cosmetics, medical and food packaging due to their sustainable and eco-friendly attributes. Therefore, numerous scientific studies have been done in this sense. This include the use of natural polymers or synthetic biodegradable polymers that can be use as matrices and/or reinforcing agents; and bioactive compounds, which are used to improve the biological properties of the final materials.

Among the polymers, chitin (poly(β-(1-4)-N-acetyl-D-glucosamine), is a biopolymer found in the exoskeleton of crustaceans like crabs, lobster and shrimps; and is one of the biggest residues in fishing industry [18,257]. However, it can also be found in the cell walls of fungi and in cuticle of insects. Being a supporting material in nature, chitin presents a highly organized micro- and nano-fibrillated structure. Under acid hydrolysis it is possible to obtain chitin nanocrystals (CHNC) with dimensions that can range from 6-60 nm in width and 100-800 nm in length [23,32]. These chitin nanocrystals present excellent properties namely low density, biocompatibility, low toxicity, biodegradability and antimicrobial properties. In

addition, its use as reinforcement agents in biocomposite films, improves the thermal stability and the mechanical properties [11,19]. A very interesting synthetic polymer, that can be used for the mentioned applications, is poly(vinyl alcohol), PVA. It is a biodegradable, non-toxic, biocompatible and soluble in water polymer presenting good film-forming and mechanical properties [258–260].

Among the bioactive agents, essential oils (EOs) are one of the most important products of agriculture-based industry due to its bioactive properties that include antimicrobial, antiviral, antioxidant, anticancer and immunomodulatory [54,57,115]. Their production is superior to 70,000 tons per year. EOs are aromatic compounds with low molecular weight extracted from plants namely barks (cinnamon), leaves (eucalyptus), flowers (lavender) and peels of fruits (orange) [115,260]. They possess various applications in health, agriculture, cosmetic, food and medicine industries. Moreover, are recognized by the Generally Recognized as Safe (GRAS) by the US Food and Drug Administration (USFDA) as safe foods [57]. Due to its medicinal and culinary properties, oregano essential oil (*Origanum vulgare),* which belongs to the *Lamiaceae* family, is one of the most employed oil since ancient times. Its properties are attributed to the presence of monoterpenes among which carvacrol and thymol stand out [59,261].

The use of EOs is quite limited because of their high volatile properties and easily decomposition during handling, heating, exposure to oxygen or ultraviolet light, etc. [37,42]. For these reasons, EOs need to be encapsulated/incorporated in materials that could

present the form of films, coatings, nanocapsules and emulsions, in order to preserve their bioactive activities. Therefore, different polymeric matrices have been used such as chitosan, polylactic acid (PLA), soy protein, fish gelatine among others [43,65,245,262]. For instance, Munhuweyi *et al.* used chitosan as matrix with oregano oil, and Wu J. *et al.* used a mixture of gelatine with chitosan by incorporating this oil to make films [213,263]. Also, PVA films were developed by mixing this polymer with clove oil and apple pomace as bioactive agents [259,260,264,265]. Hashemi *et al.* prepared a basil seed gum coating with oregano oil and Fraj *et al.* obtained polycaprolactone nanocapsules using this oil as an active ingredient [264,266]. On the other hand, Hosseini et al. studied emulsions of chitosan with oregano oil and Ribes et al. prepared an emulsion with clove and oregano oil mixed with xanthan gum [59,267].

Nonetheless, there are few works in which nanocrystals or nanofibers like nanocellulose or nanochitin, have been used to reinforce the final mechanical and biological properties of the films. Some examples are the research done by Luzi *et al.* [268] where the authors used PVA and chitosan, as a matrix adding carvacrol, as bioactive agent and cellulose nanocrystals as reinforcing agent; or by Ardekani *et al.* [221] that assessed the properties of PVA, *Zataria multiflora* oil and mats nanofiber films; or by Jahed *et al.* [29] that studied the physicochemical properties of *Carum copticum* essential oil loaded chitosan films containing organic nanoreinforcements.

In this context, the aim of this research was to developed bioactive nanocomposite films using two different sources of alpha-chitin nanocrystals (α-CHNC) as reinforcing agents to improve the final

properties of PVA and *Origanum vulgare* essential oil (OEO) films. To the best of our knowledge, chitin nanocrystals have not been studied as reinforcing agents in PVA with EOs, in particular with oregano oil. The effect of the different concentrations of EO and the origin of chitin nanocrystals on the final properties of the nanocomposite films, were assessed. Therefore, their thermal, mechanical and antioxidant properties were studied in order to evaluate their potential use in food packaging applications.

2. MATERIALS AND METHODS

2.1. Materials

For this work, two different α-chitin nanocrystals were isolated from chitin from: i) yellow lobster (*Cervimunida johni*) extracted in-house kindly supplied by Antarctic Seafood S.A. (Chile); (ii) shrimp (*Parapenaeus longirostris*) kindly provided by Mahtani Chitosan Pvt. Ltd. (India). The two α-chitin nanocrystal (α-CHNC) samples were obtained under the conditions of 125 W during 10 min using 1 M HCl solution (exp. 6-**Chapter 1**) employing the MAE technique described in **PART III**. The degrees of acetylation (DA), determined by solid ^{13}C NMR (see **PART III**) and were found to be 85 % and 90 % for shrimp and lobster chitin nanocrystals, respectively [128]. The crystallinity index (CI %), was 89 % for shrimp chitin nanocrystals and 94 % for lobster chitin nanocrystals, as obtained by XRD (see **PART III**).

Oregano oil FCC (OEO, *Origanum vulgare,* with Food Grade) was supplied by Sigma-Aldrich. *Origanum vulgare* essential oil composition was determined using GC/MS (see **Part III**). The identification of the different compounds was carried out by using the National Institute of Standards Library (NIST). The obtained data is

summarized in the Table IV-22. Only compounds with areas superior to 0.4 were accounted for. 14 compounds of OEO were identified representing 97.4 % of the total essential oil. The main components were carvacrol representing 75 % and ϒ-terpinene at around 5.96 %. These results are in agreement with those obtained previously by Munhuweyi et al. [213] and Hosseini et al. [59].

Table IV-22. Composition of Origanum vulgare assessed by GC/MS.

Component	Area (%)	Retention Time (min)
1R-α-Pinene	0.51	5.07
β-Pinene	0.40	5.69
β-Myrcene	0.56	5.81
α-Terpinene	0.92	6.24
o-cymenene	5.87	6.36
Eucalyptol	0.60	6.47
γ-Terpinene	5.96	6.86
β-Linalool	1.46	7.44
Borneol	0.82	8.76
1-terpinen-4-ol	0.52	8.98
Thymol	1.97	11.99
Carvacrol	75.05	12.50
Caryophyllene	2.33	15.55
α-Humulene	0.43	16.22
Total	**97.4**	-

All the reagents employed are presented in Appendix B.

2.2. Preparation of the nanocomposite films

PVA solutions (2 % w/v) were prepared by dissolving PVA in a mixture of ethanol (60 % v/v) and distilled water under stirring

overnight at 55 °C. The oregano essential oil (OEO) concentration varied from 0.5 to 2 % v/v with respect to PVA solution. The nanocomposite films were prepared by adding 0.5 % w/v of chitin nanocrystals (α-CHNC, from shrimp or lobster). The dispersion of α-CHNC in the PVA solutions was done using an Ultra-Turrax (Heidolph Silent Crusher M., Germany) at 13 500 rpm for 10 min. A second set of samples was prepared without α-CHNC. All suspensions or solutions were degassed in order to remove entrapped air. The films were then prepared by casting at room temperature using 50 mm-diameter silicon molds for 72 hours. The ensuing materials were kept in a conditioning cabinet at 50 ± 5 % relative humidity (RH) and 25 °C.

The nanocomposite films were characterised by physico-chemical, structural (ATR-FTIR), thermal (TGA) and mechanical properties analyses. In addition, the total phenolic content and antioxidant properties were measured at 12, 24, 48 and 72 h. The techniques were described in **PART III**.

In order to assess the impact of the ultraviolet (UV) irradiation on the nanocomposite films, the samples were exposed to UV light into a dark room with an UV lamp at 364 nm during 3 days according to the method described by Morales *et al.* [258]. The effect of the UV irradiation was evaluated by measuring the mechanical properties of the films. The identification and composition of the nanocomposite films in terms of α-CHNC and OEO are listed in Table IV-23.

Table IV-23. Identification and composition of the nanocomposite films.

Samples identification	Source of α - CHNC	PVA (% w/v)	α-CHNC (% w/v)	OEO (% v/v)
P-0		2	0	0
P-0.5		2	0	0.5
P-1	-	2	0	1
P-1.5		2	0	1.5
P-2		2	0	2
PNCS-0		2	0.5	0
PNCS-0.5		2	0.5	0.5
PNCS-1	Shrimp	2	0.5	1
PNCS-1.5		2	0.5	1.5
PNCS-2		2	0.5	2
PNCL-0		2	0.5	0
PNCL-0.5		2	0.5	0.5
PNCL-1	Lobster	2	0.5	1
PNCL-1.5		2	0.5	1.5
PNCL-2		2	0.5	2

2.3. Statistical analysis

The statistical analysis was performed using one-way analysis of variance (ANOVA) by SPSS software (Version 24, Inc. Chicago, IL, USA). The values of the significant differences were determined by Duncan's multiple range test. The experiments were carried out at least three times for each condition. The results are expressed as average ± standard deviation and values of $p < 0.05$ were considered statistically significant.

3. RESULTS AND DISCUSSION

3.1. Physico-chemical characterization of the nanocomposite films

Our main aim in this study was to developed bioactive nanocomposite films using two different sources of alpha-chitin nanocrystals (α-CHNC) as reinforcing agents to improve the final properties of PVA and *Origanum vulgare* essential oil (OEO) films. Herein, we specifically focus on the effect of the different concentrations of OEO and the origin of chitin nanocrystals on the final properties of the PVA-based nanocomposite films. As a first step, we focused on the general aspect of the films and on their physicochemical characterization. Afterwards, their thermal and mechanical properties, as well as their stability against UV light and their antioxidant properties were assessed in order to evaluate their potential use for packaging-food applications.

One of the most important parameters in films for food applications is their transparency because it has a direct impact on the consumer acceptance. To evaluate the impact of the incorporation of OEO and chitin nanocrystals on the transparency of the final materials, pictures were taken and the transmittance and opacity of the nanocomposite films were measured and calculated, respectively.

3.1.1. *Appearance and optical properties of films*

Figure IV-21, displays the general aspect of the final films. The obtained films are homogeneous and translucent. Figure IV-22 represents the transmittance (measured in the range between 400 - 750 nm) profiles of the nanocomposite films and confirms the qualitative analyse of Figure IV-21.
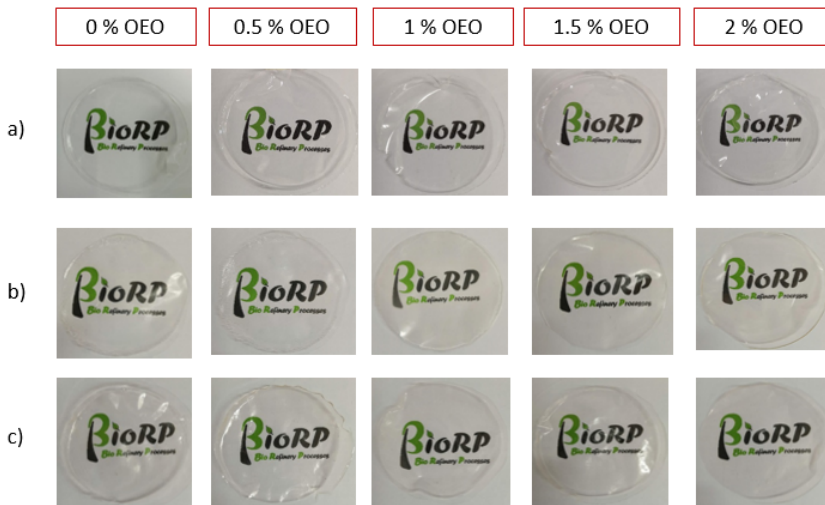
Figure IV-21. General appearance of the nanocomposite films. From left to right: a) P-O, P0.5/P1/P1.5/P2; b) PNCS-O/PNCS-0.5/PNCS-1/PNCS-1.5/PNCS-2; c) PNCL-O/PNCL-0.5/PNCL-1/PNCL-1.5/PNCL-2.

As demonstrated in Figure IV-22, in the range of the visible light (400 to 750 nm), the highest transmittance were ascribed to the unfilled PVA film (P-0, around 90 % at 600 nm) and to the films prepared with low concentrations of OEO. However, our data showed that the incorporation of high concentration of OEO (P-2) decreases the transmittance of the films. On the other hand, as expected, the addition of chitin nanocrystals decreases the transmittance of the nanocomposite films (PNCS-0 and PNCL-0), as previously demonstrated with other matrices [32,125]. Interestingly, the incorporation of OEO into the nanocomposite films showed a decrease of the transmittance of the final materials. Previous studies, have demonstrated the influence of the addition of EOs on different matrices, namely the work described by Sahraee et al. [42] and Gomes et al. [217], where the authors prepared materials using chitosan as

matrix with different concentrations of essential oils; or described by Kanatt et al. [247], where CS and PVA were blended with plants extract.
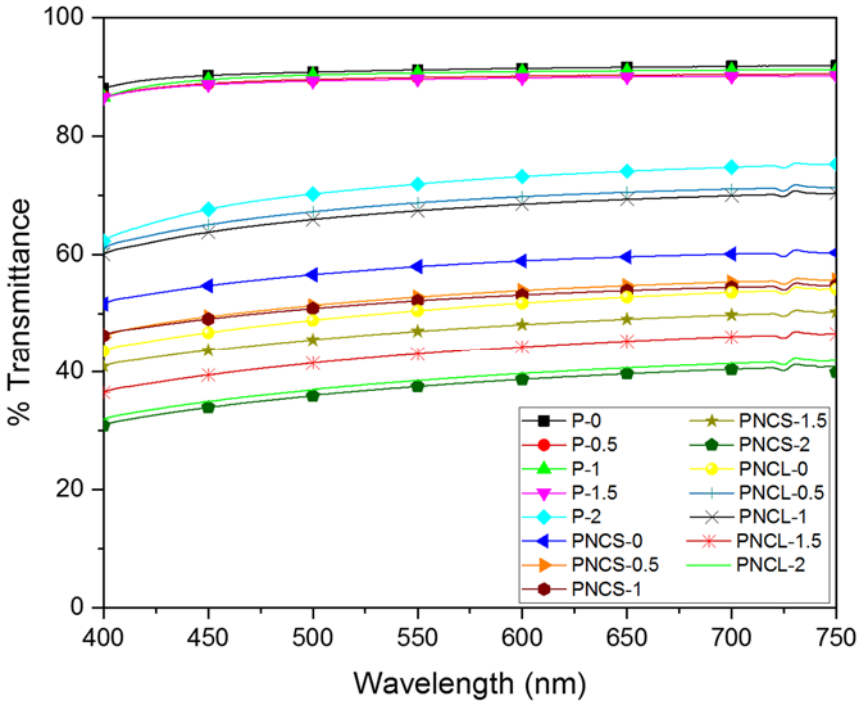
Figure IV-22. Transmittance from 400 to 750 nm of the nanocomposites films.

To underline these data, the opacity of the films was also calculated (equation III-7, see in **PART III)** that take in account the absorbance of the films at 600 nm and the thickness). The results are listed in Table IV-24. The lowest opacity value was observed in the pure PVA film (P-0) presenting an opacity of 0.65 ± 0.01. Similar to the data obtained by Chen et al. [259], by incorporating clove essential oil or apple pomace into PVA films, the opacity of our nanocomposite films increases with the incorporation of high concentrations of OEO

(P-1.5 and P-2). In addition, the addition of nanocrystals resulted in a consequent increase of the opacity of the films. No significant differences were observed between the 2 types of chitin nanocrystals: 2.16 to 2.99 and 2.43 to 2.84 for films prepared with shrimp and lobster chitin nanocrystals, respectively.

Table IV-24. Data concerning the thickness, opacity and MC (moisture content) of the nanocomposite films. The values were average ± standard deviation (thickness n=6; opacity and moisture content n=3). Superscript letters depict significant differences (Duncan's test, p < 0.05) among OEO concentration with in each chitin nanocrystals treatment.

Samples	Thickness (µm)	Opacity	MC (%)
P-0	48.0± 1.8[a]	0.65 ± 0.01[a]	11.0 ± 0.2[a]
P-0.5	49.0 ± 3.5[a]	0.66 ± 0.02[a]	10.8 ± 0.8[a]
P-1	60.2 ± 3.6[b]	0.68 ± 0.06[a]	8.0 ± 0.1[b]
P-1.5	66.7 ± 2.3[c]	0.75 ± 0.02[b]	5.9 ± 0.7[c]
P-2	72.8 ± 2.0[d]	0.93 ± 0.04[c]	5.1 ± 0.2[d]
PNCS-0	48.2 ± 2.1[a]	2.16 ± 0.12[a]	13.2 ± 3.2[a]
PNCS-0.5	53.2 ± 2.0[b]	2.36 ± 0.34[ab]	10.0 ± 2.7[a]
PNCS-1	56.2 ± 3.0[b]	2.38 ± 0.05[ab]	9.1 ± 1.2[a]
PNCS-1.5	61.8 ± 3.8[c]	2.44 ± 1.94[b]	7.7 ± 2.9[a]
PNCS-2	64.3 ± 3.8[c]	2.99 ± 0.19[b]	7.4 ± 1.9[a]
PNCL-0	51.1 ± 4.3[a]	2.43 ± 1.40[a]	13.1 ± 0.5[a]
PNCL-0.5	65.1 ± 1.1[b]	1.96 ± 0.04[b]	11.4 ± 1.3[ab]
PNCL-1	71.2 ± 3.0[c]	2.14 ± 0.07[c]	10.4 ± 1.6[b]
PNCL-1.5	76.0 ± 4.8[cd]	2.56 ± 0.04[d]	8.1 ± 0.5[c]
PNCL-2	79.2 ± 5.8[d]	2.84 ± 1.64[e]	6.0 ± 0.4[d]

3.1.2. *Moisture content*

Another important aspect for food-packaging materials is their water absorbance capacity, because being in contact with food can cause the damage of the product. Table IV-24 reports the results of the moisture content of the nanocomposite films. The data listed in Table IV-24 show that the incorporation of OEO decreases the moisture content of the PVA films. The lowest value of moisture content was observed for the P-2 films (5.1 ± 0.2 %). Interestingly, even for the nanocomposite films that have an important amount of OH groups, the incorporation of OEO induces the decrease of moisture content. These results are attributed to the hydrophobic properties of the OEO, and good interaction between OEO, α-CHNC and PVA leaving least possibility for them to interact with water molecules [269].

3.1.3. *ATR-FTIR*

In Table IV-25 are listed the ATR-FTIR band assignments of OEO and PVA. For instance, the OEO spectra presented a broad peak at 3397 cm^{-1} belonging to the O-H stretching which was attributed to carvacrol, and the phenolic ring was assigned to the peaks between 1622 and 1424 cm^{-1}. The peak at 941 cm^{-1} showed C-H bending and at 810 cm^{-1} revealed the characteristic peak of thymol [221,266].

Regarding the PVA, for example, the peaks at 1732 cm^{-1} and 1573 cm^{-1} were attributed to ester C=O stretching vibration and C=C stretching vibration, respectively. Other representative bands of PVA are the C-C stretching vibration at 1090 cm^{-1} and 1022 cm^{-1}, and C-C and C-O stretching vibration at 843 cm^{-1} [221,270]. In addition, the C-H$_2$

bending vibration and C-CH$_3$ deformation vibration were observed at 1428 cm^{-1} and 1377 cm^{-1}, respectively [258,265,271].

Table IV-25. ATR-FTIR band assignments of OEO and PVA.

	Band (cm^{-1})	Functional group assignment
OEO	3397	O-H stretching
	2960	symmetric C-H stretching
	2872	asymmetric C-H stretching
	1622 - 1424	phenolic ring
	1586	N-H bending
	1456	C-H$_2$ bending
	1250 - 1112	C-O-C stretching
	941	C-H bending
PVA	3295	O-H tensile vibration
	2914 - 2943	alkyl asymmetric stretching
	1732	ester C=O stretching vibration
	1573	C=C stretching vibration
	1428	C-H$_2$ bending vibration
	1377	C-CH$_3$ deformation vibration
	1247	C-O stretching
	1090 - 1022	C-C stretching vibration
	843	C-C and C-O stretching vibration

Figure IV-23, displays the ATR-FTIR spectra of OEO, PVA, PNCS-2 and PNCL-2. All nanocomposite films (not showed) showed characteristics bands corresponding to each component, as demonstrated with the representative examples. For instance, when compared to OEO, P-0 and P-2 spectra, the PNCS-2 and PNCL-2 spectra, showed an increase of the intensity of the band corresponding to the O-H stretching vibrations (around 3400 cm^{-1}); of the bands corresponding to the C-H stretching (around 2950 cm^{-1}); and of the bands at 1657 and 1620 cm^{-1} attributed to amide I and at 1556 cm^{-1}, corresponding to amide II, which is due to the presence of the chitin nanocrystals.
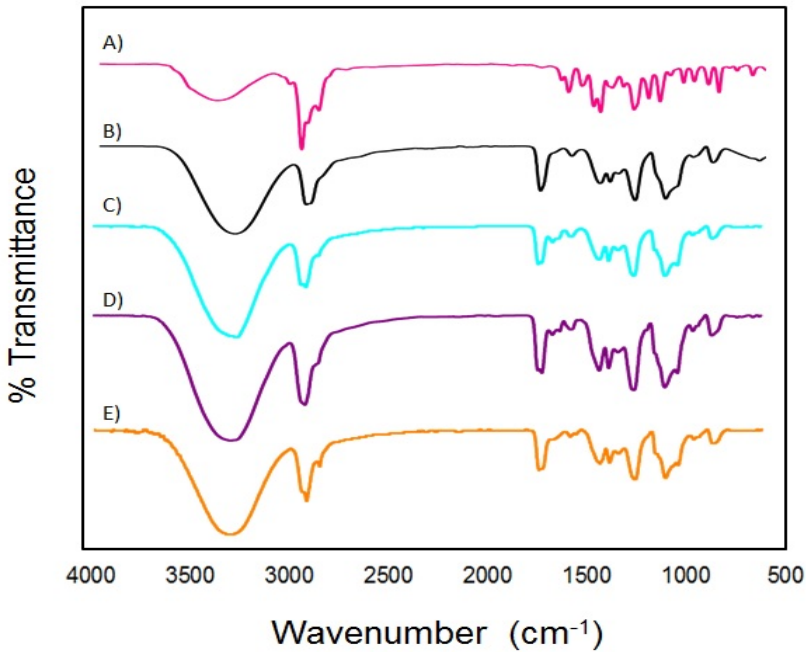
Figure IV-23. FTIR spectrum of a) OEO, b) P-0, c) P-2, d) PNCS-2, e) PNCL-2.

3.2. Thermal and mechanical properties

The effect of the incorporation of chitin nanocrystals into the PVA/OEO films was evaluated in terms of thermal and mechanical properties. The TGA serves as a proof for chemical interactions and the formation of hydrogen bonds in the final materials. Figure IV-24 shows the thermogravimetric analysis (TGA) and derivative (dTGA) curves of the PVA and PVA/OEO films and of the nanocomposite films. The results from TGA and dTGA, clearly showed that the PVA film displayed two-stages of degradation a first step with a maximum degradation at 319 °C attributed to the degradation of the amorphous parts of the polymer, and a second step at around 420 °C that corresponds to the degradation of the higher thermal stability crystalline parts. The PVA/OEO films depicted 4 degradation steps

and presented lower thermal stability compared to control. The first step occurred at around 100 °C and was attributed to the loss of water; the second step was observed at 180 °C and was ascribed to the degradation of the OEO [259]. The third and fourth steps were attributed to the PVA degradation, but their maximum temperature of degradation decreased between 15-20 °C. Nevertheless, it was observed that the incorporation of both chitin nanocrystals showed an improvement of the thermal stability of the PVA/OEO films. This fact was attributed to the high temperature of degradation of chitin nanocrystals (around 380 °C, degradation of chitin macromolecules) and to the good homogeneity and interactions between the chitin nanocrystals and the PVA, the increasing of crystallinity of PVA molecules in the presence of the chitin nanocrystals is also a possibility. Like for PVA/OEO films, the nanocomposite's dTGA curves exhibited 4 degradation steps. However, the maximum temperature of degradation of the materials increased (for instance, 318 °C for PNCL-1 and -2, Figure IV-24).
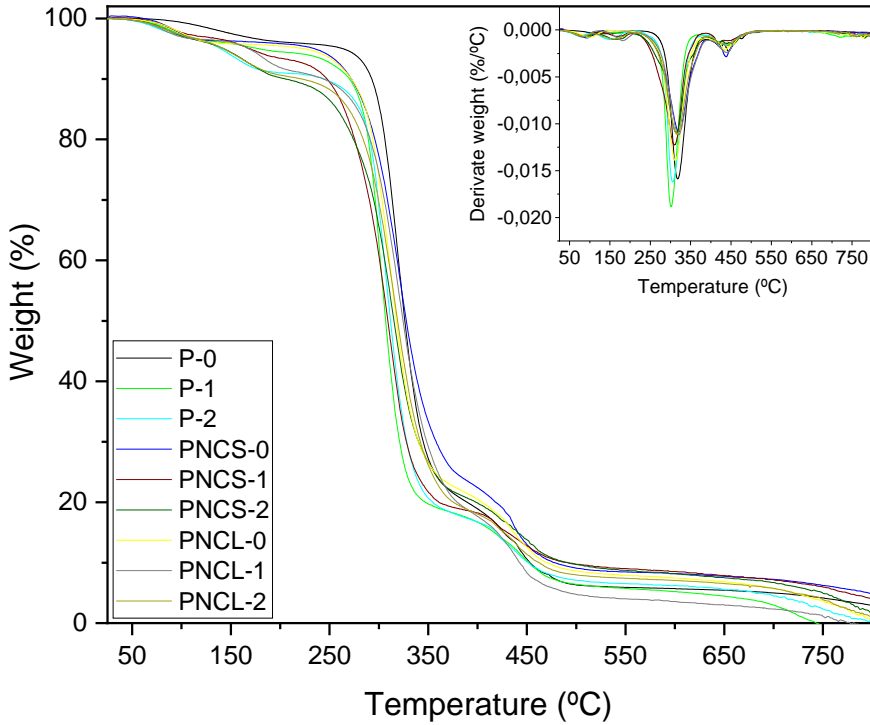
*Figure IV-24. TGA and dTGA curves nanocomposite films: P-0, P-1, P-2,
PNCS-0, PNCS-1, PNCS-2, PNCL-0, PNCL-1, and PNCL-2.*

The data of the mechanical properties of the nanocomposite films is summarized in Table IV-26. The results showed no significant differences ($p > 0.05$) regarding the TS values of the unfilled PVA films (without α-CHNC) with the increasing of the concentration of OEO (P-0 to P-2). However, the TS of the nanocomposite films decreased significantly ($p < 0.05$) with the concentration of OEO. These results are in accordance with those obtained by Gaikwad et al. [260], in which the TS values decreased with the concentration of apple pomace in PVA films; or with Chen et al. [259] that observed a decrease in TS values in PVA films with clove oil. Nonetheless, the

incorporation of the chitin nanocrystals allowed increase the TS with respect to PVA/OEO films making the nanocomposite films more resistant, as demonstrated before in other matrices [32,125,204].

Table IV-26. Mechanical properties of the nanocomposite films before and after UV radiation no irradiation and irradiation films (TS: tensile strength, MPa; YM: Young's modulus, MPa; and E: elongation, %). The values were average ± standard deviation (n = 10). Superscript letters depict significant differences (Duncan's test, p < 0.05) among oil concentration with in each chitin nanocrystals treatment.

Samples Identification	Not UV-irradiated samples			UV-irradiated samples		
	TS (MPa)	YM (MPa)	E (%)	TS (MPa)	YM (MPa)	E (%)
P-0	16.02 ± 7.73[a]	575.61 ± 41.89[a]	176.44 ± 64.11[a]	17.68 ± 3.23[ab]	291.44 ± 93.21[a]	117.00 ± 10.73[a]
P-0.5	13.74 ± 1.58[a]	574.41 ± 5.79[a]	202.85 ± 72.24[a]	19.43 ± 1.14[b]	287.52 ± 98.59[a]	177.80 ± 6.75[b]
P-1	14.11 ± 2.71[a]	555.89 ± 30.84[a]	224.38 ± 81.11[a]	12.45 ± 1.82[a]	260.45 ± 69.77[a]	172.00 ± 56.87[b]
P-1.5	14.44 ± 7.43[a]	512.48 ± 65.98[a]	295.34 ± 81.89[b]	11.63 ± 4.95[a]	243.65 ± 75.53[a]	186.71 ± 45.93[b]
P-2	13.06 ± 3.85[a]	237.99 ± 3.31[b]	298.97 ± 85.50[b]	11.44 ± 3.98[a]	170.89 ± 94.89[a]	208.51 ± 18.23[b]

PNCS-0	33.39 ± 2.93[a]	756.56 ± 197.89[a]	139.45 ± 82.56[a]	25.19 ± 4.21[a]	468.96 ± 179.09[a]	135.40 ± 38.71[a]
PNCS-0.5	27.22 ± 2.87[c]	579.00 ± 69.85[b]	128.73 ± 56.96[a]	26.83 ± 1.58[a]	454.99 ± 156.37[a]	185.70 ± 8.68[ab]
PNCS-1	30.10 ± 2.55[b]	397.89 ± 125.62[c]	195.14 ± 57.95[ab]	21.05 ± 3.89[b]	401.03 ± 112.64[a]	187.29 ± 25.33[b]
PNCS-1.5	23.82 ± 3.70[d]	377.39 ± 91.94[c]	222.83 ± 88.49[b]	16.49 ± 3.21[c]	346.16 ± 117.03[ab]	198.22 ± 51.04[b]
PNCS-2	21.07 ± 1.04[d]	307.85 ± 86.15[c]	225.53 ± 68.78[b]	16.78 ± 2.29[bc]	373.79 ± 102.16[b]	198.53 ± 12.43[b]
PNCL-0	37.88 ± 1.38[a]	754.20 ± 186.71[a]	194.79 ± 29.04[a]	19.79 ± 2.49[a]	487.70 ± 93.21[a]	68.50 ± 18.17[a]
PNCL-0.5	22.52 ± 4.69[b]	385.08 ± 98.10[b]	224.86 ± 60.41[a]	15.24 ± 2.45[b]	322.34 ± 112.59[b]	75.17 ± 9.59[a]
PNCL-1	13.99 ± 1.71[c]	234.18 ± 32.28[c]	214.07 ± 57.73[a]	13.28 ± 2.43[bc]	211.56 ± 69.77[c]	90.24 ± 31.92[a]
PNCL-1.5	12.80 ± 3.11[b]	295.38 ± 57.93[b]	226.33 ± 37.34[b]	12.62 ± 1.95[c]	211.12 ± 75.53[c]	160.03 ± 25.59[b]
PNCL-2	12.67 ± 2.11[c]	242.26 ± 20.97[c]	241.13 ± 43.99[b]	12.35 ± 1.96[c]	186.51 ± 94.89[c]	161.37 ± 72.48[b]

As it could be seen in Table IV-26, like for TS, no significant differences were observed regarding Young's modulus of PVA films with the OEO concentration. However, the Young's modulus of the nanocomposite films decreased with the OEO concentration; but the incorporation of chitin nanocrystals made that the Young's modulus values are higher PVA/OEO films. Similar results were found by Ardekani et al. [221], the authors used wound dressing of PVA with *Zataria multiflora* oil reinforced with nanofibers of mats, and used new mats fibers consisting of blend electrospun chitosan / poly (ε-caprolactone) with oregano essential oil.

On the other hand, the addition of the OEO improved the elongation (E %) of the nanocomposite films and consequently their flexibility due to the OEO plasticizing effect [100,259,272].

3.3. Effect of the UV irradiation on the nanocomposite films

The effect of the UV irradiation on the nanocomposite films was assessed by measuring the mechanical properties of the films after irradiation. The samples were exposed to UV light radiation (364 nm) for 72 h and the data are listed in Table IV-26. No significant changes were observed in the general aspect of the films after the 72 h (images not showed).

In general, comparing the results of the films exposed to UV irradiation with those not irradiated (Table IV-26), a decrease in mechanical properties was observed. The TS values decreased between 25-50 % for the films without α-CHNC and 25-30 % for the nanocomposite films.

Rodriguez-Felix et al. [273] observed this trend in chitosan and polyethylene films. With this work, the authors demonstrated that TS values decrease between 80-90 % during 135 days. Other researchers such

as Bai et al. [274], showed that after 30 days of exposure to UV light, the values of TS decrease in EDTA/Fe^{3+}/Alginate.

Regarding the Young's modulus (YM) results, it was observed that films irradiated during 72 h had lost stiffness since they showed lower values than the films that have not been irradiated. These results are in accordance with Morales et al. [258], which demonstrated that YM decreased to 1750 MPa in the bio-oil film when irradiated during 60 h. Furthermore, the YM values of the films PNCL (between 468-373 MPa with the content of OEO) were higher than the films PNCS (between 487-186 MPa with OEO concentration). The data also showed that the PNCL nanocomposite films were the ones that showed the highest reduction when they were irradiated with respect to the non-irradiated, observing a drop between 33-67 % in their YM.

Summarizing, the addition of both α-CHNC as reinforcing agents, for one hand, allowed the increase in mechanical properties of the unfilled PVA/OEO films; and for the other hand, causes an increased of the stability of the final materials when they were submitted to UV radiation.

3.4. Total phenolic content and antioxidant activity

In order to avoid the use of synthetic compounds to protect food from oxidation, today there is an increasing demand for active packaging to release natural compounds, in particular essential oils. In this work, to assess the antioxidant activity of the nanocomposite films, two different assays were done: (i) total phenolic content (TPC) used to determine the total amount of phenolic compounds that are important constituents with redox properties responsible for antioxidant activity [70]; and (ii) DPPH assay, in which the antioxidant activity of the samples was measured

through the ability of the samples to donate hydrogen to the radical DPPH [29].

Therefore, herein, the profile of total phenolic content and antioxidant release of the OEO from the films and nanocomposite films were studied by immersion in a methanol solution for 12 h, 24 h, 48 and 72 h. The results of the TPC and DPPH assays are shown in Figures IV-25 and 26, respectively.

In both assays, the pure PVA film (P-0) did not show any antioxidant activity, as demonstrated earlier [128,265]. However, the films prepared with OEO and α-CHNC showed antioxidant activity. This is consistent with other studies in which it was shown that the OEO contains antioxidant compounds such as carvacrol or thymol [59,261]. Furthermore, the data also demonstrated that the total phenolic content and antioxidant activity of the samples, gradually increased with the increasing of the immersion time and OEO concentration (Figure IV-25 and 26).

More specifically, regarding to the TPC data (Figure IV-25), the P-2 film, which contains a higher concentration of OEO, showed the greater release of phenolic compounds with 36.47 ± 0.04 mg GAE/g film value at 72 h. On the other hand, it was observed that in films without nanocrystals there was a huge increase in phenolic content from 12h to 72 h. For instance, for the films P-1, P-1.5 and P-2 an increase of 85 %, 78 % and 95 % was observed, respectively.
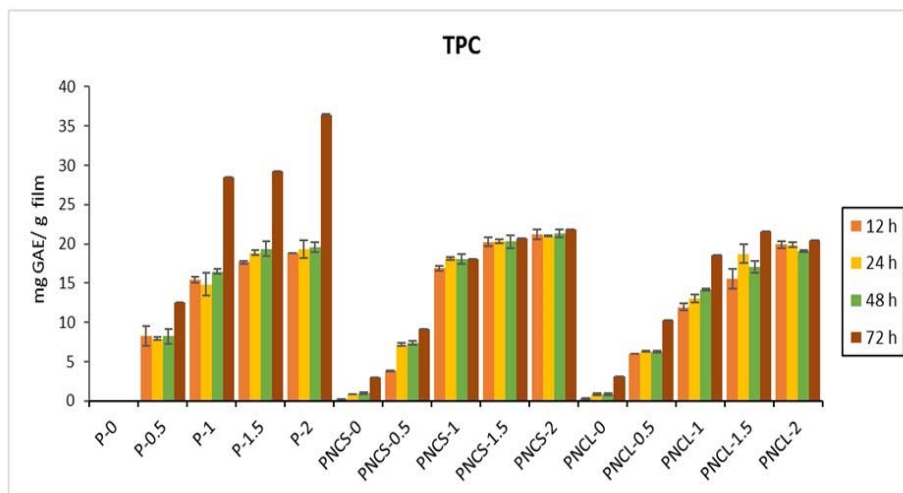
Figure IV-25. Total phenolic compounds (TPC) of the films at different time. The values were average ± standard deviation (n = 3).

In Figure IV-25 when comparing the films with shrimp and lobster nanocrystals (PNCS and PNCL), it was observed that the films prepared with shrimp nanocrystals showed slightly higher values of TPC for all release times, in particular for PNCS-1 film. On the other hand, the release of phenolic compound over the time for the films PNCS-1.5 and PNCS-2 was practically constant, keeping its values constant around 20 and 21 mg GAE /g film, respectively. Interestingly, the materials made of shrimp nanocrystals showed better results than the unfilled films over the first 48 h, and then the nanocomposite films made of lobster shrimp over the 72 h.

Figure IV-26 shows the antioxidant activity of the films obtained by DPPH assay. Among all materials, the antioxidant activity of P-2 film reflected the highest value after 72 h (2.12 ± 0.02 μmol TE/g film). In the films made of PVA and OEO, an important increase in the antioxidant activity was observed from 12 to 72 h. The higher growth occurred in the P-1 film with an increase of around 86 %. The nanocomposite films made of

shrimp nanocrystals showed better results than the nanocomposites prepared with lobster nanocrystals, but just the samples PNCS-1.5 and PNCS-2 over the first 48 h.
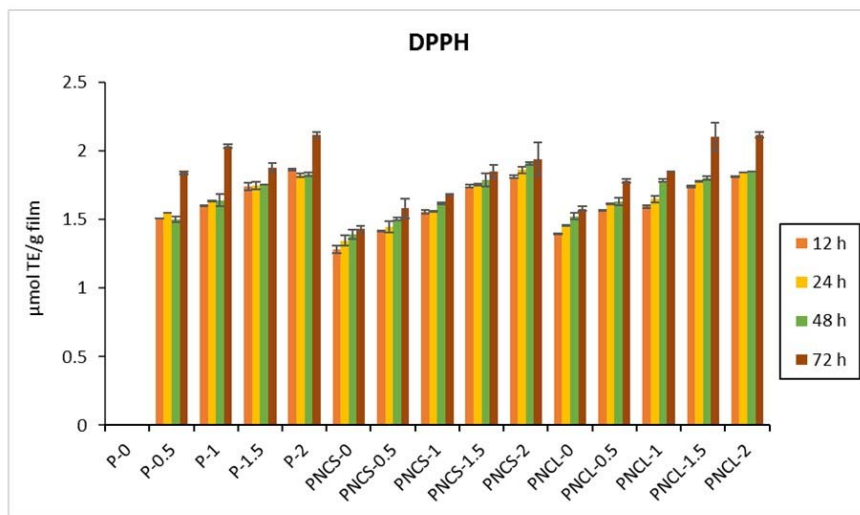
FigureIV-26. DPPH (2,2-diphenyl-1-picrylhydrazyl) radical scavenging assay of the films at different times. The values were the average ± standard deviation (n = 3).

In general, films containing nanocrystals (PNCS and PNCL) showed a slow release of antioxidant compounds over time (more constant release compared with unfilled films). There are different hypothesis that could explain this fact: (i) chitin nanocrystals create sinuous paths in the PVA matrix and makes that the antioxidant molecules of the OEO take longer to pass through these paths; (ii) the formation of strong interactions between nanocrystals and OEO compounds, making their release slow and constant; (iii) by adding chitin nanocrystals, the porosity of the PVA matrix decreases and therefore, there is a reduction in the segmental mobility of the OEO; and (iv) chitin nanocrystals form a network and, in addition, increase the

crystallinity of PVA molecules and this obstructs the mobility of OEO molecules [29,275].

4. CONCLUSIONS

The main aim of this study was to evaluate the effect of the incorporation of α-chitin nanocrystals from shrimp and lobster on the final properties PVA/OEO films made by solvent casting.

Our data demonstrated that the nanocomposite films were homogeneous and translucent even with a slight increase of the opacity. Nonetheless, the obtained nanocomposite films containing α-CHNC showed: (i) better thermal stability; (ii) better mechanical properties. Moreover, after exposure the nanocomposite films to UV radiation, it was demonstrated that the presence of α-CHNC had a retarding effect on their loss of mechanical properties; (iii) a more constant release of the antioxidant compounds over time for both TPC and DPPS assays; (iv) better antioxidant activity for the materials made of shrimp nanocrystals over the first 48h; and (v) no major effects were found regarding the source of chitin.

These results demonstrated that the nanocomposites films of PVA, α-CHNC and OEO could be promising biodegradable and active films for the food industry.

PART V:
GENERAL
CONCLUSIONS
& FUTURE

PART V: GENERAL CONCLUSIONS & FUTURE WORKS

This thesis report the development of nanocomposite materials based nanochitin and other (bio)polymers, in particular chitosan, as matrix and EOs as bioactive compounds. To do so, the work developed in this thesis was divided in two main parts. In the first, the valorisation of marine wastes was done, by the extraction of nanochitin (nanocrystals and nanofibres) using a new green approach and production of chitosan. The optimization of the extraction of *Curcuma longa* L. oil was also assessed. In the second part, the effect of the incorporation of EOs on the final properties of the developed nanochitin-based nanocomposite films was investigated.

In this thesis, it was demonstrated that the valorisation of marine wastes is possible by obtaining and isolating nanochitin and chitosan and their subsequent application in the development of nanocomposite films. Moreover, the use of essential oils as bioactive agents improves the biological properties of the nanocomposite films due to their antioxidant and antifungal properties.

In the **Extraction of Nanochitin and EOs** part, in the first chapter (**Chapter 1**) nanochitin was isolated from 3 different sources: yellow lobster, shrimp and squid pen by mean of a Box-Behnken experimental design using a green approach - microwave-assisted extraction. The optimised conditions were HCl concentration, reaction time and power, and their influence on the extraction yield was studied. The results showed that the obtained α-chitin nanocrystals from yellow lobster and shrimp and β-chitin nanofibres from squid pen presented the same chemical structure as chitin and better crystallinity. In addition, similar extraction yields, morphology and thermal stability to those obtained by conventional methods were found. This work demonstrated that nanocrystals and nanofibres could be

isolated using an environmentally friendly method such as microwave-assisted extraction while decreasing the reaction time (10 min and 14.34 min for α-chitin nanocrystals from yellow lobster and shrimp, respectively and 29.08 min for β-chitin nanofibres from squid pen) and 1 M HCl concentration for all nanochitins.

In **Chapter 2**, the extraction of *Curcuma longa* L. oil was optimised by means of a Box-Behnken experimental design using the microwave-assisted extraction technique. The optimized conditions were the reaction time, power and curcuma:ethanol ratio and how they affected the extraction yield. Furthermore, the yield and the properties of the extracted oil were compared with those obtained by the conventional Soxhlet method. The obtained curcuma oils with the microwave-assisted extraction method showed higher extraction yield, antioxidant properties (DPPH, FRAP and ABTS) and total phenolic content. Furthermore, the same compounds were obtained with both methods. Thus, it was confirmed that the extraction of curcuma oil by a more eco-friendly method such as microwave-assisted extraction is possible.

In the **Materials development** part, in **Chapter 3**, chitosan with β-chitin nanofibres (**Chapter 1**) active films were developed with Origanum majorana L. essential oil and its 3 fractions. The films with deterpenated fractions, which contained higher percentage of oxygenated terpene derivatives, showed higher inhibition of *Aspergillus niger's growth*. On the other hand, the film, which contained a higher percentage of terpenes, showed no cytotoxicity on the viability of L929 cell fibroblasts and totally blocked UV light below 300 nm. All this demonstrated that the type of essential oil fraction added to the films considerably determines the properties of the film and that, consequently, the addition of different essential oils provides suitability for a wide range of applications.

Chapter 4, focused on the application of curcuma oil (**Chapter 2**), anthocyanin extract and their mixture in a chitosan matrix reinforced with α-chitin nanocrystals from lobster (**Chapter 1**) in order to develop smart pH-color sensitive materials. The addition of the bioactive compounds and nanocrystals improved the mechanical properties, hydrophobicity, enhanced its role as a barrier against UV/Vis light and decreased the moisture content and water solubility. In addition, the films showed good antioxidant properties and total phenolic content. Notably, they showed colour changes at different concentrations of ammonia gas and pH solutions. The greatest colour changes and improvement in properties were observed in the CSNC-CA (8:1) film, which contained the highest percentage of curcuma oil. These results demonstrated that the mixture of curcuma oil and anthocyanins into nanochitin/chitosan films could be used as a smart food packaging.

The last chapter (**Chapter 5),** the objective was to apply the alpha-nanocrystals of yellow lobster and shrimp (extracted in **Chapter 1**) to a poly(vinyl alcohol) matrix with different concentrations of *Origanum vulgare* essential oil in order to demonstrate their reinforcement. In addition, the effect of different origins of the nanocrystals and different concentrations of oil on the properties of the films was studied. The data revealed that the addition of the nanocrystals improved the thermal stability, mechanical properties and delayed degradation after exposing the films against UV light. Antioxidant activity and total phenolic content improved with increasing oregano oil concentration and release time. However, no significant effect was found for the source of nanochitin. Owing to the translucent and homogeneous appearance of the films as well as their bioactive activity and biodegradability, the films showed potential as food packaging.

Overall, this work has substantially contributed to: (i) the valorisation of marine waste; (ii) the set-up of new environmentally friendly methods of microwave-assisted isolation and extraction of nanochitin and plant essential oils; (iii) the reinforcement of films with the addition of nanochitin; and (iv) the that the incorporation of EOs in nanochitin/(bio)polymers-based nanocomposite films, improve their functional properties, including their biological activity namely antioxidant and antifungal, and could be used as smart food packaging.

Future works

In order to continue the work in this field, the lines of research that could be considered in the future are as follows:

- Development of new and more eco-friendly techniques for nanochitin isolation.
- The application of the developed nanocomposite films in real food systems.
- Develop and characterise nanochitin and essential oils in other materials such as coatings, emulsions or encapsulations.

PART VI: REFERENCES

REFERENCES

[1]   J.G. Speight, The Refinery of the Future, Elsevier, 2011.

[2]   S. Shafiee, E. Topal, When will fossil fuel reserves be diminished?, Energy Policy. 37 (2009) 181–189. https://doi.org/10.1016/j.enpol.2008.08.016.

[3]   D. Garlotta, A Literature Review of Poly (Lactic Acid) A Literature Review of Poly (Lactic Acid), J. Polym. Environ. 9 (2001) 63–84.

[4]   C. Wang, Z. Zhang, O. Abedinia, S.G. Farkoush, Modeling and analysis of a microgrid considering the uncertainty in renewable energy resources, energy storage systems and demand management in electrical retail market, J. Energy Storage. 33 (2021) 102111. https://doi.org/10.1016/j.est.2020.102111.

[5]   R. Fernández-Marín, J. Labidi, M.Á. Andrés, S.C.M. Fernandes, Using α-chitin nanocrystals to improve the final properties of poly (vinyl alcohol) films with Origanum vulgare essential oil, Polym. Degrad. Stab. (2020) 109227. https://doi.org/10.1016/j.polymdegradstab.2020.109227.

[6]   S. Zhao, T. Wang, L. Zhu, P. Xu, X. Wang, L. Gao, D. Li, Analysis of suspended microplastics in the Changjiang Estuary : Implications for riverine plastic load to the ocean, Water Res. 161 (2019) 560–569. https://doi.org/10.1016/j.watres.2019.06.019.

[7]   T.H. Silva, A. Alves, B.M. Ferreira, J.M. Oliveira, L.L. Reys, R.J.F. Ferreira, R.A. Sousa, S.S. Silva, J.F. Mano, R.L. Reis, Materials of marine origin: A review on polymers and ceramics of biomedical interest, Int. Mater. Rev. 57 (2012) 276–307. https://doi.org/10.1179/1743280412Y.0000000002.

[8]   B. Joseph, R.M. Sam, P. Balakrishnan, H.J. Maria, S. Gopi, T. Volova, S.C.M. Fernandes, S. Thomas, Extraction of nanochitin from marine resources and fabrication of polymer nanocomposites: Recent advances, Polymers (Basel). 12 (2020). https://doi.org/10.3390/POLYM12081664.

[9]   M.J. Hülsey, Shell biorefinery: A comprehensive introduction, Green
        Energy Environ. 3 (2018) 318–327. https://doi.org/10.1016/j.gee.2018.07.007.

[10]   A.M. Salaberria, J. Labidi, S.C.M. Fernandes, Different routes to turn chitin
        into stunning nano-objects, Eur. Polym. J. 68 (2015) 503–515.
        https://doi.org/10.1016/j.eurpolymj.2015.03.005.

[11]   A.M. Salaberria, S.C.M. Fernandes, R.H. Diaz, J. Labidi, Processing of α-
        chitin nanofibers by dynamic high pressure homogenization:
        Characterization and antifungal activity against A. niger, Carbohydr.
        Polym. 116 (2015) 286–291. https://doi.org/10.1016/j.carbpol.2014.04.047.

[12]   Q. Li, J. Zhou, L. Zhang, Structure and Properties of the Nanocomposite
        Films of Chitosan Reinforced with Cellulose Whiskers, InterScience.
        (2009) 15–17. https://doi.org/10.1002/polb.

[13]   H. Celebi, A. Kurt, Effects of processing on the properties of
        chitosan/cellulose nanocrystal films, Carbohydr. Polym. 133 (2015) 284–293.
        https://doi.org/10.1016/j.carbpol.2015.07.007.

[14]   J.K.P. Martim, L.T. Maranho, T.A. Costa-Casagrande, Review: Role of the
        chemical compounds present in the essential oil and in the extract of
        Cordia verbenacea DC as an anti-inflammatory, antimicrobial and healing
        product, J. Ethnopharmacol. 265 (2021) 113300.
        https://doi.org/10.1016/j.jep.2020.113300.

[15]   J. Bravo, V. Carbonell, B. Sepúlveda, C. Delporte, C.E. Valdovinos, R.
        Martín-Hernández, M. Higes, Antifungal activity of the essential oil
        obtained from Cryptocarya alba against infection in honey bees by Nosema
        ceranae, J. Invertebr. Pathol. 149 (2017) 141–147.
        https://doi.org/10.1016/j.jip.2017.08.012.

[16]   F.M. Pelissari, M.V.E. Grossmann, F. Yamashita, E.A.G. Pined,
        Antimicrobial, mechanical, and barrier properties of cassava starch-
        chitosan films incorporated with oregano essential oil, J. Agric. Food
        Chem. 57 (2009) 7499–7504. https://doi.org/10.1021/jf9002363.

[17] R.A.A. Muzzarelli, J. Boudrant, D. Meyer, N. Manno, M. DeMarchis, M.G. Paoletti, Current views on fungal chitin/chitosan, human chitinases, food preservation, glucans, pectins and inulin: A tribute to Henri Braconnot, precursor of the carbohydrate polymers science, on the chitin bicentennial, Carbohydr. Polym. 87 (2011) 995–1012. https://doi.org/10.1016/j.carbpol.2011.09.063.

[18] M. Rinaudo, Chitin and chitosan : Properties and applications, Prog. Polym. Sci. 31 (2006) 603–632. https://doi.org/10.1016/j.progpolymsci.2006.06.001.

[19] A.M. Salaberria, J. Labidi, S.C.M. Fernandes, Chitin nanocrystals and nanofibers as nano-sized fillers into thermoplastic starch-based biocomposites processed by melt-mixing, Chem. Eng. J. 256 (2014) 356–364. https://doi.org/10.1016/j.cej.2014.07.009.

[20] H. Ngoc Cuong, N. Cong Minh, N. Van Hoa, T. Si Trung, Preparation and characterization of high purity b -chitin from squid pens (Loligo chenisis), Int. J. Biol. Macromol. 93 (2016) 442–447.

[21] F. Duman, M. Kaya, Crayfish chitosan for microencapsulation of coriander (Coriandrum sativum L .) essential oil, Int. J. Biol. Macromol. 92 (2016) 125–133. https://doi.org/10.1016/j.ijbiomac.2016.06.068.

[22] F. Larbi, A. García, J. Luis, A. Hamou, J. Puiggalí, Comparison of nanocrystals and nano fi bers produced from shrimp shell α - chitin : From energy production to material cytotoxicity and Pickering emulsion properties, Carbohydr. Polym. 196 (2018) 385–397. https://doi.org/10.1016/j.carbpol.2018.04.094.

[23] J.-B. Zeng, Y.-S. He, S.-L. Li, Y.-Z. Wang, Chitin Whiskers : An Overview, Biomacromolecules. 13 (2012) 1–11. https://doi.org/10.1021/bm201564a.

[24] Y. Ogawa, K. Azuma, H. Izawa, M. Morimoto, K. Ochi, T. Osaki, N. Ito, Y. Okamoto, H. Saimoto, S. Ifuku, Preparation and biocompatibility of a chitin nanofiber/gelatin composite film, Int. J. Biol. Macromol. 104 (2017)

1882–1889. https://doi.org/10.1016/j.ijbiomac.2017.02.041.

[25]   C. Chen, D. Li, H. Yano, K. Abe, Bioinspired hydrogels: Quinone
       crosslinking reaction for chitin nanofibers with enhanced mechanical
       strength via surface deacetylation, Carbohydr. Polym. 207 (2019) 411–417.
       https://doi.org/10.1016/j.carbpol.2018.12.007.

[26]   I. Gülseren, M. Corredig, Interactions of chitin nanocrystals with β_L -
       lactoglobulin at the oil – water interface , studied by drop shape
       tensiometry, Colloids Surfaces B Biointerfaces. 111 (2013) 672–679.
       https://doi.org/10.1016/j.colsurfb.2013.06.058.

[27]   H. Liu, W. Liu, B. Luo, W. Wen, M. Liu, X. Wang, C. Zhou, Electrospun
       composite nanofiber membrane of poly (l -lactide) and surface grafted
       chitin whiskers : Fabrication , mechanical properties and
       cytocompatibility, 147 (2016) 216–225.

[28]   R. Priyadarshi, B. Kumar, F. Deeba, A. Kulshreshtha, Chitosan films
       incorporated with Apricot (Prunus armeniaca) kernel essential oil as
       active food packaging material, Food Hydrocoll. 85 (2018) 158–166.
       https://doi.org/10.1016/j.foodhyd.2018.07.003.

[29]   E. Jahed, M.A. Khaledabad, H. Almasi, R. Hasanzadeh, Physicochemical
       properties of Carum copticum Essential Oil Loaded Chitosan Films
       Containing Organic Nanoreinforcements, Carbohydr. Polym. 164 (2017)
       325–338. https://doi.org/10.1016/j.carbpol.2017.02.022.

[30]   S. Ojagh Mahdi, M. Rezaei, S. Razavi Hadi, S. Mohamad, H. Hosseini,
       Development and evaluation of a novel biodegradable film made from
       chitosan and cinnamon essential oil with low affinity toward water, Food
       Chem. 122 (2010) 161–166. https://doi.org/10.1016/j.foodchem.2010.02.033.

[31]   A. Espadín, L.T. De Dios, E. Ruvalcaba, J. Valadez-García, C. Velasquillo, I.
       Bustos-Jaimes, H. Vázquez-Torres, M. Gimeno, K. Shirai, Production and
       characterization of a nanocomposite of highly crystalline nanowhiskers

from biologically extracted chitin in enzymatic poly(ε-caprolactone),
Carbohydr. Polym. 181 (2018) 684–692.
https://doi.org/10.1016/j.carbpol.2017.11.094.

[32]   A.M. Salaberria, R.H. Diaz, J. Labidi, S.C.M. Fernandes, Role of chitin
       nanocrystals and nanofibers on physical, mechanical and functional
       properties in thermoplastic starch films, Food Hydrocoll. 46 (2015) 93–102.
       https://doi.org/10.1016/j.foodhyd.2014.12.016.

[33]   G. Yuan, X. Chen, D. Li, Chitosan films and coatings containing essential
       oils: The antioxidant and antimicrobial activity, and application in food
       systems, Food Res. Int. 89 (2016) 117–128.
       https://doi.org/10.1016/j.foodres.2016.10.004.

[34]   M. Hadian, A. Rajaei, A. Mohsenifar, M. Tabatabaei, Encapsulation of
       Rosmarinus of ficinalis essential oils in chitosan-benzoic acid nanogel with
       enhanced antibacterial activity in beef cutlet against Salmonella
       typhimurium during refrigerated storage, LWT - Food Sci. Technol. 84
       (2017) 394–401. https://doi.org/10.1016/j.lwt.2017.05.075.

[35]   N. Noshirvani, B. Ghanbarzadeh, C. Gardrat, Cinnamon and ginger
       essential oils to improve antifungal , physical and mechanical properties of
       chitosan-carboxymethyl cellulose fi lms, Food Hydrocoll. 70 (2017) 36–45.
       https://doi.org/10.1016/j.foodhyd.2017.03.015.

[36]   Y. Ruiz-Navajas, M. Viuda-Martos, E. Sendra, J.A. Perez-Alvarez, J.
       Fernández-López, In vitro antibacterial and antioxidant properties of
       chitosan edible fi lms incorporated with Thymus moroderi or Thymus
       piperella essential oils, Food Control. 30 (2013) 386–392.
       https://doi.org/10.1016/j.foodcont.2012.07.052.

[37]   Á. Perdones, M. Vargas, L. Atarés, A. Chiralt, Physical , antioxidant and
       antimicrobial properties of chitosan e cinnamon leaf oil fi lms as affected
       by oleic acid, Food Hydrocoll. 36 (2014) 256–264.
       https://doi.org/10.1016/j.foodhyd.2013.10.003.

[38]   A. Mojaddar, H. Tajik, T. Mehdizadeh, M. Moradi, E. Moghaddas, A. Mahmoudian, Effects of sumac extract dipping and chitosan coating enriched with Zataria multi fl ora Boiss oil on the shelf-life of meat in modi fi ed atmosphere packaging, LWT - Food Sci. Technol. 98 (2018) 372–380. https://doi.org/10.1016/j.lwt.2018.08.063.

[39]   E. Jahed, M.A. Khaledabad, H. Almasi, R. Hasanzadeh, Physicochemical properties of Carum copticum essential oil loaded chitosan films containing organic nanoreinforcements, Carbohydr. Polym. 164 (2017) 325–338. https://doi.org/10.1016/j.carbpol.2017.02.022.

[40]   M. Sabaghi, Y. Maghsoudlou, M. Khomeiri, Postharvest Biology and Technology Active edible coating from chitosan incorporating green tea extract as an antioxidant and antifungal on fresh walnut kernel, Postharvest Biol. Technol. 110 (2015) 224–228. https://doi.org/10.1016/j.postharvbio.2015.08.025.

[41]   M. V Tzoumaki, T. Moschakis, V. Kiosseoglou, C.G. Biliaderis, Oil-in-water emulsions stabilized by chitin nanocrystal particles, Food Hydrocoll. 25 (2011) 1521–1529. https://doi.org/10.1016/j.foodhyd.2011.02.008.

[42]   S. Sahraee, J.M. Milani, B. Ghanbarzadeh, H. Hamishehkar, Effect of corn oil on physical , thermal , and antifungal properties of gelatin-based nanocomposite fi lms containing nano chitin, LWT - Food Sci. Technol. 76 (2017) 33–39. https://doi.org/10.1016/j.lwt.2016.10.028.

[43]   F. Duman, M. Kaya, Crayfish chitosan for microencapsulation of coriander (Coriandrum sativum L .) essential oil, 92 (2016) 125–133.

[44]   G.C. Feyzioglu, F. Tornuk, Development of chitosan nanoparticles loaded with summer savory (Satureja hortensis L .) essential oil for antimicrobial and antioxidant delivery applications, LWT - Food Sci. Technol. 70 (2016) 104–110. https://doi.org/10.1016/j.lwt.2016.02.037.

[45]   G. Yuan, H. Lv, B. Yang, X. Chen, H. Sun, Physical properties, antioxidant and antimicrobial activity of chitosan films containing carvacrol and

pomegranate peel extract, Molecules. 20 (2015) 11034–11045.
https://doi.org/10.3390/molecules200611034.

[46]   M. Hadian, A. Rajaei, A. Mohsenifar, M. Tabatabaei, Encapsulation of
Rosmarinus of fi cinalis essential oils in chitosan-benzoic acid nanogel
with enhanced antibacterial activity in beef cutlet against Salmonella
typhimurium during refrigerated storage, LWT - Food Sci. Technol. 84
(2017) 394–401. https://doi.org/10.1016/j.lwt.2017.05.075.

[47]   M.Z. Elsabee, E.S. Abdou, Chitosan based edible films and coatings: A
review, Mater. Sci. Eng. C. 33 (2013) 1819–1841.
https://doi.org/10.1016/j.msec.2013.01.010.

[48]   A.F.M.S. Ud-daula, F. Demirci, K. Abu, B. Demirci, L.B.L. Lim, K. Hüsnü,
C. Baser, N. Ahmad, Chemical composition , antioxidant and antimicrobial
activities of essential oils from leaves , aerial stems , basal stems , and
rhizomes of Etlingera fimbriobracteata (K . Schum .) R . M . Sm ., Ind.
Crop. Prod. 84 (2016) 189–198. https://doi.org/10.1016/j.indcrop.2015.12.034.

[49]   M.M.A. Rashed, Q. Tong, A. Nagi, J. Li, N. Ullah, L. Chen, A. Rotail, A.M.
Bakry, Isolation of essential oil from Lavandula angustifolia by using
ultrasonic-microwave assisted method preceded by enzymolysis treatment
, and assessment of its biological activities, Ind. Crop. Prod. 100 (2017) 236–
245. https://doi.org/10.1016/j.indcrop.2017.02.033.

[50]   S.S. Cheng, C.G. Huang, Y.J. Chen, J.J. Yu, W.J. Chen, S.T. Chang, Chemical
compositions and larvicidal activities of leaf essential oils from two
eucalyptus species, Bioresour. Technol. 100 (2009) 452–456.
https://doi.org/10.1016/j.biortech.2008.02.038.

[51]   E. Jahed, M. Alizadeh, H. Almasi, R. Hasanzadeh, Physicochemical
properties of Carum copticum essential oil loaded chitosan films
containing organic nanoreinforcements, Carbohydr. Polym. 164 (2017) 325–
338. https://doi.org/10.1016/j.carbpol.2017.02.022.

[52]   H. Xiang, L. Zhang, Z. Yang, F. Chen, X. Zheng, X. Liu, Chemical

compositions, antioxidative, antimicrobial, anti-inflammatory and antitumor activities of Curcuma aromatica Salisb. essential oils, Ind. Crops Prod. 108 (2017) 6–16. https://doi.org/10.1016/j.indcrop.2017.05.058.

[53]   I. Bajalan, R. Rouzbahani, A.G. Pirbalouti, F. Maggi, Antioxidant and antibacterial activities of the essential oils obtained from seven Iranian populations of Rosmarinus officinalis, Ind. Crops Prod. 107 (2017) 305–311. https://doi.org/10.1016/j.indcrop.2017.05.063.

[54]   A. El Asbahani, K. Miladi, W. Badri, M. Sala, E.H.A. Addi, H. Casabianca, A. El Mousadik, D. Hartmann, A. Jilale, F.N.R. Renaud, A. Elaissari, C.B. Lyon, Essential oils : From extraction to encapsulation, Int. J. Pharm. 483 (2015) 220–243. https://doi.org/10.1016/j.ijpharm.2014.12.069.

[55]   R. Ribeiro-santos, M. Andrade, ScienceDirect Application of encapsulated essential oils as antimicrobial agents in food packaging, Curr. Opin. Food Sci. 14 (n.d.) 78–84. https://doi.org/10.1016/j.cofs.2017.01.012.

[56]   C. Dima, M. Cotârlet, P. Alexe, S. Dima, Reprint of "Microencapsulation of essential oil of pimento [Pimenta dioica (L) Merr.] by chitosan/k-carrageenan complex coacervation method," Innov. Food Sci. Emerg. Technol. 25 (2014) 97–105. https://doi.org/10.1016/j.ifset.2014.07.008.

[57]   S. Manso, D. Pezo, R. Gómez-Lus, C. Nerín, Diminution of aflatoxin B1 production caused by an active packaging containing cinnamon essential oil, Food Control. 45 (2014) 101–108. https://doi.org/10.1016/j.foodcont.2014.04.031.

[58]   C. Dima, S. Dima, Essential oils in foods : extraction , stabilization , and toxicity, Curr. Opin. Food Sci. 5 (2015) 29–35. https://doi.org/10.1016/j.cofs.2015.07.003.

[59]   S. Hosseini Fakhreddin, M. Zandi, M. Rezaei, F. Farahmandghavi, Two-step method for encapsulation of oregano essential oil in chitosan nanoparticles : Preparation , characterization and in vitro release study, Carbohydr. Polym. 95 (2013) 50–56.

https://doi.org/10.1016/j.carbpol.2013.02.031.

[60]   A. Mohammadi, M. Hashemi, S. Masoud, Postharvest Biology and
        Technology Chitosan nanoparticles loaded with Cinnamomum zeylanicum
        essential oil enhance the shelf life of cucumber during cold storage,
        Postharvest Biol. Technol. 110 (2015) 203–213.
        https://doi.org/10.1016/j.postharvbio.2015.08.019.

[61]   Y. Peng, Y. Li, Combined effects of two kinds of essential oils on physical,
        mechanical and structural properties of chitosan films, Food Hydrocoll. 36
        (2014) 287–293. https://doi.org/10.1016/j.foodhyd.2013.10.013.

[62]   E. Jahed, M.A. Khaledabad, M.R. Bari, H. Almasi, Effect of cellulose and
        lignocellulose nano fibers on the properties of Origanum vulgare ssp .
        gracile essential oil-loaded chitosan films, 117 (2017) 70–80.
        https://doi.org/10.1016/j.reactfunctpolym.2017.06.008.

[63]   L. Atarés, C. De Jesús, P. Talens, A. Chiralt, Characterization of SPI-based
        edible films incorporated with cinnamon or ginger essential oils, J. Food
        Eng. 99 (2010) 384–391. https://doi.org/10.1016/j.jfoodeng.2010.03.004.

[64]   A. Acevedo-fani, L. Salvia-trujillo, M.A. Rojas-graü, O. Martín-belloso,
        Edible films from essential-oil-loaded nanoemulsions : Physicochemical
        characterization and antimicrobial properties, Food Hydrocoll. 47 (2015)
        168–177. https://doi.org/10.1016/j.foodhyd.2015.01.032.

[65]   M. Ahmad, S. Benjakul, T. Prodpran, T.W. Agustini, Physico-mechanical
        and antimicrobial properties of gelatin film from the skin of unicorn
        leatherjacket incorporated with essential oils, Food Hydrocoll. 28 (2012)
        189–199. https://doi.org/10.1016/j.foodhyd.2011.12.003.

[66]   M.H. Hosseini, S.H. Razavi, M.A. Mousavi, ANTIMICROBIAL , PHYSICAL
        AND MECHANICAL PROPERTIES OF CHITOSAN-BASED FILMS
        INCORPORATED WITH THYME , 33 (2008) 727–743.
        https://doi.org/10.1111/j.1745-4549.2008.00307.x.

215

[67] V. Falguera, J.P. Quintero, A. Jiménez, J.A. Muñoz, A. Ibarz, Edible films and coatings: Structures, active functions and trends in their use, Trends Food Sci. Technol. 22 (2011) 292–303. https://doi.org/10.1016/j.tifs.2011.02.004.

[68] J. Bonilla, L. Atarés, M. Vargas, A. Chiralt, Effect of essential oils and homogenization conditions on properties of chitosan-based fi lms, Food Hydrocoll. 26 (2012). https://doi.org/10.1016/j.foodhyd.2011.03.015.

[69] Á. Perdones, I. Escriche, A. Chiralt, M. Vargas, Effect of chitosan – lemon essential oil coatings on volatile profile of strawberries during storage, Food Chem. 197 (2016) 979–986. https://doi.org/10.1016/j.foodchem.2015.11.054.

[70] J. Hafsa, M. ali Smach, M.R. Ben Khedher, B. Charfeddine, K. Limem, H. Majdoub, S. Rouatbi, Physical, antioxidant and antimicrobial properties of chitosan films containing Eucalyptus globulus essential oil, LWT - Food Sci. Technol. 68 (2016) 356–364. https://doi.org/10.1016/j.lwt.2015.12.050.

[71] L. Sánchez-gonzález, M. Cháfer, C. González-martínez, A. Chiralt, Study of the release of limonene present in chitosan films enriched with bergamot oil in food simulants, 105 (2011) 138–143. https://doi.org/10.1016/j.jfoodeng.2011.02.016.

[72] H. Wang, J. Qian, F. Ding, Emerging Chitosan-Based Films for Food Packaging Applications, J. Agric. Food Chem. 66 (2018) 395–413. https://doi.org/10.1021/acs.jafc.7b04528.

[73] S. Galus, J. Kadzińska, Food applications of emulsion-based edible films and coatings, Trends Food Sci. Technol. 45 (2015) 273–283. https://doi.org/10.1016/j.tifs.2015.07.011.

[74] K. Munhuweyi, O.J. Caleb, C.L. Lennox, A.J. Van Reenen, U. Linus, In vitro and in vivo antifungal activity of chitosan-essential oils against pomegranate fruit pathogens, Postharvest Biol. Technol. 129 (2017) 9–22. https://doi.org/10.1016/j.postharvbio.2017.03.002.

216

[75] G.G. Santos Frazão, A.F. Blank, L.C.L. de Aquino Santana, Optimisation of edible chitosan coatings formulations incorporating Myrcia ovata Cambessedes essential oil with antimicrobial potential against foodborne bacteria and natural microflora of mangaba fruits, LWT - Food Sci. Technol. 79 (2017) 1–10. https://doi.org/10.1016/j.lwt.2017.01.011.

[76] F. Donsì, G. Ferrari, Essential oil nanoemulsions as antimicrobial agents in food, J. Biotechnol. 233 (2016) 106–120. https://doi.org/10.1016/j.jbiotec.2016.07.005.

[77] R. Severino, K.D. Vu, F. Donsì, S. Salmieri, G. Ferrari, M. Lacroix, Antibacterial and physical effects of modified chitosan based-coating containing nanoemulsion of mandarin essential oil and three non-thermal treatments against Listeria innocua in green beans, Int. J. Food Microbiol. 191 (2014) 82–88. https://doi.org/10.1016/j.ijfoodmicro.2014.09.007.

[78] S. Khalili Tahereh, A. Mohsenifar, M. Beyki, S. Zhaveh, T. Rahmani-cherati, A. Abdollahi, M. Bayat, M. Tabatabaei, Encapsulation of Thyme essential oils in chitosan-benzoic acid nanogel with enhanced antimicrobial activity against Aspergillus fl avus, LWT - Food Sci. Technol. 60 (2015) 502–508. https://doi.org/10.1016/j.lwt.2014.07.054.

[79] D.J. McCLEMENTS, Principles, Practicies, and Techniques, 2005.

[80] M. Atarian, A. Rajaei, M. Tabatabaei, A. Mohsenifar, H. Bodaghi, Formulation of Pickering sunflower oil-in-water emulsion stabilized by chitosan-stearic acid nanogel and studying its oxidative stability, Carbohydr. Polym. 210 (2019) 47–55. https://doi.org/10.1016/j.carbpol.2019.01.008.

[81] E. Dickinson, Use of nanoparticles and microparticles in the formation and stabilization of food emulsions, Trends Food Sci. Technol. 24 (2012) 4–12. https://doi.org/10.1016/j.tifs.2011.09.006.

[82] X. Song, Y. Pei, M. Qiao, F. Ma, H. Ren, Q. Zhao, Preparation and characterizations of Pickering emulsions stabilized by hydrophobic starch

particles, Food Hydrocoll. 45 (2015) 256–263.
https://doi.org/10.1016/j.foodhyd.2014.12.007.

[83] M. Errezma, A. Ben Mabrouk, A. Magnin, A. Dufresne, S. Boufi, Surfactant-free emulsion Pickering polymerization stabilized by aldehyde-functionalized cellulose nanocrystals, Carbohydr. Polym. 202 (2018) 621–630. https://doi.org/10.1016/j.carbpol.2018.09.018.

[84] M. Beyki, S. Zhaveh, S. Tahere, T. Rahmani-cherati, A. Abollahi, M. Bayat, M. Tabatabaei, A. Mohsenifar, Encapsulation of Mentha piperita essential oils in chitosan – cinnamic acid nanogel with enhanced antimicrobial activity against Aspergillus flavus, 54 (2014) 310–319.

[85] S. Zhaveh, A. Mohsenifar, M. Beiki, S.T. Khalili, A. Abdollahi, T. Rahmani-Cherati, M. Tabatabaei, Encapsulation of Cuminum cyminum essential oils in chitosan-caffeic acid nanogel with enhanced antimicrobial activity against Aspergillus flavus, Ind. Crops Prod. 69 (2015) 251–256. https://doi.org/10.1016/j.indcrop.2015.02.028.

[86] L.J. Pérez-Córdoba, I.T. Norton, H.K. Batchelor, K. Gkatzionis, F. Spyropoulos, P.J.A. Sobral, Physico-chemical, antimicrobial and antioxidant properties of gelatin-chitosan based films loaded with nanoemulsions encapsulating active compounds, Food Hydrocoll. 79 (2018) 544–559. https://doi.org/10.1016/j.foodhyd.2017.12.012.

[87] I. Gülseren, M. Corredig, Interactions of chitin nanocrystals with β-lactoglobulin at the oil-water interface, studied by drop shape tensiometry, Colloids Surfaces B Biointerfaces. 111 (2013) 672–679. https://doi.org/10.1016/j.colsurfb.2013.06.058.

[88] A. Shetta, J. Kegere, W. Mamdouh, Comparative study of encapsulated peppermint and green tea essential oils in chitosan nanoparticles: Encapsulation, thermal stability, in-vitro release, antioxidant and antibacterial activities, Int. J. Biol. Macromol. 126 (2019) 731–742. https://doi.org/10.1016/j.ijbiomac.2018.12.161.

[89]   J. Rodríguez, M.J. Martín, M.A. Ruiz, B. Clares, Current encapsulation
        strategies for bioactive oils: From alimentary to pharmaceutical
        perspectives, Food Res. Int. 83 (2016) 41–59.
        https://doi.org/10.1016/j.foodres.2016.01.032.

[90]   C.E. Mora-Huertas, H. Fessi, A. Elaissari, Polymer-based nanocapsules for
        drug delivery, Int. J. Pharm. 385 (2010) 113–142.
        https://doi.org/10.1016/j.ijpharm.2009.10.018.

[91]   N. Hasheminejad, F. Khodaiyan, M. Safari, Improving the antifungal
        activity of clove essential oil encapsulated by chitosan nanoparticles, Food
        Chem. 275 (2019) 113–122. https://doi.org/10.1016/j.foodchem.2018.09.085.

[92]   N. Sowasod, K. Nakagawa, T. Charinpanitkul, W. Tanthapanichakoon,
        Encapsulation of Curcumin Loaded Oil Droplets with Chitosan Based
        Cryogel: Influence of Freezing Condition on Nanocapsule Properties, Food
        Sci. Technol. Res. 19 (2013) 633–640. https://doi.org/10.3136/fstr.19.633.

[93]   S. Woranuch, R. Yoksan, Eugenol-loaded chitosan nanoparticles: I.
        Thermal stability improvement of eugenol through encapsulation,
        Carbohydr. Polym. 96 (2013) 578–585.
        https://doi.org/10.1016/j.carbpol.2012.08.117.

[94]   F.O.M.S. Abreu, E.F. Oliveira, H.C.B. Paula, R.C.M. De Paula, Chitosan /
        cashew gum nanogels for essential oil encapsulation, Carbohydr. Polym.
        89 (2012) 1277–1282. https://doi.org/10.1016/j.carbpol.2012.04.048.

[95]   U. Siripatrawan, B.R. Harte, Physical properties and antioxidant activity of
        an active film from chitosan incorporated with green tea extract, Food
        Hydrocoll. 24 (2010) 770–775.
        https://doi.org/10.1016/j.foodhyd.2010.04.003.

[96]   M. Moradi, H. Tajik, S. Mehdi, R. Rohani, A. Rasoul, H. Malekinejad, J.
        Aliakbarlu, M. Hadian, Characterization of antioxidant chitosan film
        incorporated with Zataria multiflora Boiss essential oil and grape seed
        extract, LWT - Food Sci. Technol. 46 (2012) 477–484.

https://doi.org/10.1016/j.lwt.2011.11.020.

[97]   D. Huang, O.U. Boxin, R.L. Prior, The chemistry behind antioxidant
         capacity assays, J. Agric. Food Chem. 53 (2005) 1841–1856.
         https://doi.org/10.1021/jf030723c.

[98]   W. Brand-Williams, M.E. Cuvelier, C. Berset, Use of a Free Radical Method
         to Evaluate Antioxidant Activity, 28 (1995) 25–30.
         https://doi.org/10.1016/S0023-6438(95)80008-5.

[99]   N.J. Miller, C. Rice-Evans, M.J. Davies, V. Gopinathan, A. Milner, A Novel
         Method for Measuring Antioxidant Capacity and its Application to
         Monitoring the Antioxidant Status in Premature Neonates, Clin. Sci. 84
         (1993) 407–412. https://doi.org/10.1042/cs0840407.

[100]   J. Bonilla, T. Poloni, R. V Lourenço, P.J.A. Sobral, Antioxidant potential of
         eugenol and ginger essential oils with gelatin / chitosan fi lms ☆, Food
         Biosci. J. 23 (2018) 107–114. https://doi.org/10.1016/j.fbio.2018.03.007.

[101]   E.T. Silva Damasceno, R.R. Almeida, S.Y.B. de Carvalho, G.S.G. de
         Carvalho, V. Mano, A.C. Pereira, L.G. de Lima Guimarães, Lippia
         origanoides Kunth. essential oil loaded in nanogel based on the chitosan
         and ρ-coumaric acid: Encapsulation efficiency and antioxidant activity,
         Ind. Crops Prod. 125 (2018) 85–94.
         https://doi.org/10.1016/j.indcrop.2018.08.074.

[102]   D. Kadam, S.S. Lele, Cross-linking effect of polyphenolic extracts of
         Lepidium sativum seedcake on physicochemical properties of chitosan
         films, Int. J. Biol. Macromol. 114 (2018) 1240–1247.
         https://doi.org/10.1016/j.ijbiomac.2018.04.018.

[103]   A. Riaz, S. Lei, S. Akhtar, P. Wan, D. Chen, S. Jabbar, M. Abid, M.
         Muhammad, X. Zeng, Preparation and characterization of chitosan-based
         antimicrobial active food packaging fi lm incorporated with apple peel
         polyphenols, Int. J. Biol. Macromol. 114 (2018) 547–555.

https://doi.org/10.1016/j.ijbiomac.2018.03.126.

[104] N.M. Hromiš, V.L. Lazic, S.L. Markov, G. Vaštag, S.Z. Popovic, D.Z. Šuput, A.S. Velic, L.M. Popovic, Optimization of chitosan biofilm properties by addition of caraway essential oil and beeswax ˇ uz, 158 (2015) 86–93. https://doi.org/10.1016/j.jfoodeng.2015.01.001.

[105] K.T. Trifkovi, N.Z. Milašinovic, V.B. Djordjevi, Z.D. Knežević-Jugovićˇ, M.T.K. Krušic, Chitosan microbeads for encapsulation of thyme (Thymus serpyllum L .) polyphenols, 111 (2014) 901–907. https://doi.org/10.1016/j.carbpol.2014.05.053.

[106] M. Moradi, H. Tajik, S. Mehdi, R. Rohani, A. Rasoul, H. Malekinejad, J. Aliakbarlu, M. Hadian, Characterization of antioxidant chitosan fi lm incorporated with Zataria multi fl ora Boiss essential oil and grape seed extract, LWT - Food Sci. Technol. 46 (2012) 477–484. https://doi.org/10.1016/j.lwt.2011.11.020.

[107] E. Jahed, M.A. Khaledabad, H. Almasi, R. Hasanzadeh, Physicochemical properties of Carum copticum essential oil loaded chitosan films containing organic nanoreinforcements, Carbohydr. Polym. 164 (2017) 325–338. https://doi.org/10.1016/j.carbpol.2017.02.022.

[108] M. Viuda-Martos, M.A. Mohamady, J. Fernández-López, K.A. Abd ElRazik, E.A. Omer, J.A. Pérez-Alvarez, E. Sendra, In vitro antioxidant and antibacterial activities of essentials oils obtained from Egyptian aromatic plants, Food Control. 22 (2011) 1715–1722. https://doi.org/10.1016/j.foodcont.2011.04.003.

[109] L. Atarés, A. Chiralt, Essential oils as additives in biodegradable fi lms and coatings for active food packaging, Trends Food Sci. Technol. J. 48 (2016) 51–62. https://doi.org/10.1016/j.tifs.2015.12.001.

[110] J. Sangsuwan, T. Pongsapakworawat, P. Bangmo, Effect of chitosan beads incorporated with lavender or red thyme essential oils in inhibiting Botrytis cinerea and their application in strawberry packaging system,

LWT - Food Sci. Technol. 74 (2016) 14–20.
https://doi.org/10.1016/j.lwt.2016.07.021.

[111]   J. Gómez-Estaca, A.L. de Lacey, M.E. López-Caballero, M.C. Gómez-
        Guillén, P. Montero, Biodegradable gelatin e chitosan fi lms incorporated
        with essential oils as antimicrobial agents for fi sh preservation, Food
        Microbiol. 27 (2010) 889–896. https://doi.org/10.1016/j.fm.2010.05.012.

[112]   P. Cazón, G. Velazquez, J.A. Ramírez, M. Vázquez, Polysaccharide-based
        films and coatings for food packaging: A review, Food Hydrocoll. 68 (2017)
        136–148. https://doi.org/10.1016/j.foodhyd.2016.09.009.

[113]   J.R. Calo, P.G. Crandall, C.A. O'Bryan, S.C. Ricke, Essential oils as
        antimicrobials in food systems - A review, Food Control. 54 (2015) 111–119.
        https://doi.org/10.1016/j.foodcont.2014.12.040.

[114]   S. Burt, Essential oils: Their antibacterial properties and potential
        applications in foods - A review, Int. J. Food Microbiol. 94 (2004) 223–253.
        https://doi.org/10.1016/j.ijfoodmicro.2004.03.022.

[115]   R. Ribeiro-Santos, M. Andrade, N.R. de Melo, A. Sanches-Silva, Use of
        essential oils in active food packaging: Recent advances and future trends,
        Trends Food Sci. Technol. 61 (2017) 132–140.
        https://doi.org/10.1016/j.tifs.2016.11.021.

[116]   S. Kakaei, Y. Shahbazi, Effect of chitosan-gelatin fi lm incorporated with
        ethanolic red grape seed extract and Ziziphora clinopodioides essential oil
        on survival of Listeria monocytogenes and chemical , microbial and
        sensory properties of mince, LWT - Food Sci. Technol. 72 (2016) 432–438.
        https://doi.org/10.1016/j.lwt.2016.05.021.

[117]   A. Paparella, G. Mazzarrino, C. Chaves-López, C. Rossi, G. Sacchetti, O.
        Guerrieri, A. Serio, Chitosan boosts the antimicrobial activity of Origanum
        vulgare essential oil in modi fi ed atmosphere packaged pork, 59 (2016) 23–
        31. https://doi.org/10.1016/j.fm.2016.05.007.

[118] A. Mohammadi, M. Hashemi, S. Masoud, Integration between chitosan and Zataria multi fl ora or Cinnamomum zeylanicum essential oil for controlling Phytophthora drechsleri , the causal agent of cucumber fruit rot, LWT - Food Sci. Technol. 65 (2016) 349–356. https://doi.org/10.1016/j.lwt.2015.08.015.

[119] R. Severino, G. Ferrari, K.D. Vu, F. Donsì, S. Salmieri, M. Lacroix, Antimicrobial effects of modified chitosan based coating containing nanoemulsion of essential oils, modified atmosphere packaging and gamma irradiation against Escherichia coli O157:H7 and Salmonella Typhimurium on green beans, Food Control. 50 (2015) 215–222. https://doi.org/10.1016/j.foodcont.2014.08.029.

[120] J. Wu, S. Ge, H. Liu, S. Wang, S. Chen, J. Wang, J. Li, Q. Zhang, Properties and antimicrobial activity of silver carp (Hypophthalmichthys molitrix) skin gelatin-chitosan films incorporated with oregano essential oil for fish preservation, Food Packag. Shelf Life. 2 (2014) 7–16. https://doi.org/10.1016/j.fpsl.2014.04.004.

[121] S. Shankar, J.P. Reddy, J.W. Rhim, H.Y. Kim, Preparation, characterization, and antimicrobial activity of chitin nanofibrils reinforced carrageenan nanocomposite films, Carbohydr. Polym. 117 (2015) 468–475. https://doi.org/10.1016/j.carbpol.2014.10.010.

[122] F. Silva, S. Ferreira, J.A. Queiroz, F.C. Domingues, Coriander (Coriandrum sativum L.) essential oil: Its antibacterial activity and mode of action evaluated by flow cytometry, J. Med. Microbiol. 60 (2011) 1479–1486. https://doi.org/10.1099/jmm.0.034157-0.

[123] P. LO Cantore, N.S. Iacobellis, A. DE Marco, F. Capasso, F. Senatore, Antibacterial activity of Coriandrum sativum L. and Foeniculum vulgare Miller Var. vulgare (Miller) essential oils., J. Agric. Food Chem. 52 (2004) 7862–7866. https://doi.org/10.1021/jf0493122.

[124] N. Hasheminejad, F. Khodaiyan, M. Safari, Improving the antifungal

activity of clove essential oil encapsulated by chitosan nanoparticles, Food Chem. 275 (2019) 113–122. https://doi.org/10.1016/j.foodchem.2018.09.085.

[125]   A.M. Salaberria, R.H. Diaz, J. Labidi, S.C.M. Fernandes, Preparing valuable renewable nanocomposite films based exclusively on oceanic biomass - Chitin nanofillers and chitosan, React. Funct. Polym. 89 (2015) 31–39. https://doi.org/10.1016/j.reactfunctpolym.2015.03.003.

[126]   Priyanka, S. Khanam, Influence of operating parameters on supercritical fluid extraction of essential oil from turmeric root, J. Clean. Prod. 188 (2018) 816–824. https://doi.org/10.1016/j.jclepro.2018.04.052.

[127]   Y. Li, Y. Ying, Y. Zhou, Y. Ge, C. Yuan, C. Wu, Y. Hu, A pH-indicating intelligent packaging composed of chitosan-purple potato extractions strength by surface-deacetylated chitin nanofibers, Int. J. Biol. Macromol. 127 (2019) 376–384. https://doi.org/10.1016/j.ijbiomac.2019.01.060.

[128]   M.R. Kasaai, Determination of the degree of N -acetylation for chitin and chitosan by various NMR spectroscopy techniques : A review, Carbohydr. Polym. 79 (2010) 801–810. https://doi.org/10.1016/j.carbpol.2009.10.051.

[129]   F.A.A. Sagheer, M.A. Al-Sughayer, S. Muslim, M.Z. Elsabee, Extraction and characterization of chitin and chitosan from marine sources in Arabian Gulf, Carbohydr. Polym. 77 (2009) 410–419. https://doi.org/10.1016/j.carbpol.2009.01.032.

[130]   B. Gullón, G. Eibes, M.T. Moreira, I. Dávila, J. Labidi, P. Gullón, Antioxidant and antimicrobial activities of extracts obtained from the refining of autohydrolysis liquors of vine shoots, Ind. Crops Prod. 107 (2017) 105–113. https://doi.org/10.1016/j.indcrop.2017.05.034.

[131]   M. Mujtaba, A.M. Salaberria, M.A. Andres, M. Kaya, A. Gunyakti, J. Labidi, Utilization of flax (Linum usitatissimum) cellulose nanocrystals as reinforcing material for chitosan films, Int. J. Biol. Macromol. 104 (2017) 944–952. https://doi.org/10.1016/j.ijbiomac.2017.06.127.

[132]   X. Zhai, J. Shi, X. Zou, S. Wang, C. Jiang, J. Zhang, X. Huang, W. Zhang, M. Holmes, Novel colorimetric films based on starch/polyvinyl alcohol incorporated with roselle anthocyanins for fish freshness monitoring, Food Hydrocoll. 69 (2017) 308–317. https://doi.org/10.1016/j.foodhyd.2017.02.014.

[133]   H. El Knidri, R. Belaabed, A. Addaou, A. Laajeb, A. Lahsini, Extraction, chemical modification and characterization of chitin and chitosan, Int. J. Biol. Macromol. 120 (2018) 1181–1189. https://doi.org/10.1016/j.ijbiomac.2018.08.139.

[134]   M. Claverie, C. McReynolds, A. Petitpas, M. Thomas, S.C.M. Fernandes, Marine-derived polymeric materials and biomimetics: An overview, Polymers (Basel). 12 (2020). https://doi.org/10.3390/POLYM12051002.

[135]   H. El Knidri, R. El Khalfaouy, A. Laajeb, A. Addaou, A. Lahsini, Eco-friendly extraction and characterization of chitin and chitosan from the shrimp shell waste via microwave irradiation, Process Saf. Environ. Prot. 104 (2016) 395–405. https://doi.org/10.1016/j.psep.2016.09.020.

[136]   V. Zubillaga, A. Alonso-varona, S.C.M. Fernandes, A.M. Salaberria, T. Palomares, Adipose-derived mesenchymal stem cell chondrospheroids cultured in hypoxia and a 3D porous chitosan/chitin nanocrystal scaffold as a platform for cartilage tissue engineering, Int. J. Mol. Sci. 21 (2020) 1–17. https://doi.org/10.3390/ijms21031004.

[137]   R.D. Pinto Rodrigues, A.S. e. Silva, T.A.V. Carlos, A.K.P. Bastos, R.S. de Santiago-Aguiar, M.V.P. Rocha, Application of protic ionic liquids in the microwave-assisted extraction of phycobiliproteins from Arthrospira platensis with antioxidant activity, Sep. Purif. Technol. 252 (2020) 117448. https://doi.org/10.1016/j.seppur.2020.117448.

[138]   C.L. Teo, A. Idris, Evaluation of direct transesterification of microalgae using microwave irradiation, Bioresour. Technol. 174 (2014) 281–286. https://doi.org/10.1016/j.biortech.2014.10.035.

[139]   F.A. Al Sagheer, M.A. Al-sughayer, S. Muslim, M.Z. Elsabee, Extraction and

characterization of chitin and chitosan from marine sources in Arabian Gulf, Carbohydr. Polym. J. 77 (2009) 410–419. https://doi.org/10.1016/j.carbpol.2009.01.032.

[140] T.T. Nguyen, A.R. Barber, P. Smith, X. Luo, W. Zhang, Application and optimization of the highly efficient and environmentally-friendly microwave-intensified lactic acid demineralization of deproteinized Rock lobster shells (Jasus edwardsii) for chitin production, Food Bioprod. Process. 102 (2017) 367–374. https://doi.org/10.1016/j.fbp.2017.02.005.

[141] Y. Xiao, Y. Liu, X. Wang, M. Li, H. Lei, H. Xu, Cellulose nanocrystals prepared from wheat bran: Characterization and cytotoxicity assessment, Int. J. Biol. Macromol. 140 (2019) 225–233. https://doi.org/10.1016/j.ijbiomac.2019.08.160.

[142] A. Morales, B. Gullón, I. Dávila, G. Eibes, J. Labidi, P. Gullón, Optimization of alkaline pretreatment for the co-production of biopolymer lignin and bioethanol from chestnut shells following a biore fi nery approach, Ind. Crop. Prod. 124 (2018) 582–592. https://doi.org/10.1016/j.indcrop.2018.08.032.

[143] Y. Yuan, S. Hong, H. Lian, K. Zhang, H. Liimatainen, Comparison of acidic deep eutectic solvents in production of chitin nanocrystals, Carbohydr. Polym. 236 (2020) 116095. https://doi.org/10.1016/j.carbpol.2020.116095.

[144] J. Araki, Y. Yamanaka, K. Ohkawa, Chitin-chitosan nanocomposite gels: Reinforcement of chitosan hydrogels with rod-like chitin nanowhiskers, Polym. J. 44 (2012) 713–717. https://doi.org/10.1038/pj.2012.11.

[145] N.E. Mushi, N. Butchosa, M. Salajkova, Q. Zhou, L.A. Berglund, Nanostructured membranes based on native chitin nanofibers prepared by mild process, Carbohydr. Polym. 112 (2014) 255–263. https://doi.org/10.1016/j.carbpol.2014.05.038.

[146] S. Phongying, S. ichi Aiba, S. Chirachanchai, Direct chitosan nanoscaffold formation via chitin whiskers, Polymer (Guildf). 48 (2007) 393–400.

https://doi.org/10.1016/j.polymer.2006.10.049.

[147] B. Ma, A. Qin, X. Li, X. Zhao, C. He, Structure and properties of chitin
       whisker reinforced chitosan membranes, Int. J. Biol. Macromol. 64 (2014)
       341–346. https://doi.org/10.1016/j.ijbiomac.2013.12.015.

[148] S. Cao, W. Gu, W. Ou-yang, D. Chen, B. Yang, Y. Ma, Y. An, Preparation ,
       characterization and application of rod-like chitin nanocrystal by using p-
       toluenesulfonic acid / choline chloride deep eutectic solvent as a
       hydrolytic media, Carbohydr. Polym. 213 (2019) 304–310.
       https://doi.org/10.1016/j.carbpol.2019.02.092.

[149] N. Lin, S. Zhao, L. Gan, P.R. Chang, T. Xia, J. Huang, Preparation of
       fungus-derived chitin nanocrystals and their dispersion stability evaluation
       in aqueous media, 173 (2017) 610–618.

[150] H.N. Cuong, N.C. Minh, N. Van Hoa, T.S. Trung, Preparation and
       characterization of high purity β-chitin from squid pens (Loligo chenisis),
       Int. J. Biol. Macromol. 93 (2016) 442–447.
       https://doi.org/10.1016/j.ijbiomac.2016.08.085.

[151] A. Oberemko, A.M. Salaberria, R. Saule, G. Saulis, M. Kaya,
       Physicochemical and in vitro cytotoxic properties of chitosan from
       mushroom species (Boletus bovinus and Laccaria laccata), Carbohydr.
       Polym. 221 (2019) 1–9. https://doi.org/10.1016/j.carbpol.2019.05.073.

[152] M. Kaya, I. Sargin, K.Ö. Tozak, T. Baran, S. Erdogan, G. Sezen, Chitin
       extraction and characterization from Daphnia magna resting eggs, Int. J.
       Biol. Macromol. 61 (2013) 459–464.
       https://doi.org/10.1016/j.ijbiomac.2013.08.016.

[153] A. Tolaimate, J. Desbrières, M. Rhazi, A. Alagui, M. Vincendon, P. Vottero,
       On the influence of deacetylation process on the physicochemical
       characteristics of chitosan from squid chitin, Polymer (Guildf). 41 (2000)
       2463–2469. https://doi.org/10.1016/S0032-3861(99)00400-0.

[154]   J.D. Goodrich, W.T. Winter, alpha-Chitin Nanocrystals Prepared from Shrimp Shells and Their Specific Surface Area Measurement, Biomacromolecules. 8 (2007) 252–257.

[155]   Q. Wu, E. Jungstedt, M. Šoltésová, N.E. Mushi, L.A. Berglund, High strength nanostructured films based on well-preserved β-chitin nanofibrils, Nanoscale. 11 (2019) 11001–11011. https://doi.org/10.1039/c9nr02870f.

[156]   J.N.I. Balitaan, J.M. Yeh, K.S. Santiago, Marine waste to a functional biomaterial: Green facile synthesis of modified-β-chitin from Uroteuthis duvauceli pens (gladius), Int. J. Biol. Macromol. (2019). https://doi.org/10.1016/j.ijbiomac.2019.11.041.

[157]   B.A. Juárez-De La Rosa, P. Quintana, P.L. Ardisson, J.M. Yáñez-Limón, J.J. Alvarado-Gil, Effects of thermal treatments on the structure of two black coral species chitinous exoskeleton, J. Mater. Sci. 47 (2012) 990–998. https://doi.org/10.1007/s10853-011-5878-9.

[158]   V. Aylanc, S. Ertosun, L. Akyuz, B. Koc Bilican, S. Gokdag, I. Bilican, Y.S. Cakmak, B.A. Yilmaz, M. Kaya, Natural β-chitin-protein complex film obtained from waste razor shells for transdermal capsaicin carrier, Int. J. Biol. Macromol. 155 (2020) 508–515. https://doi.org/10.1016/j.ijbiomac.2020.03.232.

[159]   I.F. Nata, T.M. Wu, J.K. Chen, C.K. Lee, A chitin nanofibril reinforced multifunctional monolith poly(vinyl alcohol) cryogel, J. Mater. Chem. B. 2 (2014) 4108–4113. https://doi.org/10.1039/c4tb00175c.

[160]   R. Mishra, A.K. Gupta, R.K. Lal, T. Jhang, N. Banerjee, Genetic variability, analysis of genetic parameters, character associations and contribution for agronomical traits in turmeric (Curcuma longa L.), Ind. Crops Prod. 76 (2015) 204–208. https://doi.org/10.1016/j.indcrop.2015.06.049.

[161]   S.R. Shirsath, S.S. Sable, S.G. Gaikwad, S.H. Sonawane, D.R. Saini, P.R. Gogate, Intensification of extraction of curcumin from Curcuma amada

using ultrasound assisted approach: Effect of different operating parameters, Ultrason. Sonochem. 38 (2017) 437–445. https://doi.org/10.1016/j.ultsonch.2017.03.040.

[162] L. Zhang, Z. Yang, F. Chen, P. Su, D. Chen, W. Pan, Y. Fang, C. Dong, X. Zheng, Z. Du, Composition and bioactivity assessment of essential oils of Curcuma longa L. collected in China, Ind. Crops Prod. 109 (2017) 60–73. https://doi.org/10.1016/j.indcrop.2017.08.009.

[163] S.C. Gupta, B. Sung, J.H. Kim, S. Prasad, S. Li, B.B. Aggarwal, Multitargeting by turmeric, the golden spice: From kitchen to clinic, Mol. Nutr. Food Res. 57 (2013) 1510–1528. https://doi.org/10.1002/mnfr.201100741.

[164] A. Chaaban, E.N. Gomes, V.S. Richardi, C.E.N. Martins, J.S. Brum, M.A. Navarro-Silva, C. Deschamps, M.B. Molento, Essential oil from Curcuma longa leaves: Can an overlooked by-product from turmeric industry be effective for myiasis control?, Ind. Crops Prod. 132 (2019) 352–364. https://doi.org/10.1016/j.indcrop.2019.02.030.

[165] M. Valizadeh Kiamahalleh, G. Najafpour-Darzi, M. Rahimnejad, A.A. Moghadamnia, M. Valizadeh Kiamahalleh, High performance curcumin subcritical water extraction from turmeric (Curcuma longa L.), J. Chromatogr. B Anal. Technol. Biomed. Life Sci. 1022 (2016) 191–198. https://doi.org/10.1016/j.jchromb.2016.04.021.

[166] S.Y. Park, D.S.H.L. Kim, Discovery of natural products from Curcuma longa that protect cells from beta-amyloid insult: A drug discovery effort against Alzheimer's disease, J. Nat. Prod. 65 (2002) 1227–1231. https://doi.org/10.1021/np010039x.

[167] T. Hamaguchi, K. Ono, M. Yamada, Curcumin and Alzheimer's disease, CNS Neurosci. Ther. 16 (2010) 285–297. https://doi.org/10.1111/j.1755-5949.2010.00147.x.

[168] M.E.M. Braga, P.F. Leal, J.E. Carvalho, M.A.A. Meireles, Comparison of Yield, Composition, and Antioxidant Activity of Turmeric (Curcuma longa

L.) Extracts Obtained Using Various Techniques, J. Agric. Food Chem. 51 (2003) 6604–6611. https://doi.org/10.1021/jf0345550.

[169]   T.T. Dao, P.H. Nguyen, H.K. Won, E.H. Kim, J. Park, B.Y. Won, W.K. Oh, Curcuminoids from Curcuma longa and their inhibitory activities on influenza A neuraminidases, Food Chem. 134 (2012) 21–28. https://doi.org/10.1016/j.foodchem.2012.02.015.

[170]   N.G. Das, S. Dhiman, P.K. Talukdar, B. Rabha, D. Goswami, V. Veer, Synergistic mosquito-repellent activity of Curcuma longa, Pogostemon heyneanus and Zanthoxylum limonella essential oils, J. Infect. Public Health. 8 (2015) 323–328. https://doi.org/10.1016/j.jiph.2015.02.005.

[171]   M.R.M. da Silva, E. Ricci-Júnior, An approach to natural insect repellent formulations: from basic research to technological development, Acta Trop. 212 (2020) 105419. https://doi.org/10.1016/j.actatropica.2020.105419.

[172]   B. Gopalan, M. Goto, A. Kodama, T. Hirose, Supercritical carbon dioxide extraction of turmeric (Curcuma longa), J. Agric. Food Chem. 48 (2000) 2189–2192. https://doi.org/10.1021/jf9908594.

[173]   F. Sahne, M. Mohammadi, G.D. Najafpour, A.A. Moghadamnia, Enzyme-assisted ionic liquid extraction of bioactive compound from turmeric (Curcuma longa L.): Isolation, purification and analysis of curcumin, Ind. Crops Prod. 95 (2017) 686–694. https://doi.org/10.1016/j.indcrop.2016.11.037.

[174]   L.H. Chang, T.T. Jong, H.S. Huang, Y.F. Nien, C.M.J. Chang, Supercritical carbon dioxide extraction of turmeric oil from Curcuma longa Linn and purification of turmerones, Sep. Purif. Technol. 47 (2006) 119–125. https://doi.org/10.1016/j.seppur.2005.06.018.

[175]   A.L. Chassagnez-Méndez, N.T. Machado, M.E. Araujo, J.G. Maia, M.A.A. Meireles, Supercritical CO_2 extraction of curcumins and essential oil from the rhizomes of turmeric (Curcuma longa L.), Ind. Eng. Chem. Res. 39 (2000) 4729–4733. https://doi.org/10.1021/ie000171c.

[176] P.S. Wakte, B.S. Sachin, A.A. Patil, D.M. Mohato, T.H. Band, D.B. Shinde, Optimization of microwave, ultra-sonic and supercritical carbon dioxide assisted extraction techniques for curcumin from Curcuma longa, Sep. Purif. Technol. 79 (2011) 50–55. https://doi.org/10.1016/j.seppur.2011.03.010.

[177] H.A. Martinez-Correa, J.T. Paula, A.C.A.V. Kayano, C.L. Queiroga, P.M. Magalhães, F.T.M. Costa, F.A. Cabral, Composition and antimalarial activity of extracts of Curcuma longa L. obtained by a combination of extraction processes using supercritical CO2, ethanol and water as solvents, J. Supercrit. Fluids. 119 (2017) 122–129. https://doi.org/10.1016/j.supflu.2016.08.017.

[178] B.Z. Hmar, D. Kalita, B. Srivastava, Optimization of microwave power and curing time of turmeric rhizome (Curcuma Longa L.) based on textural degradation, Lwt-Food Sci. Technol. 76 (2017) 48–56. https://doi.org/10.1016/j.lwt.2016.10.044.

[179] Q.Q. Yang, L.Z. Cheng, T. Zhang, S. Yaron, H.X. Jiang, Z.Q. Sui, H. Corke, Phenolic profiles, antioxidant, and antiproliferative activities of turmeric (Curcuma longa), Ind. Crops Prod. 152 (2020) 112561. https://doi.org/10.1016/j.indcrop.2020.112561.

[180] W. Ye, X. Wang, Y. Liu, J. Chen, Analysis and prediction of the performance of free- piston Stirling engine using response surface methodology and artificial neural network, Appl. Therm. Eng. 188 (2021) 116557. https://doi.org/10.1016/j.applthermaleng.2021.116557.

[181] B. Gullón, P. Gullón, T.A. Lú-chau, M. Teresa, J.M. Lema, Optimization of solvent extraction of antioxidants from Eucalyptus globulus leaves by response surface methodology : Characterization and assessment of their bioactive properties, Ind. Crop. Prod. 108 (2017) 649–659. https://doi.org/10.1016/j.indcrop.2017.07.014.

[182] U.K. Vijayan, S. Varakumar, R.S. Singhal, A comparative account of extraction of oleoresin from Curcuma aromatica Salisb by solvent and

supercritical carbon dioxide: Characterization and bioactivities, Lwt-Food Sci. Technol. 116 (2019) 108564. https://doi.org/10.1016/j.lwt.2019.108564.

[183]   E. Rohaeti, M. Rafi, U.D. Syafitri, R. Heryanto, Fourier transform infrared spectroscopy combined with chemometrics for discrimination of Curcuma longa, Curcuma xanthorrhiza and Zingiber cassumunar, Spectrochim. Acta - Part A Mol. Biomol. Spectrosc. 137 (2015) 1244–1249. https://doi.org/10.1016/j.saa.2014.08.139.

[184]   T.M. Sampath Udeni Gunathilake, Y.C. Ching, C.H. Chuah, H.A. Illias, K.Y. Ching, R. Singh, L. Nai-Shang, Influence of a nonionic surfactant on curcumin delivery of nanocellulose reinforced chitosan hydrogel, Int. J. Biol. Macromol. 118 (2018) 1055–1064. https://doi.org/10.1016/j.ijbiomac.2018.06.147.

[185]   Z. Chen, L. Quan, H. Zhou, Y. Zhao, P. Chen, L. Hu, Z. Yang, C. Hu, D. Cao, Screening of active fractions from Curcuma Longa Radix isolated by HPLC and GC-MS for promotion of blood circulation and relief of pain, J. Ethnopharmacol. 234 (2019) 68–75. https://doi.org/10.1016/j.jep.2018.09.035.

[186]   F.A.L. de Carvalho, P.E.S. Munekata, A. Lopes de Oliveira, M. Pateiro, R. Domínguez, M.A. Trindade, J.M. Lorenzo, Turmeric (Curcuma longa L.) extract on oxidative stability, physicochemical and sensory properties of fresh lamb sausage with fat replacement by tiger nut (Cyperus esculentus L.) oil, Food Res. Int. 136 (2020) 109487. https://doi.org/10.1016/j.foodres.2020.109487.

[187]   S.S. Patil, V.K. Rathod, Synergistic Effect of Ultrasound and Three Phase Partitioning for the Extraction of Curcuminoids from Curcuma longa and its Bioactivity Profile, Process Biochem. 93 (2020) 85–93. https://doi.org/10.1016/j.procbio.2020.02.031.

[188]   K. Hayat, S. Abbas, S. Hussain, S.A. Shahzad, M.U. Tahir, Effect of microwave and conventional oven heating on phenolic constituents, fatty

acids, minerals and antioxidant potential of fennel seed, Ind. Crops Prod. 140 (2019) 111610. https://doi.org/10.1016/j.indcrop.2019.111610.

[189]   Z. Sanchez-Reinoso, W.I. Mora-Adames, C.A. Fuenmayor, A.E. Darghan-Contreras, C. Gardana, L.F. Gutiérrez, Microwave-assisted extraction of phenolic compounds from Sacha Inchi shell: Optimization, physicochemical properties and evaluation of their antioxidant activity, Chem. Eng. Process. - Process Intensif. 153 (2020) 107922. https://doi.org/10.1016/j.cep.2020.107922.

[190]   H. Liang, W. Wang, J. Xu, Q. Zhang, Z. Shen, Z. Zeng, Q. Li, Optimization of ionic liquid-based microwave-assisted extraction technique for curcuminoids from Curcuma longa L., Food Bioprod. Process. 104 (2017) 57–65. https://doi.org/10.1016/j.fbp.2017.04.003.

[191]   C. Pan, L. Zhao, D. Zhao, Microwave-assisted green extraction of antioxidant components from Osmanthus fragrans (Lour) flower using natural deep eutectic solvents, J. Appl. Res. Med. Aromat. Plants. 20 (2021) 100285. https://doi.org/10.1016/j.jarmap.2020.100285.

[192]   R. Fernández-Marín, J. Labidi, M.Á. Andrés, S.C.M. Fernandes, Using α-chitin nanocrystals to improve the final properties of poly (vinyl alcohol) films with Origanum vulgare essential oil, Polym. Degrad. Stab. 179 (2020). https://doi.org/10.1016/j.polymdegradstab.2020.109227.

[193]   S. Lago, H. Rodríguez, A. Soto, A. Arce, Deterpenation of citrus essential oil by liquid-liquid extraction with 1-alkyl-3-methylimidazolium bis(trifluoromethylsulfonyl)amide ionic liquids, J. Chem. Eng. Data. 56 (2011) 1273–1281. https://doi.org/10.1021/je1011339.

[194]   W.P. Silvestre, F. Agostini, L.A.R. Muniz, G.F. Pauletti, Fractionating of green Mandarin (Citrus deliciosa Tenore) essential oil by vacuum fractional distillation, J. Food Eng. 178 (2016) 90–94. https://doi.org/10.1016/j.jfoodeng.2016.01.011.

[195]   M. Francisco, S. Lago, A. Soto, A. Arce, Essential oil deterpenation by

solvent extraction using 1-ethyl-3-methylimidazolium 2-(2-methoxyethoxy) ethylsulfate ionic liquid, Fluid Phase Equilib. 296 (2010) 149–153. https://doi.org/10.1016/j.fluid.2010.03.019.

[196]   J.F. Perini, W.P. Silvestre, F. Agostini, D. Toss, G.F. Pauletti, Fractioning of orange (Citrus sinensis L.) essential oil using vacuum fractional distillation, Sep. Sci. Technol. 52 (2017) 1397–1403. https://doi.org/10.1080/01496395.2017.1290108.

[197]   D. Gonçalves, P. Costa, C.E.C. Rodrigues, A.E. Rodrigues, Effect of citrus sinensis essential oil deterpenation on the aroma profile of the phases obtained by solvent extraction, J. Chem. Thermodyn. 116 (2018) 166–175. https://doi.org/10.1016/j.jct.2017.09.011.

[198]   K. Sakamoto, K. Fujii, A. Inoue, H. Kozuka, H. Ohta, Differential recovery of terpene hydrocarbons and oxygenated compounds from condensates containing essential oil discharged during concentration of citrus juices using a ceramic membrane, Food Sci. Technol. Res. 9 (2003) 11–16. https://doi.org/10.3136/fstr.9.11.

[199]   G. Ben Salha, R. Herrera Díaz, J. Labidi, M. Abderrabba, Deterpenation of Origanum majorana L . essential oil by reduced pressure steam distillation, Ind. Crop. Prod. 109 (2017) 116–122. https://doi.org/10.1016/j.indcrop.2017.08.016.

[200]   G. Ben Salha, R. Herrera Díaz, J. Labidi, M. Abderrabba, Deterpenation of Origanum majorana L. essential oil by reduced pressure steam distillation, Ind. Crops Prod. 109 (2017) 116–122. https://doi.org/10.1016/j.indcrop.2017.08.016.

[201]   R. Fernández-Marín, S.C. M. Fernandes, C. McReynolds, J. Labidi, M.Á. Sánchez Andrés, Chapter 22-Chitosan-based materials as templates for essential oils, in: Handb. Chitin Chitosan-Volume 3 Chitina-and Chitosan-Based Polym. Mater. Var. Appl., Elsevier, 2020: pp. 689–720.

[202]   M. Kaya, P. Ravikumar, S. Ilk, M. Mujtaba, L. Akyuz, J. Labidi, A.M.

Salaberria, Y.S. Cakmak, S.K. Erkul, Production and characterization of chitosan based edible films from Berberis crataegina's fruit extract and seed oil, Innov. Food Sci. Emerg. Technol. 45 (2018) 287–297. https://doi.org/10.1016/j.ifset.2017.11.013.

[203] M. Salari, M. Sowti Khiabani, R. Rezaei Mokarram, B. Ghanbarzadeh, H. Samadi Kafil, Development and evaluation of chitosan based active nanocomposite films containing bacterial cellulose nanocrystals and silver nanoparticles, Food Hydrocoll. 84 (2018) 414–423. https://doi.org/10.1016/j.foodhyd.2018.05.037.

[204] V. Zubillaga, A.M. Salaberria, T. Palomares, A. Alonso-Varona, S. Kootala, J. Labidi, S.C.M. Fernandes, Chitin Nanoforms Provide Mechanical and Topological Cues to Support Growth of Human Adipose Stem Cells in Chitosan Matrices, Biomacromolecules. 19 (2018) 3000–3012. https://doi.org/10.1021/acs.biomac.8b00570.

[205] A.M. Salaberría, R. Teruel-Juanes, J.D. Badia, S.C.M. Fernandes, V. Sáenz de Juano-Arbona, J. Labidi, A. Ribes-Greus, Influence of chitin nanocrystals on the dielectric behaviour and conductivity of chitosan-based bionanocomposites, Compos. Sci. Technol. 167 (2018) 323–330. https://doi.org/10.1016/j.compscitech.2018.08.019.

[206] A. Saralegi, S.C.M. Fernandes, A. Alonso-Varona, T. Palomares, E.J. Foster, C. Weder, A. Eceiza, M.A. Corcuera, Shape-memory bionanocomposites based on chitin nanocrystals and thermoplastic polyurethane with a highly crystalline soft segment, Biomacromolecules. 14 (2013) 4475–4482. https://doi.org/10.1021/bm401385c.

[207] I.K. Sani, S. Pirsa, Ş. Tağı, Preparation of chitosan/zinc oxide/Melissa officinalis essential oil nano-composite film and evaluation of physical, mechanical and antimicrobial properties by response surface method, Polym. Test. 79 (2019). https://doi.org/10.1016/j.polymertesting.2019.106004.

[208] Y. Peng, Y. Li, Combined effects of two kinds of essential oils on physical, mechanical and structural properties of chitosan films, Food Hydrocoll. 36 (2014) 287–293. https://doi.org/10.1016/j.foodhyd.2013.10.013.

[209] J. Hafsa, M. ali Smach, M.R. Ben Khedher, B. Charfeddine, K. Limem, H. Majdoub, S. Rouatbi, Physical, antioxidant and antimicrobial properties of chitosan films containing Eucalyptus globulus essential oil, LWT - Food Sci. Technol. 68 (2016) 356–364. https://doi.org/10.1016/j.lwt.2015.12.050.

[210] M. Pereda, A. Dufresne, M.I. Aranguren, N.E. Marcovich, Polyelectrolyte films based on chitosan/olive oil and reinforced with cellulose nanocrystals, Carbohydr. Polym. 101 (2014) 1018–1026. https://doi.org/10.1016/j.carbpol.2013.10.046.

[211] C. Shin, D. Kim, W. Shin, Characterization of chitosan extracted from Mealworm Beetle (Tenebrio molitor , Zophobas morio) and Rhinoceros Beetle (Allomyrina dichotoma) and their antibacterial activities, Int. J. Biol. Macromol. 125 (2019) 72–77.

[212] A. Kumar, Navneet, S.S. Gautam, Volatile Constituents of Curcuma caesia Roxb. Rhizome from North India, Natl. Acad. Sci. Lett. 43 (2020) 607–610. https://doi.org/10.1007/s40009-020-00926-y.

[213] K. Munhuweyi, O.J. Caleb, C.L. Lennox, A.J. van Reenen, U.L. Opara, In vitro and in vivo antifungal activity of chitosan-essential oils against pomegranate fruit pathogens, Postharvest Biol. Technol. 129 (2017) 9–22. https://doi.org/10.1016/j.postharvbio.2017.03.002.

[214] A. Morales, M.Á. Andrés, J. Labidi, P. Gullón, UV–vis protective poly(vinyl alcohol)/bio-oil innovative films, Ind. Crops Prod. 131 (2019) 281–292. https://doi.org/10.1016/j.indcrop.2019.01.071.

[215] S. Hajji, H. Kchaou, I. Bkhairia, R. Ben Slama-Ben, S. Boufi, F. Debeaufort, N. Moncef, Conception of active food packaging films based on 1 crab chitosan and 2 gelatin enriched with crustacean protein hydrolysates with improved 3 functional and biological properties, Food Hydrocoll. (2021)

135907. https://doi.org/10.1016/j.foodhyd.2021.106639.

[216]   A.G. Cunha, S.C.M. Fernandes, C.S.R. Freire, A.J.D. Silvestre, C.P. Neto, A.
        Gandini, What is the real value of chitosan's surface energy?,
        Biomacromolecules. 9 (2008) 610–614. https://doi.org/10.1021/bm701199g.

[217]   V.G.L. Souza, J.R.A. Pires, P. Freitas Rodrigues, A.A.S. Lopes, F.M.B.
        Fernandes, M. Paula, I.M. Coelhoso, A. Luisa, Bionanocomposites of
        chitosan / montmorillonite incorporated with Rosmarinus o ffi cinalis
        essential oil : Development and physical characterization, Food Packag.
        Shelf Life. 16 (2018) 148–156. https://doi.org/10.1016/j.fpsl.2018.03.009.

[218]   S. Valizadeh, M. Naseri, S. Babaei, S.M.H. Hosseini, A. Imani, Development
        of bioactive composite films from chitosan and carboxymethyl cellulose
        using glutaraldehyde, cinnamon essential oil and oleic acid, Int. J. Biol.
        Macromol. 134 (2019) 604–612.
        https://doi.org/10.1016/j.ijbiomac.2019.05.071.

[219]   A. Khan, R.A. Khan, S. Salmieri, C. Le, B. Riedl, J. Bouchard, V. Tan, M.R.
        Kamal, M. Lacroix, Mechanical and barrier properties of nanocrystalline
        cellulose reinforced chitosan based nanocomposite films, Carbohydr.
        Polym. 90 (2012) 1601–1608. https://doi.org/10.1016/j.carbpol.2012.07.037.

[220]   Z. Shen, D.P. Kamdem, Development and characterization of
        biodegradable chitosan films containing two essential oils, Int. J. Biol.
        Macromol. 74 (2015) 289–296.
        https://doi.org/10.1016/j.ijbiomac.2014.11.046.

[221]   N. Ardekani Torabi, M. Khorram, K. Zomorodian, S. Yazdanpanah, H.
        Veisi, V. Hojat, Evaluation of electrospun poly (vinyl alcohol) -based nano
        fi ber mats incorporated with Zataria multi fl ora essential oil as potential
        wound dressing, Int. J. Biol. Macromol. 125 (2019) 743–750.
        https://doi.org/10.1016/j.ijbiomac.2018.12.085.

[222]   M. Mohammadi, S. Mirabzadeh, R. Shahvalizadeh, H. Hamishehkar,
        Development of novel active packaging films based on whey protein

isolate incorporated with chitosan nanofiber and nano-formulated cinnamon oil, Int. J. Biol. Macromol. 149 (2020) 11–20. https://doi.org/10.1016/j.ijbiomac.2020.01.083.

[223] T. Kulisic, A. Radonic, V. Katalinic, M. Milos, Use of different methods for testing antioxidative activity of oregano essential oil, Food Chem. 85 (2004) 633–640. https://doi.org/10.1016/j.foodchem.2003.07.024.

[224] S. Inouye, K. Uchida, H. Yamaguchi, T. Miyara, S. Gomi, M. Amano, Volatile aroma constituents of three labiatae herbs growing wild in the karakoram-himalaya district and their antifungal activity by vapor contact, J. Essent. Oil Res. 13 (2001) 68–72. https://doi.org/10.1080/10412905.2001.9699610.

[225] P.S. P., K.S. T., Antioxidant, antibacterial and cytotoxic potential of silver nanoparticles synthesized using terpenes rich extract of Lantana camara L. leaves, Biochem. Biophys. Reports. 10 (2017) 76–81. https://doi.org/10.1016/j.bbrep.2017.03.002.

[226] Q. Ma, T. Liang, L. Cao, L. Wang, Intelligent poly (vinyl alcohol)-chitosan nanoparticles-mulberry extracts films capable of monitoring pH variations, Int. J. Biol. Macromol. 108 (2018) 576–584. https://doi.org/10.1016/j.ijbiomac.2017.12.049.

[227] S. Chen, M. Wu, P. Lu, L. Gao, S. Yan, S. Wang, Development of pH indicator and antimicrobial cellulose nanofibre packaging film based on purple sweet potato anthocyanin and oregano essential oil, Int. J. Biol. Macromol. 149 (2020) 271–280. https://doi.org/10.1016/j.ijbiomac.2020.01.231.

[228] M. Alizadeh-Sani, M. Tavassoli, D.J. McClements, H. Hamishehkar, Multifunctional halochromic packaging materials: Saffron petal anthocyanin loaded-chitosan nanofiber/methyl cellulose matrices, Food Hydrocoll. 111 (2021) 106237. https://doi.org/10.1016/j.foodhyd.2020.106237.

[229] X. Zhang, Y. Liu, H. Yong, Y. Qin, J. Liu, J. Liu, Development of

multifunctional food packaging films based on chitosan, TiO $_2$ nanoparticles and anthocyanin-rich black plum peel extract, Food Hydrocoll. 94 (2019) 80–92. https://doi.org/10.1016/j.foodhyd.2019.03.009.

[230] S. Kalpana, S.R. Priyadarshini, M. Maria Leena, J.A. Moses, C. Anandharamakrishnan, Intelligent packaging: Trends and applications in food systems, Trends Food Sci. Technol. 93 (2019) 145–157. https://doi.org/10.1016/j.tifs.2019.09.008.

[231] H. Yong, X. Wang, X. Zhang, Y. Liu, Y. Qin, J. Liu, Effects of anthocyanin-rich purple and black eggplant extracts on the physical, antioxidant and pH-sensitive properties of chitosan film, Food Hydrocoll. 94 (2019) 93–104. https://doi.org/10.1016/j.foodhyd.2019.03.012.

[232] V.A. Pereira, I.N.Q. de Arruda, R. Stefani, Active chitosan/PVA films with anthocyanins from Brassica oleraceae (Red Cabbage) as Time-Temperature Indicators for application in intelligent food packaging, Food Hydrocoll. 43 (2015) 180–188. https://doi.org/10.1016/j.foodhyd.2014.05.014.

[233] T. Liang, G. Sun, L. Cao, J. Li, L. Wang, A pH and NH3 sensing intelligent film based on Artemisia sphaerocephala Krasch. gum and red cabbage anthocyanins anchored by carboxymethyl cellulose sodium added as a host complex, Food Hydrocoll. 87 (2019) 858–868. https://doi.org/10.1016/j.foodhyd.2018.08.028.

[234] K. Halász, L. Csóka, Black chokeberry (Aronia melanocarpa) pomace extract immobilized in chitosan for colorimetric pH indicator film application, Food Packag. Shelf Life. 16 (2018) 185–193. https://doi.org/10.1016/j.fpsl.2018.03.002.

[235] C. Wu, Y. Li, J. Sun, Y. Lu, C. Tong, L. Wang, Z. Yan, J. Pang, Novel konjac glucomannan films with oxidized chitin nanocrystals immobilized red cabbage anthocyanins for intelligent food packaging, Food Hydrocoll. 98 (2020) 105245. https://doi.org/10.1016/j.foodhyd.2019.105245.

[236] R. Fernández-Marín, S. C M Fernandes, M.A. Andrés, J. Labidi, Microwave

- Assisted Extraction of Curcuma longa L . Oil : Optimization , Chemical Structure and Composition , Antioxidant Activity and Comparison with Conventional Soxhlet Extraction, Molecules. (2021) 1616.

[237]   H. zhi Chen, M. Zhang, B. Bhandari, C. hui Yang, Novel pH-sensitive films containing curcumin and anthocyanins to monitor fish freshness, Food Hydrocoll. 100 (2020) 105438. https://doi.org/10.1016/j.foodhyd.2019.105438.

[238]   X. Zhu, J. Chen, Y. Hu, N. Zhang, Y. Fu, X. Chen, Tuning complexation of carboxymethyl cellulose/ cationic chitosan to stabilize Pickering emulsion for curcumin encapsulation, Food Hydrocoll. 110 (2021) 106135. https://doi.org/10.1016/j.foodhyd.2020.106135.

[239]   H. Yong, X. Wang, R. Bai, Z. Miao, X. Zhang, J. Liu, Development of antioxidant and intelligent pH-sensing packaging films by incorporating purple-fleshed sweet potato extract into chitosan matrix, Food Hydrocoll. 90 (2019) 216–224. https://doi.org/10.1016/j.foodhyd.2018.12.015.

[240]   Y. Liu, Y. Qin, R. Bai, X. Zhang, L. Yuan, J. Liu, Preparation of pH-sensitive and antioxidant packaging films based on κ-carrageenan and mulberry polyphenolic extract, Int. J. Biol. Macromol. 134 (2019) 993–1001. https://doi.org/10.1016/j.ijbiomac.2019.05.175.

[241]   R.R. Koshy, J.T. Koshy, S.K. Mary, S. Sadanandan, S. Jisha, L.A. Pothan, Preparation of pH sensitive film based on starch/carbon nano dots incorporating anthocyanin for monitoring spoilage of pork, Food Control. 126 (2021) 108039. https://doi.org/10.1016/j.foodcont.2021.108039.

[242]   X. Zhang, Y. Li, M. Guo, T.Z. Jin, S.A. Arabi, Q. He, B.B. Ismail, Y. Hu, D. Liu, Antimicrobial and UV Blocking Properties of Composite Chitosan Films with Curcumin Grafted Cellulose Nanofiber, Food Hydrocoll. 112 (2021) 106337. https://doi.org/10.1016/j.foodhyd.2020.106337.

[243]   A.M. Salaberria, R.H. Diaz, M.A. Andrés, S.C.M. Fernandes, J. Labidi, The antifungal activity of functionalized chitin nanocrystals in poly (Lactid Acid) films, Materials (Basel). 10 (2017) 1–16.

https://doi.org/10.3390/ma10050546.

[244] P. Ezati, J.W. Rhim, pH-responsive chitosan-based film incorporated with alizarin for intelligent packaging applications, Food Hydrocoll. 102 (2020) 105629. https://doi.org/10.1016/j.foodhyd.2019.105629.

[245] X. Chen, X. He, B. Zhang, X. Fu, J. Jane, Q. Huang, Effects of adding corn oil and soy protein to corn starch on the physicochemical and digestive properties of the starch, Int. J. Biol. Macromol. 104 (2017) 481–486.

[246] M. Kaya, P. Ravikumar, S. Ilk, M. Mujtaba, L. Akyuz, J. Labidi, A.M. Salaberria, Y.S. Cakmak, S.K. Erkul, Production and characterization of chitosan based edible films from Berberis crataegina's fruit extract and seed oil, Innov. Food Sci. Emerg. Technol. 45 (2018) 287–297. https://doi.org/10.1016/j.ifset.2017.11.013.

[247] S.R. Kanatt, M.S. Rao, S.P. Chawla, A. Sharma, Active chitosan e polyvinyl alcohol fi lms with natural extracts, Food Hydrocoll. 29 (2012) 290–297. https://doi.org/10.1016/j.foodhyd.2012.03.005.

[248] Q. Ma, L. Wang, Preparation of a visual pH-sensing film based on tara gum incorporating cellulose and extracts from grape skins, Sensors Actuators, B Chem. 235 (2016) 401–407. https://doi.org/10.1016/j.snb.2016.05.107.

[249] H. Yong, J. Liu, Recent advances in the preparation, physical and functional properties, and applications of anthocyanins-based active and intelligent packaging films, Food Packag. Shelf Life. 26 (2020) 100550. https://doi.org/10.1016/j.fpsl.2020.100550.

[250] S. Roy, J.W. Rhim, Antioxidant and antimicrobial poly(vinyl alcohol)-based films incorporated with grapefruit seed extract and curcumin, J. Environ. Chem. Eng. 9 (2021) 104694. https://doi.org/10.1016/j.jece.2020.104694.

[251] Q. Ma, K. Pang, K. Wang, S. Huang, B. Ding, Y. Duan, J. Zhang, Ultrafine and carboxylated β-chitin nanofibers prepared from squid pen and its transparent hydrogels, Carbohydr. Polym. 211 (2019) 118–123.

https://doi.org/10.1016/j.carbpol.2019.02.001.

[252] X. Zhou, X. Yu, F. Xie, Y. Fan, X. Xu, J. Qi, G. Xiong, pH-responsive double-layer indicator films based on konjac glucomannan / camellia oil and carrageenan / anthocyanin / curcumin for monitoring meat freshness, Food Hydrocoll. (2021) 106695. https://doi.org/10.1016/j.foodhyd.2021.106695.

[253] M.C. Silva-Pereira, J.A. Teixeira, V.A. Pereira-Júnior, R. Stefani, Chitosan/corn starch blend films with extract from Brassica oleraceae (red cabbage) as a visual indicator of fish deterioration, Lwt. 61 (2015) 258–262. https://doi.org/10.1016/j.lwt.2014.11.041.

[254] J. Zhang, X. Zou, X. Zhai, X.W. Huang, C. Jiang, M. Holmes, Preparation of an intelligent pH film based on biodegradable polymers and roselle anthocyanins for monitoring pork freshness, Food Chem. 272 (2019) 306–312. https://doi.org/10.1016/j.foodchem.2018.08.041.

[255] D. Yun, H. Cai, Y. Liu, L. Xiao, J. Song, J. Liu, Development of active and intelligent films based on cassava starch and Chinese bayberry (: Myrica rubra Sieb. et Zucc.) anthocyanins, RSC Adv. 9 (2019) 30905–30916. https://doi.org/10.1039/c9ra06628d.

[256] G.T. Sigurdson, R.J. Robbins, T.M. Collins, M.M. Giusti, Molar absorptivities (ε) and spectral and colorimetric characteristics of purple sweet potato anthocyanins, Food Chem. 271 (2019) 497–504. https://doi.org/10.1016/j.foodchem.2018.07.096.

[257] Y. Ruiz-Navajas, M. Viuda-Martos, E. Sendra, J.A. Perez-Alvarez, J. Fernández-López, In vitro antibacterial and antioxidant properties of chitosan edible fi lms incorporated with Thymus moroderi or Thymus piperella essential oils, Food Control. 30 (2013) 386–392. https://doi.org/10.1016/j.foodcont.2012.07.052.

[258] A. Morales, M.Á. Andrés, J. Labidi, P. Gullón, UV – vis protective poly (vinyl alcohol)/ bio-oil innovative fi lms, Ind. Crop. Prod. 131 (2019) 281–

292. https://doi.org/10.1016/j.indcrop.2019.01.071.

[259] C. Chen, Z. Xu, Y. Ma, J. Liu, Q. Zhang, Properties , vapour-phase antimicrobial and antioxidant activities of active poly (vinyl alcohol) packaging fi lms incorporated with clove oil, Food Control. 88 (2018) 105–112. https://doi.org/10.1016/j.foodcont.2017.12.039.

[260] K.K. Gaikwad, J.Y. Lee, Y.S. Lee, Development of polyvinyl alcohol and apple pomace bio-composite film with antioxidant properties for active food packaging application, J. Food Sci. Technol. 53 (2016) 1608–1619. https://doi.org/10.1007/s13197-015-2104-9.

[261] H. Baydar, O. Sagdic, G. Özkan, T. Karadogan, Antibacterial activity and composition of essential oils from Origanum , Thymbra and Satureja species with commercial importance in Turkey, Food Control. 15 (2004) 169–172. https://doi.org/10.1016/S0956-7135(03)00028-8.

[262] H. Chi, S. Song, M. Luo, C. Zhang, W. Li, L. Li, Y. Qin, Effect of PLA nanocomposite films containing bergamot essential oil , TiO 2 nanoparticles , and Ag nanoparticles on shelf life of mangoes, Sci. Hortic. (Amsterdam). 249 (2019) 192–198. https://doi.org/10.1016/j.scienta.2019.01.059.

[263] L. Wu, S. Huang, J. Zheng, Z. Qiu, X. Lin, Y. Qin, Synthesis and characterization of biomass lignin-based PVA super-absorbent hydrogel, Int. J. Biol. Macromol. 140 (2019) 538–545. https://doi.org/10.1016/j.ijbiomac.2019.08.142.

[264] S.M.B. Hashemi, A.M. Khaneghah, Progress in Organic Coatings Characterization of novel basil-seed gum active edible fi lms and coatings containing oregano essential oil, Prog. Org. Coatings. 110 (2017) 35–41. https://doi.org/10.1016/j.porgcoat.2017.04.041.

[265] S. Singh, K.K. Gaikwad, Y.S. Lee, Antimicrobial and antioxidant properties of polyvinyl alcohol bio composite films containing seaweed extracted cellulose nano-crystal and basil leaves extract, Int. J. Biol. Macromol. 107

(2018) 1879–1887. https://doi.org/10.1016/j.ijbiomac.2017.10.057.

[266]   A. Fraj, F. Jaâfar, M. Marti, L. Coderch, N. Ladhari, A comparative study of oregano (Origanum vulgare L .) essential oil-based polycaprolactone nanocapsules / microspheres : Preparation , physicochemical characterization , and storage stability, Ind. Crop. Prod. 140 (2019) 111669. https://doi.org/10.1016/j.indcrop.2019.111669.

[267]   S. Ribes, A. Fuentes, J.M. Barat, Effect of oregano (Origanum vulgare L . ssp . hirtum) and clove (Eugenia spp .) nanoemulsions on Zygosaccharomyces bailii survival in salad dressings, Food Chem. 295 (2019) 630–636. https://doi.org/10.1016/j.foodchem.2019.05.173.

[268]   F. Luzi, E. Fortunati, G. Giovanale, A. Mazzaglia, L. Torre, G. Mariano, Cellulose nanocrystals from Actinidia deliciosa pruning residues combined with carvacrol in PVA CH films with antioxidant / antimicrobial properties for packaging applications, Int. J. Biol. Macromol. 104 (2017) 43–55. https://doi.org/10.1016/j.ijbiomac.2017.05.176.

[269]   C.W. Chen, J. Xie, F.X. Yang, H.L. Zhang, Z.W. Xu, J.L. Liu, Y.J. Chen, Development of moisture-absorbing and antioxidant active packaging film based on poly(vinyl alcohol) incorporated with green tea extract and its effect on the quality of dried eel, J. Food Process. Preserv. 42 (2018) 1–11. https://doi.org/10.1111/jfpp.13374.

[270]   Z. Yu, B. Li, J. Chu, P. Zhang, Silica in situ enhanced PVA / chitosan biodegradable fi lms for food packages, Carbohydr. Polym. 184 (2018) 214–220. https://doi.org/10.1016/j.carbpol.2017.12.043.

[271]   J.-P. Fan, J.-J. Luo, X.-H. Zhang, B. Zhen, C.-Y. Dong, Y. Li, J. Shen, Y.-T. Cheng, H.-P. Chen, A novel electrospun β -CD / CS / PVA nano fi ber membrane for simultaneous and rapid removal of organic micropollutants and heavy metal ions from water, Chem. Eng. J. 378 (2019) 122232. https://doi.org/10.1016/j.cej.2019.122232.

[272]   S. Yoon, Y. Kim, B. Il, J. Je, Preparation and antibacterial activities of

chitosan-gallic acid / polyvinyl alcohol blend film by LED-UV irradiation, J. Photochem. Photobiol. B Biol. 176 (2017) 145–149. https://doi.org/10.1016/j.jphotobiol.2017.09.024.

[273] D.E. Rodríguez-Félix, J.M. Quiroz-castillo, H. Grijalva-monteverde, T. Castillo-castro, S.E. Burruel-ibarra, F. Rodríguez-Félix, T. Madera-Santana, R.E. Cabanillas, P.J. Herrera-Franco, Degradability of Extruded Polyethylene / Chitosan Blends Compatibilized with Polyethylene- Graft - Maleic Anhydride Under Natural Weathering, Appl. Polym. Sci. 41045 (2014) 1–7. https://doi.org/10.1002/app.41045.

[274] Y. Bai, Y. Zhao, Y. Li, J. Xu, X. Fu, X. Gao, X. Mao, Z. Li, UV-shielding alginate films crosslinked with Fe_{3+} containing EDTA, Carbohydr. Polym. (2019) 115–480. https://doi.org/10.1016/j.carbpol.2019.115480.

[275] H. Almasi, B. Ghanbarzadeh, J. Dehghannya, A.A. Entezami, A. Khosrowshahi Asl, Development of a novel controlled-release nanocomposite based on poly(lactic acid) to increase the oxidative stability of soybean oil, Food Addit. Contam. - Part A Chem. Anal. Control. Expo. Risk Assess. 31 (2014) 1586–1597. https://doi.org/10.1080/19440049.2014.935962.

Appendix A: Publications

BOOK CHAPTER:

- **Publication 1**

Rut Fernández-Marín, Susana C M Fernandes, Colin McReynolds, Jalel Labidi, María Ángeles Andrés Sánchez

Chapter 22: Chitosan-based materials as templates for essential oils

Handbook of Chitin and Chitosan: Volume 3: Chitin and Chitosan based Polymer Materials for Various Applications, 3 (2020) 689-720. https://doi.org/10.1016/B978-0-12-817966-6.00022-4

PAPERS IN SCIENTIFIC JOURNALS:

(JC: Journal Category, JR: Journal Ranking)

- **Publication 2**

Rut Fernández-Marín, Fabio Hernández-Ramos, Asier M. Salaberria, Mª Ángeles Andrés Sánchez, Jalel Labidi, Susana C.M. Fernandes

Optimization of microwave irradiation for the isolation of nanochitin from different origins by response surface methodology: an eco-friendly alternative.

International Journal of Biological Macromolecules (Under revision)

Impact factor: 5.162 (2019); JC: Biochemistry & molecular biology; JR: 51/297

- **Publication 3**

Rut Fernández-Marín, Susana C.M. Fernandes, Mª Ángeles Andrés Sánchez, Jalel Labidi
Microwave-assisted extraction of Curcuma longa L. oil: Optimization, chemical structure and composition, antioxidant activity and comparison with

conventional Soxhlet extraction, Molecules, 26 (2021) 1516.
https://doi.org/10.3390/molecules26061516

Impact factor: 3.267 (2019); JC: Biochemistry & molecular biology; JR: 142/297

- **Publication 4**

Rut Fernández-Marín, Muhammad Mujtaba, Demet Cansaran Duman, Mª Ángeles Andrés Sánchez, Corinne Nardin, Susana C.M. Fernandes, Jalel Labidi

Nanocomposite films based on beta-chitin nanofibres, chitosan & deterpenated fractions of Origanum majorana L. essential oil

Polymers, (accepted)

Impact factor: 3.426 (2019); JC: Polymer Science; JR: 16/89

- **Publication 5**

Rut Fernández-Marín, Susana C.M. Fernandes, Mª Ángeles Andrés Sánchez, Jalel Labidi

Halocromic and antioxidant capacity of smart pH- and volatile ammonia-sensitive chitosan/chitin nanocrystals nanocomposite films prepared with curcuma oil and anthocyanins

 (in process)

- **Publication 6**

Rut Fernández-Marín, Jalel Labidi, María Ángeles Andrés, Susana C. M. Fernandes

Using α-chitin nanocrystals to improve the final properties of poly(vinyl alcohol) films with Origanum vulgare essential oil, Polymer Degradation and Stability, 179 (2020) 109227. https://doi.org/10.1016/j.polymdegradstab.2020.109227

Impact factor: 4.032 (2019); JC: Polymer science; JR: 13/89

CONFERENCES:

- **Rut Fernández-Marín**, Asier M. Salaberria, Mª Ángeles Andrés Sánchez, Susana C.M. Fernandes, Jalel Labidi

An eco-friendly approach to obtain chitin nanocrystals

13th Internacional Conference of the European Chitin Society-8th symposium of the Iberoamerican Chitin Society (EUCHIS-2017)

31 May - 3 June 2017, Sevilla, Spain

(Poster)

- **Rut Fernández-Marín**, Asier M. Salaberria, Jalel Labidi, Mª Ángeles Andrés Sánchez, Susana C.M. Fernandes

Preparation of alpha-chitin nanocrystals and their nanocomposite films with poly(vinyl alcohol) and Origanum vulgare oil by microwave technique

4th Iberoamerican Congress on Biorefineries (CIAB)

24 - 26 October 2018, Jaén, Spain

(Poster)

- **Rut Fernández-Marín**, Susana C.M. Fernandes, Jalel Labidi, Mª Ángeles Andrés Sánchez

α-chitin nanocrystals/PVA nanocomposites films with Oreganum vulgare essential oil

7th international conference on biodegradable and biobased polymers (BIOPOL2019)

17-19 June 2019, Stockholm, Sweden

(Oral presentation)

Appendix

COLLABORATIONS:

- *Publication 1*

Amaia Morales, Fabio Hernández-Ramos, Leyre Sillero, **Rut Fernández-Marín**, Izaskun Dávila, Patricia Gullón, Xabier Erdocia, Jalel Labidi

Multiproduct biorefinery based on almond shells: Impact of the delignification stage on the manufacture of valuable products. Bioresource Technology, 315 (2020) 123896. https://doi.org/10.1016/j.biortech.2020.123896

Impact factor: 7.539 (2019); JC: Agricultural engineering; JR: 1/13

- *Publication 2*

Leyre Sillero, Amaia Morales, **Rut Fernández-Marín**, Fabio Hernández-Ramos, Izaskun Dávila, Xabier Erdocia, Jalel Labidi

Science of the Total EnvironmentComparative Life Cycle Assessment of a multiproduct almond shells biorefinery

Journal of Environmental Chemical Engineering *(Under revision)*

Impact factor: 4.3 (2019); JC: Chemical engineering; JR: 29/143

- *Publication 3*

Leyre Sillero, Amaia Morales, **Rut Fernández-Marín**, Fabio Hernández-Ramos, Izaskun Davila, Xabier Erdocia, Jalel Labidi

Study of different extraction methods of bioactive molecules from different tree species. Chemical Engineering Transactions, 86 (2021)

CISAP7: *7TH International Conference on Safety & Environment in Process industry. ISBN 978-88-95608-84-6; ISSN 2283-9216.*

- *Publication 4:*

Muhammad Mujtaba, **Rut Fernandez-Marín**, Eduardo Robles, Jalel Labidi, Khalid Mahmood Khaward, Bahar Akyuz Yılmaze, Houwaida Nefzif

Production of chitosan film incorporated with co-polymerized cellulose nanofibers and diatomite nanocomposite

Carbohydrates polymer *(under revision)*

EDUCATION PUBLICATIONS:

- **Publication 1**

Rut Fernández-Marín, Amaia Morales, María González-Alriols, Rodrigo Llano-Ponte

New technologies for stimulation of student engagement, 11th International Conference on Education and New Learning Technologies, (2019) 4000-4004.

- **Publication 2**

Amaia Morales, **Rut Fernández-Marín**, Leyre Sillero, Itziar Egües, Mª Ángeles Andrés

Enhancement of reflective experiential learning via new technologies, 11th International Conference on Education and New Learning Technologies, (2019) 4529-4534.

Appendix B: Chemicals

Sigma-Aldrich

- Ethanol (EtOH, analytical standard)

- Ethyl acetate ($C_4H_8O_2$, HPLC grade)
- Methanol (MeOH, HPLC grade)
- 2,2-diphenyl-1-picrylhydrazyl (DPPH)
- 6-Hydroxy-2,5,7,8-tetramethylchromane-2-carboxylic acid (Trolox)
- bis(3-ethylbenzothiazoline-6-sulphonic acid) (ABTS)

- 2,4,6-Tri(2-pyridyl)-s-triazine (TPTZ)

- Clorhidric acid (HCl, 37% w/w, ACS reagent)

- Tween 20

- Ringer solution

- Dulbecco's Phosphate (DPBS)
- DMEM medium

- 3-(4,5-dimethylthiazol- 2-yl)-2,5-diphenyltetrazolium bromide (MTT)
- dimethyl sulfoxide (DMSO, 99.9 purity, ACS reagent)

Scharlau

- Folin-Ciocalteu reagent

- Gallic acid monohydrate ($C_7H_6O_5 \cdot H_2O$, extra pure).

Panreac AppliChem

- Glycerol anhydrous

- Sodium hydrogen phosphate (Na_2HPO_4)
- Potassium chloride (KCl)

- sodium hydroxide (NaOH, ACS reagent)
- Acetic acid glacial (CHCOOH, technical grade)

- Sodium chloride (NaCl)

- Potassium di-hydrogen phosphate (KH_2PO_4)
- Sodium acetate (CH_3COONa)

- Potassium peroxodisulphate ($K_2S_2O_8$)

Fischer

- Sodium carbonate anhydrous (NaCO, general-purpose grade)
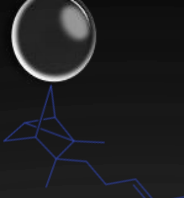
Appendix

Acros Organics
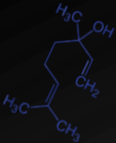
- Iron (III) chloride hexahydrate (FeCl$_3$·6H$_2$O)
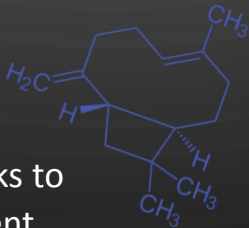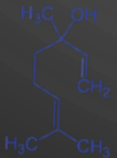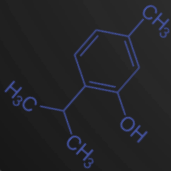
Merck

- Potato dextrose agar (PDA)

Biowest

- penicillin/streptomycin

Biological Industries

- Trypsinized and fetal bovine serum (FBS)

In recent years, the isolation of chitin, which is the second most abundant natural polymer after cellulose, from crustacean shell waste has generated great interest for its application in different fields. this is due to its interesting properties such as biocompatibility and biodegradability. Chitin is a support material in nature, and presents a highly organised micro and nanofibrillated structure, which makes it possible to obtain nanochitin (nanocrystals and nanofibres). These have excellent properties such as low density, low toxicity, and high biodegradability. Additionally, they improve the mechanical properties by acting as reinforcement of films. on the other hand, essential oils are a complex mixture of volatile compounds extracted from different parts of plants that are a good source of bioactive metabolites with antioxidant and antimicrobial properties. Therefore, the aim of this thesis was to develop nanocomposite films based on nanochitin and bio)polymers (in particular chitosan as matrix) essential oils as bioactive compounds, in order to promote the revalorisation of marine waste. The results showed that the addition of nanochitin reinforced the films and, moreover, the essential oils improved their functional properties, and including their biological activity (antioxidant and antifungal). They could therefore be applied as smart food packaging.